Open Quantum Systems: Time (non)-locality, Fixed Points, and Renormalization Groups

Von der Fakultät für Mathematik, Informatik und Naturwissenschaften der RWTH Aachen University zur Erlangung des akademischen Grades eines Doktors der Naturwissenschaften genehmigte Dissertation

vorgelegt von

Konstantin Nestmann, M. Sc.

aus Chemnitz

Berichter: apl.-Prof. Dr. rer. nat. Maarten Rolf Wegewijs
Univ.-Prof. Dr. phil. Herbert Schoeller

Tag der mündlichen Prüfung: 23. Mai 2022

Diese Dissertation ist auf den Internetseiten der Universitätsbibliothek online verfügbar.

Eidesstattliche Erklärung

Ich, Konstantin Nestmann, erkläre hiermit, dass diese Dissertation und die darin dargelegten Inhalte die eigenen sind und selbstständig, als Ergebnis der eigenen originären Forschung, generiert wurden.

Hiermit erkläre ich an Eides statt:

1. Diese Arbeit wurde vollständig oder größtenteils in der Phase als Doktorand dieser Fakultät und Universität angefertigt;
2. Sofern irgendein Bestandteil dieser Dissertation zuvor für einen akademischen Abschluss oder eine andere Qualifikation an dieser oder einer anderen Institution verwendet wurde, wurde dies klar angezeigt;
3. Wenn immer andere eigene- oder Veröffentlichungen Dritter herangezogen wurden, wurden diese klar benannt;
4. Wenn aus anderen eigenen- oder Veröffentlichungen Dritter zitiert wurde, wurde stets die Quelle hierfür angegeben. Diese Dissertation ist vollständig meine eigene Arbeit, mit der Ausnahme solcher Zitate;
5. Alle wesentlichen Quellen von Unterstützung wurden benannt;
6. Wenn immer ein Teil dieser Dissertation auf der Zusammenarbeit mit anderen basiert, wurde von mir klar gekennzeichnet, was von anderen und was von mir selbst erarbeitet wurde;
7. Teile dieser Arbeit wurden zuvor veröffentlicht und zwar in den Referenzen [1–5].

Ort, Datum	Konstantin Nestmann

List of publications

- V. Reimer, M. R. Wegewijs, **K. Nestmann** and M. Pletyukhov
  "Five approaches to exact open-system dynamics: Complete positivity, divisibility, and time-dependent observables"
  J. Chem. Phys. **151**, 044101 (2019)

- **K. Nestmann**, V. Bruch and M. R. Wegewijs
  "How Quantum Evolution with Memory is Generated in a Time-Local Way"
  Phys. Rev. X **11**, 021041 (2021)

- V. Bruch, **K. Nestmann**, J. Schulenborg and M. R. Wegewijs
  "Fermionic duality: General symmetry of open systems with strong dissipation and memory"
  SciPost Phys. **11**, 53 (2021)

- **K. Nestmann** and M. R. Wegewijs
  "General connection between time-local and time-nonlocal perturbation expansions"
  Phys. Rev. B **104**, 155407 (2021)

- **K. Nestmann** and M. R. Wegewijs
  "Renormalization group for open quantum systems using environment temperature as flow parameter"
  SciPost Phys. **12**, 121 (2022)

Acknowledgments

First and foremost, I am deeply grateful to my supervisor Maarten Wegewijs for his support and guidance. Thank you for encouraging me to follow my (sometimes unconventional) ideas, for being available for hundreds of whiteboard discussions (including those taking place virtually), and for injecting the whole stressful process with humor and ease.

I want to thank my collaborators Valentin Bruch, Viktor Reimer, Mikhail Pletyukhov, Jens Schulenborg and Jan Vanberg – it was a pleasure working with you. I thoroughly enjoyed our lively research discussions.

I would also like to thank Herbert Schoeller for co-refereeing this dissertation and for his inspiring lectures about open quantum systems.

I am grateful to the Research Training Group 1995 for their financial support, which, in addition to funding my own research at RWTH Aachen, afforded me the opportunity to participate in conferences and visit the universities at Lund and Chalmers. Thank you, Martin Leijnse and Janine Splettstoesser for your great hospitality. I very much enjoyed my time with you and your groups.

Thank you to those involved in the organization of the RTG, my colleagues at the RTG, and to all of my office mates at the Institute for Quantum Information, who provided an open and friendly work environment.

I thank my family for supporting me, particularly when things got difficult.

Finally, I would like to thank my soon-to-be-wife, Catherine. Thank you for encouraging me without question, for believing in me without conditions, and for convincing me to write a short email asking about open positions in Aachen.

Short Summary

In this thesis we consider the dynamics of generic open quantum systems described using quantum master equations (QMEs). Motivated by the puzzling fact that there are *two* exact QMEs, the time-nonlocal (Nakajima-Zwanzig) and the time-local (time-convolutionless) QME, our focus is finding the general connection between these two canonical approaches. The result takes the form of an elegant functional fixed-point relation between the time-local generator $\mathcal{G}$ and the time-nonlocal memory kernel $\mathcal{K}$, $\mathcal{G} = \hat{\mathcal{K}}[\mathcal{G}]$. This leads to several new insights into important topics in open system dynamics, including the construction of non-perturbative Markov approximations, their relation to initial slip corrections, and a memory expansion used in studies of driven quantum dynamics and transport. Furthermore, it naturally suggests a novel construction of time-local descriptions from iterations of the fixed-point functional, which we explore in detail for the Jaynes-Cummings model describing atomic decay in a radiation field and the resonant level model describing non-interacting transport to an electron reservoir.

We further leverage this relation to derive the general connection between time-local and time-nonlocal perturbation expansions, a long-standing problem. This allows the technically more advanced time-nonlocal approximation strategies to be translated into a corresponding time-local picture, which is advantageous from the quantum information vantage point. We exemplify this using the Anderson model of an interacting quantum dot coupled to voltage-biased electron reservoirs to show how the well-known diagrammatic expansion of the time-nonlocal memory kernel can be translated into its time-local form term-by-term. Additionally, we apply this technique to investigate a powerful renormalized series, which reveals limitations of the time-local approach.

Finally, based on this series we introduce a time-nonlocal renormalization group to address the interesting low-temperature dynamics of Anderson-like models. This method works by lowering the environment temperature and calculating the higher order coupling effects this generates. One of its key features is that a single renormalization group trajectory contains the full temperature dependence of dynamical and transport quantities. The method can be formulated in real-time, which brings several advantages, in particular for analyzing transient dynamics. Our numerical results are benchmarked against several other advanced methods, such as the functional renormalization group, the density-matrix renormalization group, and the quantum Monte Carlo method.

Kurzzusammenfassung

In dieser Arbeit untersuchen wir die Dynamik generischer offener Quantensysteme mithilfe von Quantenmastergleichungen (QMG). Motiviert durch die überraschende Tatsache, dass es *zwei* exakte QMG gibt, die zeitnichtlokale (Nakajima-Zwanzig) und die zeitlokale (zeitfaltungsfreie) QMG, leiten wir die allgemeine Beziehung zwischend diesen beiden kanonischen Grundgleichungen ab. Als Ergebnis finden wir, dass der zeitlokale Generator $\mathcal{G}$ und der zeitnichtlokale Gedächtniskern $\mathcal{K}$ durch die elegante Fixpunktbeziehung $\mathcal{G} = \hat{\mathcal{K}}[\mathcal{G}]$ miteinander verbunden sind. Dies führt zu mehreren neuen Erkenntnissen über die Dynamik offener Quantensysteme, z.B. über die Konstruktion von nicht-perturbativen Markov Näherungen, deren Beziehung zu initialen Ausrutschkorrekturen und über eine Gedächtnisreihenentwicklung, die in Studien zu getriebener Quantendynamik und -transport genutzt wird. Außerdem legt dies auf natürliche Weise nahe, zeitlokale Beschreibungen der Dynamik durch Iterationen des Fixpunktfunktionals zu konstruieren. Dies untersuchen wir im Detail für das Jaynes-Cummings Modell eines Atoms in einem Strahlungsfeld und das Resonanzniveau Modell, das nichtwechselwirkenden Transport zu elektronischen Reservoiren beschreibt.

Wir nutzen diese Fixpunktbeziehung außerdem, um die allgemeine Verbindung zwischen zeitlokalen und zeitnichtlokalen Störungsreihen abzuleiten, ein seit langem offenes Problem. Dies ermöglicht es technisch fortgeschrittenere zeitnichtlokale Näherungsverfahren in eine korrespondierende zeitlokale Form zu bringen, was vorteilhaft ist für Betrachtungen aus der Quanteninformation. Wir veranschaulichen dies am Beispiel eines wechselwirkenden Anderson-Quantenpunktes gekoppelt an elektronische Reservoire unter einem Spannungs-Bias, indem wir die wohlbekannte diagrammatische Entwicklung des zeitnichtlokalen Gedächtniskerns Term für Term in eine zeitlokale Form übersetzen. Des Weiteren nutzen wir diese Technik, um eine mächtigere renormalisierte Reihe zu analysieren, was Limitationen des zeitlokalen Ansatzes offenbart.

Schließlich führen wir basierend auf dieser renormalisierten Reihe eine zeitnichtlokale Renormierungsgruppe ein, die die interessante Tieftemperaturedynamik von Anderson-Quantenpunkt ähnlichen Modellen beschreibt. Diese Methode berechnet Kopplungseffekte höherer Ornung, die durch ein Verringern der Temperature entstehen. Ein Hauptmerkmal ist, dass einzelne Renormierungsgruppentrajektorien bereits die vollständige Temperaturabhängigkeit von dynamischen Kenngrößen enthalten. Die Methode kann in Echtzeit formuliert werden, was mehrere Vorteile mit sich bringt,

insbesondere für die Analyse von transienter Dynamik. Wir vergleichen unsere numerischen Ergebnisse mit verschiedenen anderen fortgeschrittenen Methoden, wie z.B. der funktionalen Renormierungsgruppe, der Dichtematrix-Renormierungsgruppe und der Quanten-Monte-Carlo-Methode.

Contents

1

Introduction

The field of open quantum systems encompasses many topics, ranging from quantum optics [6–8], quantum transport [9] and chemical physics [10, 11] to more modern areas such as quantum information [12], quantum thermodynamics [13–15] and quantum (non)-Markovianity [16–19]. Each of these topics is significantly impacted by the fact that quantum systems cannot be regarded as perfectly isolated from their environment, but instead require an account of its interaction with the environment responsible for measurable exchange of energy and/or particles. Although the environment's influence is sometimes unwanted in practice, most notably in the construction of quantum computers, it can lead to interesting but very complex many-body effects worth studying in their own right. This is particularly the case when the system-environment coupling is strong.

This thesis focuses on the dynamical equations that describe such physically interesting open systems. Specifically, it addresses a number of essential questions about the interrelation between the fundamental laws governing open systems with applications to basic problems in perturbation theory, transient time-dependent dynamics, but also more advanced renormalization groups.

1.1 | Dynamical equations of a quantum system

Typically, it is not possible to microscopically describe the degrees of freedom of a total system, i.e., of a system and its environment together. This practically forces one to find a simpler, reduced description of the open system alone, even if a (reasonably good) model of the total system is known. As a consequence, quantum states can no longer be mathematically described as wavefunctions $|\psi(t)\rangle$, but instead as density operators $\rho(t)$. Furthermore, these open-system density operators do not evolve unitarily, but

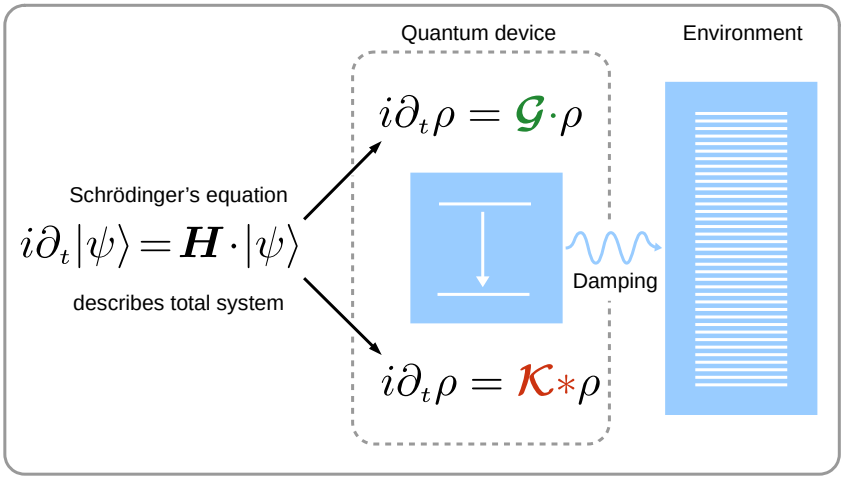

Figure 1.1. Interaction of a quantum system with its environment. When integrating out the environment to find an effective description of the quantum device alone, two fundamental laws emerge: One features a time-nonlocal convolution (denoted by $*$) over a memory kernel $\mathcal{K}$, the other a time-local generator $\mathcal{G}$.

according to so-called completely positive and trace preserving propagators, denoted by Π, which leads to physically richer dynamics in comparison to closed systems. These dynamics can be conveniently described using a quantum master equation (QME). In stark contrast to closed quantum systems which always evolve according to a single fundamental law – the Schrödinger equation – there are *two* exact QMEs: the so-called *time-nonlocal* (Nakajima-Zwanzig) and the *time-local* (time-convolutionless) QME.

The main difference between these two equivalent descriptions lies in their treatment and understanding of *memory*. Although it is clear that memory is a key feature of open systems (as opposed to closed ones), this term has no universal definition. Nevertheless it is central to the physics of open-system dynamics and therefore continues to be discussed and refined. Whereas the time-nonlocal QME is an integro-differential equation which uses a memory kernel $\mathcal{K}$ to make memory explicit from the start, the time-local QME is an ordinary differential equation that keeps memory implicit within a generator $\mathcal{G}$, which is therefore a much more complicated quantity. Thus, for open systems there are surprisingly *two* possible generalizations of the Hamiltonian H, see Fig. 1.1. As a consequence of these two starting points, a plethora of completely different approximation schemes have been developed to address various questions of interest in the field of open systems. While this has led to a variety of insights and progress, the communities have remained disconnected, focusing exclusively on one or the other QME. One reason for this – perhaps the most important – is the lack of a simple, explicit connection between these two fundamental equations of motion of open systems.

1.2 | Equivalent equations, different physical insights

The first part of this thesis addresses and, in fact, solves this outstanding issue by deriving the general connection between these two canonical approaches [Chap. 3]. This connection is then applied to derive "translation rules" for series expansions between the memory kernel $\mathcal{K}$ and the generator $\mathcal{G}$ used in numerous applications [Chap. 4], which addresses the non-trivial question of which expansion type ($\mathcal{K}$ or $\mathcal{G}$) is "better". One of the main motivations for this arose from a detailed study at the beginning of this project reported in Ref. [1], in which both approaches were worked out explicitly for a solvable yet sufficiently rich model. Parts of that study are used in Sec. 3.5. The physical models and particularly challenging phenomena we use to illustrate the differences between descriptions based on $\mathcal{K}$ or $\mathcal{G}$ are introduced in Sec. 1.4.

Of course, one might wonder why it is relevant to be able to convert between two equivalent QMEs, if one can just solve the equation one has in hand for $\rho(t)$ instead? Careful consideration of this question supports a complementary view [20–22]. Typically the memory kernel $\mathcal{K}$ is easier to compute and advanced methods have been developed to obtain it analytically [23, 24] and numerically [25, 26] with successful applications to nontrivial models [27–30] covering transient and stationary dynamics, as well as counting statistics [31–33] of observables. By contrast, the direct computation of the generator $\mathcal{G}$ using the time-convolutionless formalism [34–39] is typically more challenging.

However, some schemes that aim to solve the time-nonlocal equation ($\mathcal{K}$) approximately, while accounting for the frequency dependence (retardation) of the memory kernel, *actually* construct a corresponding time-local equation first ($\mathcal{G}$), which is subsequently solved to obtain the propagator [31, 40–42]. This may lead one to believe that "memory" is accounted for using an effective time-local equation, which can lead to much confusion if a clear view on time-local and non-local descriptions is missing.

Another physically more interesting point is that the generator $\mathcal{G}$ is *by itself* of particular interest – it allows for the inference of important properties of the propagator Π, the solution of the dynamics, which remarkably are very difficult to see otherwise, even with the propagator Π already "in hand" [1]. For example, the physical legitimacy of the propagator can in many situations be explicitly inferred [18, 43, 44] from a time-dependent canonical form of its generator $\mathcal{G}$ [45]. This is important for the phenomenological construction of QMEs [20, 21] and of microscopic models that obey prescribed QMEs [46]. Working with $\mathcal{K}$, it is considerably less clear how to construct phenomenological QMEs whose solutions make any physical sense at all (irrespective whether they accurately describe the targeted behaviour). Related to this is that $\mathcal{G}$ often has a clear operational meaning in terms of quantum jumps, which makes it advanta-

geous for stochastic simulations. For the same reason, time-local QMEs are the method of choice for constructing noise models in quantum-information science and technology. Despite continued efforts, this is much more complicated to achieve when using $\mathcal{K}$. Even though completely positive approximations [see Sec. 2.1] can in principle be computed by reorganizing the microscopic coupling expansion, this comes at the cost of violating trace preservation [47]. Beyond that, guarantees about the physicality of $\mathcal{K}$ can only be made for special parametrizations of $\mathcal{K}$, such as legitimate-pair decompositions [48, 49], semi-Markov [50, 51] or collision-models [52].

A further key property that can be directly inferred from $\mathcal{G}$, but which seems prohibitively difficult to discuss when using $\mathcal{K}$ [53], is the so-called divisibility of the evolution Π. This plays a prominent role in the field of quantum Markovianity [Sec. 2.2.2], in which one aims to define "memory" precisely, which, as we already noted, is a key physical concept of quantum dynamics. Divisibility also features in applied tasks such as quantum coding [54, 55] and tomography [56], key distribution [57], teleportation [58], and work extraction by erasure [59]. It should be noted that retardation (or frequency dependence) is often uncritically identified with "Markovianity" when working with time-nonlocal QMEs [41, 42]. Although this identification is tempting, we will see that it is misleading: memoryless dynamics can correspond to time-dependent memory kernels [Sec. 2.2.2] and consistent Markov approximations may involve finite frequency contributions [Sec. 3.2]. Finally, the time-local nature of $\mathcal{G}$ is crucial to access geometric [60–62] and possible topological [63, 64] phases in open-systems. This is a very active field with many unanswered questions and applications to pumping, full-counting statistics [65], fluctuation relations [66] and quantum thermodynamics [13]. Also here descriptions based on $\mathcal{K}$ spoil the standard assumption of time-locality made in geometric analysis of dynamical equations. Thus, there are many reasons for *explicitly* understanding the general relation between $\mathcal{K}$ and $\mathcal{G}$.

1.3 | Renormalization groups for open systems

At low temperatures interactions can have a significant and often surprising impact on the dynamics of quantum systems. This necessitates the application of methods more advanced than perturbation theory, such as renormalization group (RG) methods. Even though we will be considering open systems later on, we will first focus on discussing the RG concept for closed systems because already here the key ideas can be understood.

Historically, the development of RG techniques was in a sense motivated by measurements of the electrical resistance of a metal. Simply put, electrical resistance is

caused by electron-phonon scattering ($\propto T^5$), electron-electron scattering ($\propto T^2$) and electron-impurity scattering (T independent). Thus, for a long time it was believed that the resistance should saturate at some finite value as $T \to 0$. In the 1930s, however, it was found by measuring gold at temperatures $T < 10$K that it is also possible for the resistance to rise again if the temperature is lowered sufficiently, thus giving a *finite temperature* minimum [67]. It took some 30 years until J. Kondo found that magnetic impurities were responsible for this effect [68]. He used perturbation theory to show that, under an antiferromagnetic electron-impurity interaction, spin-flip scattering events lead to a logarithmic increase of the resistance. As a consequence all electrons become correlated and have to be described by a complicated many-body wavefunction. Interestingly, the Kondo effect, as it is now called, was also observed later in quantum dots [69], a prime example of an open quantum system, which allow for the systematic control and study of the interplay with non-equilibrium phenomena by applying a temperature or bias-voltage. We consider such quantum dot systems in Chap. 4 and 5.

Even though Kondo's insight marked a breakthrough, the unphysical logarithmic divergences produced by perturbation theory were a severe theoretical problem. This was only conclusively solved by K. Wilson in 1975 through the development of the renormalization group technique [70], building on ideas of Kadanoff [71, 72] and Anderson [73]. As formulated by Wilson, the failure of simple perturbative descriptions is generic whenever systems lack a characteristic scale. For example, in a magnet at the critical point the magnetization fluctuates with all wavelengths (missing length scale) and in quantum electrodynamics high energy scattering leads to intermediate states containing momenta of arbitrary magnitude (missing energy scale).

To describe these systems, Wilson's RG approach is, roughly speaking, to first replace the original Hamiltonian H describing the physical problem with a simpler effective Hamiltonian H_N with typical energy scale Λ^{-N} such that $H = \lim_{N\to\infty} H_N$. For example, in Wilson's work on the Kondo problem, the parameter N was the number of logarithmic intervals in which the conduction band is discretized. In the second step, one relates Hamiltonians on these successive energy scales and their ground states with each other through a map $\mathcal{F}$ called the RG transformation, $H_{N+1} = \mathcal{F}[H_N]$. One of Wilson's key insights was that, in the above-mentioned problems, energy scales are locally coupled and therefore each step $H_N \to H_{N+1}$ only represents a small perturbation which can be computed systematically. Therefore an accurate solution can be obtained by iterating $\mathcal{F}$ until an RG fixed point is reached[1].

There are several obstacles in applying the above described RG ideas to open quan-

[1] These RG fixed points are a priori not connected to the fixed points discussed in Chap. 3.

tum systems: of interest are not only *non-equilibrium* stationary states, but also the transient *dynamics* towards these stationary states. Since Wilson's work, much progress has been made. Wilson's original numerical renormalization group was extended to time-dependent [74] and non-equilibrium states [75, 76]. Additionally other prominent RG approaches applicable to non-equilibrium open systems were developed such as the density matrix renormalization group (closely tied to quantum information) [77, 78], the functional renormalization group (originating in field theory) [79, 80], quantum Monte Carlo methods [81] or path integral approaches [82], to name a few.

One may wonder how to implement RG techniques in the context of QMEs, considering our discussion of the two fundamental dynamical equations of open systems. Within the time-local approach, we know of no RG scheme that *directly* computes the generator $\mathcal{G}$. In Chap. 4 we shed some light on the complications that arise when one tries to use $\mathcal{G}$ by translating advanced approximation schemes known for $\mathcal{K}$. Not surprisingly, the problems relate to the issue of memory considered here as retardation. However, the connection between $\mathcal{K}$ and $\mathcal{G}$ which we derive in Chap. 3 suggests an indirect path to do RG for $\mathcal{K}$ first, and then transform the result to $\mathcal{G}$.

The construction of (semi-)analytical RG methods for open quantum systems is indeed possible within the time-nonlocal approach using $\mathcal{K}$, for example, the real-time renormalization group (RTRG) method is by now well-established. In its original formulation [83, 84] a real-time cutoff t_c was included into the memory kernel, $\mathcal{K} \to \mathcal{K}_{t_c}$, which effectively cut off the memory such that $\lim_{t_c\to\infty} \mathcal{K}_{t_c} = \mathcal{K}$. For technical reasons the RTRG was later reformulated in frequency space [23, 85]. In its most recent formulation, called the E-flow scheme[2], the RTRG has been successfully applied to a range of models, such as the non-equilibrium Kondo model [27, 86–89], the interacting resonant level model [90, 91] or the spin boson model [29, 92] allowing detailed analytical or numerical calculations in experimentally relevant regimes.

We follow this line of development in the last part of this thesis [Chap. 5] and introduce a new method for the computation of the memory kernel by analyzing its *temperature dependence*. At its core lies the observation that temperature sets the inverse correlation time of the reservoirs in line with common intuition about memory as retardation, and is therefore connected to the memory contained in $\mathcal{K}$ – whereas at high temperatures the correlations are short ranged (no memory), they decay very slowly (power-law like) at small temperatures. This closely connects to a dynamical version of Wilson's observation about the lack of a scale. Although this is well known, the conceptually obvious route to access low-temperature, many-body physics by literally lowering the temperature has

[2] In the E-flow reference [27] E denotes the Laplace variable, which we instead call ω in this thesis.

not been previously explored. We introduce a RG scheme dubbed the T-flow which systematically calculates the generated higher-order coupling effects when lowering the temperature in a renormalization group flow. This provides a new way of computing the memory kernel in real time, naturally describing transient dynamics. Importantly a *single* RG trajectory describes the physics at *all* traversed finite temperatures, which saves numerical effort and is physically interesting since correlation effects often express themselves in a pronounced T-dependence. Although not explored, this new approach is naturally of interest in the active field of quantum thermoelectric studies with many applications.

1.4 | Analyzed models and their applications

As the above introduction outlined, the thesis focuses on several quite general open problems surrounding quantum dynamical equations. In illustrating and exploring these topics we make use of a number of models which are well known from applications to quantum transport and quantum optics. It is tempting to say the same about the solutions of these models, but on several occasions we illustrate that this is not the case, even if the solutions can be written down analytically.

Here we briefly introduce the models discussed in this thesis. The general connection between $\mathcal{K}$ and $\mathcal{G}$ derived in Chap. 3 is illustrated for two exactly solvable models: the dissipative Jaynes-Cummings model [Sec. 3.4] and the fermionic finite temperature resonant level model [Sec. 3.5]. The Jaynes-Cummings model provides one of the most basic descriptions of atomic decay. Despite its algebraic simplicity it features a well-characterized non-Markovian regime where the generator $\mathcal{G}$ has isolated time-singularities, which represent one of the most challenging aspects of the time-local framework and has been contemplated in many works [93–97].

The resonant level model describes quantum transport while ignoring interaction and complements the Jaynes-Cummings model – even though the generator is singularity-free, the algebraic structure is more complicated due to the statistical mixing caused by temperature. Despite the solution having been known for a long time, physically interesting results, for example regarding its non-Markovianity, went unnoticed. Furthermore, we recently noted that this simple model exhibits non-intuitive reentrant behavior in time, where the level does not simply decay into a lower-lying Fermi-sea as naively expected, but significantly fills up more before eventually decaying [1].

The general connection between time-local and time-nonlocal series expansions as discussed in Chap. 4 and the renormalization group study presented in Chap. 5 are

illustrated at the example of an Anderson quantum dot [Sec. 4.3 and 5.4 respectively], which properly describes transport in the presence of interaction. This model was originally proposed to investigate the conditions under which localized magnetic moments form in bulk metals with magnetic impurities, but also accurately captures the physics of quantum dots. Quantum dots are the workhorses of nanoscale electronics with a variety of practical applications such lasers [98], solar cells [99] or displays [100] and are also at the heart of proposed solid-state quantum computers [101]. The Kondo model briefly discussed in Sec. 1.3 describes the low-energy sector of the Anderson model at the particle-hole symmetric point [102].

When analyzing transient effects in the Anderson model in Chap. 5, we show that the above-mentioned reentrant behaviour, that we first described for the non-interacting resonant level model, survives both strong interaction and finite bias transport. This transient effect seems to be generic and was overlooked so far making its experimental investigation seem of interest. Moreover, we find that the short-time behaviour of observables is temperature independent causing a collapse of the short-time data onto a single T-independent curve. This observable effect reflects the key idea that the memory time of the environment, governed by its temperature, is a natural quantity on which an RG treatment of open system dynamics can be based.

2

Theoretical background

This chapter provides the theoretical background and notation used throughout this thesis. We first discuss the two canonical time-evolution equations introduced in the previous chapter, the time-local and time-nonlocal QME. The following analysis of these equations requires that we consider which type of superoperators are allowed as solutions of these QMEs, in other words, the allowed mathematical form that a physical evolution must take. With this in hand we will have a closer look at the subtle issue of quantum Markovianity – a notion distinct from microscopic retardation. This is important since the different viewpoints on what constitutes "memory" will play a role later on. In particular, one of the standard simplifying strategies of approximating open-system quantum evolutions is to enforce a simple type of quantum Markovianity onto the dynamics (semigroup) by altering the QME. In the final section we discuss two basic approximation strategies going beyond such crude approximations, which will be important in later chapters.

2.1 | Propagators, master equations and physicality

In this thesis we consider a system S in the presence of an environment (also called reservoir) R and assume throughout that at some initial time t_0 the total state is given by a product state $\rho_{\text{tot}}(t_0) = \rho_0 \otimes \rho_R$. Typically statistics of local measurements performed on the system, contained within the density operator $\rho(t) \coloneqq \text{Tr}_R\, \rho_{\text{tot}}(t)$, are of interest, but later on we will also consider non-local observables, such as particle currents. The dynamics of the densiy operator can be computed using the propagator $\Pi(t, t_0)$,

$$\rho(t) = \Pi(t, t_0)\rho_0 \coloneqq \text{Tr}_R \left\{ U_{\text{tot}}(t, t_0)\, (\rho_0 \otimes \rho_R)\, U_{\text{tot}}^\dagger(t, t_0) \right\}. \tag{2.1}$$

This is the open-system analog to the time evolution operator $U_{\text{tot}}(t, t_0)$ for closed systems. The propagator $\Pi(t, t_0)$ maps arbitrary initial system states ρ_0 for a given initial reservoir state ρ_R.

A basic question to ask is which superoperators can represent physically meaningful propagators, i.e., what is the open-system-analog to the unitarity requirement of $U_{\text{tot}}(t, t_0)$? Clearly it is necessary that Π is trace- (TP) and positivity preserving (PP). However, these conditions are not sufficient to guarantee physicality because they don't take *entanglement* into account: It is possible that the system S is initially correlated with additional external degrees of freedom (labeled P), which neither evolve in time nor interact with system and environment for $t \geq t_0$. Therefore, the actual initial state is given by ρ_{SP} with marginal $\rho_0 = \text{Tr}_P \rho_{SP}$ and propagation is achieved via

$$\rho(t) = \text{Tr}_P \left\{ \Pi(t, t_0) \otimes \mathcal{I}_P \rho_{SP} \right\}. \tag{2.2}$$

If S and P are not entangled, then by the separability of ρ_{SP} the positivity of the evolving state is ensured if Π is PP. However, if S and P are entangled this is not the case and one must *demand* that $\Pi(t, t_0) \otimes \mathcal{I}_P$ is PP. Importantly this should hold for arbitrary dimensions of P, which is precisely the definition of complete positivity (CP). Thus CP is closely tied to the evolution of entanglement. Using the so-called Choi isomorphism [47, 103, 104] it is in fact easier to check whether a given propagator Π is CP than the weaker and irrelevant PP property.

It might be at first surprising that the presence of a "blind and dead" witness [105] P can enforce a requirement as strong as CP onto the dynamics. However, for initial product states as we consider them, CP can be shown to follow from Eq. (2.1) [106]. We note that in the case of initial system-environment correlations the possibility of defining a CP propagator, mapping initial marginal states of S to their later values $\rho(t)$, has been controversially debated [105, 107, 108]. This was recently clarified by tracing back the confusion to the issue of independently varying marginals of initially correlated states, see Ref. [109] for a detailed exposition.

2.1.1 | Time-nonlocal master equation – Microscopic retardation

In investigating general properties of the propagator or when performing practical computations it is typically advantageous to analyze the propagator's equation of motion. As was shown by Nakajima and Zwanzig [110, 111] using the projection-superoperator technique, the propagator satisfies the time-nonlocal QME

$$\dot{\Pi}(t, t_0) = -i \int_{t_0}^{t} ds \mathcal{K}(t, s) \Pi(s, t_0), \tag{2.3}$$

which can alternatively also be derived from diagrammatic arguments [23]. Typically the memory kernel $\mathcal{K}(t,s)$ contains a time-local contribution $\mathcal{K}_L(t)$ besides an inherently time-nonlocal part $\mathcal{K}_N(t,s)$:

$$\mathcal{K}(t,s) = \mathcal{K}_L(t)\bar{\delta}(t-s) + \mathcal{K}_N(t,s). \tag{2.4}$$

Here we use a $\bar{\delta}(t)$ distribution defined such that $\int_0^t \bar{\delta}(t-s)f(s) = f(t)$.

The above equations simplify for time-translation invariant systems, where the total Hamiltonian H_{tot} is constant and $U_{\text{tot}}(t-t_0)$ is a function of the time difference only. It then follows that $\Pi(t-t_0)$ and $\mathcal{K}(t-s)$ also become functions of a single time argument and $\mathcal{K}_L$ is time-constant. In this case (2.3) can be formally solved in frequency space: defining the Laplace transform of the memory kernel

$$\hat{\mathcal{K}}(\omega) := \lim_{t_0\to-\infty}\int_{t_0}^{t} ds\mathcal{K}(t-s)e^{i\omega(t-s)} = \int_0^\infty ds\mathcal{K}(s)e^{i\omega s} \tag{2.5}$$

and analogously for $\hat{\Pi}(\omega)$, one obtains the "Green's function" or resolvent for the density operator

$$\hat{\Pi}(\omega) = \frac{i}{\omega - \hat{\mathcal{K}}(\omega)}. \tag{2.6}$$

At first (2.5) is only defined for $\operatorname{Im}\omega > 0$, because only here the integral formally converges and $\hat{\Pi}$ is an analytic function of ω. However, via analytic continuation one can also extend the definition into the lower half of the complex plane, where interesting features such as poles and branch cuts emerge, which correspond to exponential and power law time-dependence of the dynamics.

From (2.6) it follows that *fixed-point frequencies* of $\hat{\mathcal{K}}$, i.e., frequencies ω_p satisfying

$$\hat{\mathcal{K}}(\omega_p)|\omega_p) = \omega_p|\omega_p) \tag{2.7}$$

for some eigenoperator[1] $|\omega_p)$, are the poles of $\hat{\Pi}$. Transforming back to time-space via integration along a clockwise oriented contour $\mathcal{C}$ closed in the lower half of the complex plane, we obtain the general time-nonlocal structure of the time-evolution:

$$\Pi(t-t_0) = \frac{1}{2\pi}\int_{\mathcal{C}} d\omega\hat{\Pi}(\omega)e^{-i\omega(t-t_0)} \tag{2.8a}$$

$$= \sum_{\omega_p}\operatorname*{Res}_{\omega=\omega_p}\left[\frac{e^{-i\omega(t-t_0)}}{\omega-\hat{\mathcal{K}}(\omega)}\right] + \frac{i}{2\pi}\int_{\text{b.c.}} d\omega\frac{e^{-i\omega(t-t_0)}}{\omega-\hat{\mathcal{K}}(\omega)}. \tag{2.8b}$$

[1]When interpreting operators $\hat{A}$ as supervectors we use the notation $|A) \equiv \hat{A}$. The Hilbert-Schmidt scalar product between two supervectors $|A)$ and $|B)$ is denoted by $(A|B) := \operatorname{Tr}\{A^\dagger B\}$. This also motivates the definition of dual maps $(A|\bullet := \operatorname{Tr}\{A^\dagger\bullet\}$.

Here the sum goes over all poles of $\hat{\Pi}(\omega)$ and "b.c." indicates integration over possible branch cut contributions. In the simplest case, where $\hat{\mathcal{K}}$ itself is analytic and thus branch cuts are absent, we can see that Π is given by a (possibly infinite) sum of pure exponentials with time-constant superoperator-valued prefactors. Taking branch cuts into account, which typically arise at zero temperature, these prefactors become time-dependent. One should note that this is not an "exotic" feature, but already appears in the simplest possible model of transient transport through a resonant level [Sec. 3.5]. This general picture forms the starting point for advanced approximation strategies such as the real-time renormalization group (RTRG) [23] and the related E-flow scheme, see Refs. [24, 27, 29, 30, 89, 92] for details and applications.

2.1.2 | Time-local master equation – Just a mathematical trick?

The time-convolution in the time-nonlocal QME (2.3) is for some considerations undesirable [1]. Therefore one idea is to transform (2.3) into an equivalent convolutionless form. This can always be achieved [112, 113]: formally defining the generator $\mathcal{G}(t,t_0) := i\dot{\Pi}(t,t_0)\Pi^{-1}(t,t_0)$, the time-local QME

$$\dot{\Pi}(t,t_0) = -i\mathcal{G}(t,t_0)\Pi(t,t_0) \tag{2.9}$$

holds *by construction*. We see that $\mathcal{G}(t,t_0)$ generates $\Pi(t,t_0)$ in the same way as $H_{\text{tot}}(t)$ generates $U_{\text{tot}}(t,t_0)$, with the important difference that $\mathcal{G}(t,t_0)$ is not hermitian and also depends on the initial time t_0 due to the presence of the environment. The formal solution can thus be expressed as

$$\Pi(t,t_0) = \mathcal{T}_{\leftarrow}\, e^{-i\int_{t_0}^{t} d\tau \mathcal{G}(\tau,t_0)}, \tag{2.10}$$

where $\mathcal{T}_{\leftarrow}$ denotes the time-ordering operator. For time-translation invariant systems only the time difference $t-t_0$ is relevant and $\mathcal{G}(t,t_0) = \mathcal{G}(t-t_0)$. In this case the generator typically converges at long times to a stationary value

$$\mathcal{G}(\infty) = \lim_{t_0\to-\infty} \mathcal{G}(t-t_0), \tag{2.11}$$

but we will also see very simple physical examples where this limit does not exist, even though the propagator $\Pi(t)$ converges to a well-defined stationary state $\Pi(\infty)$.

It is evident from the definition of the generator that it will contain singularities at any time t_* where $\Pi(t_*,t_0)$ is not invertible. Although this was noted a long ago [93], it has recently received renewed attention [94–97]. Importantly, these singularities are not spurious, noting that the product $\mathcal{G}(t,t_0)\Pi(t,t_0)$ always remains finite, even at $t\to t_*$.

In fact they are physically meaningful: by identifying the divergent matrix elements of $\mathcal{G}(t_*, t_0)$ one can already infer that certain parts of $\Pi(t_*, t_0)$ must vanish, which restricts the physically allowed subspace through which *every* evolving density operator has to pass at $t = t_*$. This subspace restriction can be so severe that $\Pi(t_*, t_0)$ becomes an entanglement breaking map [114–117], which we encounter in the model considered in Sec. 3.4.

For many applications it is advantageous to decompose $\mathcal{G}$ into the so-called (time-dependent) Gorini-Kossakowski-Sudarshan-Lindblad (GKSL) [118, 119] form,

$$-i\mathcal{G}(t,t_0)\bullet = -i[H(t,t_0),\bullet] + \sum_k j_k(t,t_0)\left(J_k(t,t_0)\bullet J_k^\dagger(t,t_0) - \tfrac{1}{2}\left\{J_k^\dagger(t,t_0)J_k(t,t_0),\bullet\right\}\right), \tag{2.12}$$

where $\bullet$ denotes some operator argument, H is an hermitian operator, j_k are the real-valued jump rates, and the jump operators J_k are traceless and orthonormal, $(J_k|J_{k'}) = \delta_{kk'}$. Importantly the form (2.12) guarantees that trace and hermicity are preserved during the evolution, but it is an open problem which constraints on the time-dependent jump rates and operators are necessary and sufficient to ensure complete positivity of the solution $\Pi(t, t_0)$. Of course the exact generator always ensures CP of the dynamics, but this is not necessarily the case if approximations or phenomenological ad-hoc constructions are made. However, in the special case where $j_k(t, t_0) \geq 0$, which will be important in the next section, it is established that CP is guaranteed [120]. This makes the GKSL jump operator representation (2.12) important for direct phenomenological modeling of experiments. The guaranteed physicality is also exploited in stochastic simulations [121].

2.2 | Quantum Markovianity

One of the central themes in the analysis of open quantum systems is the understanding of *memory effects* – roughly speaking, whether there is a backaction of the environment onto the system or not. Even though the distinction between Markovian (no backaction) and non-Markovian systems is rather fundamental, its discussion is typically not straightforward because different well-motivated definitions are used depending on the interests of involved communities [16, 18, 122]. A related question is how and under what conditions memory effects can be neglected within Markov approximations, and how systematic improvements beyond them can be made.

2.2.1 | Semigroup Markovianity

At the heart of the problem of how to clearly define "quantum Markovian" is that the classical definition of a stochastic Markov process can not be easily generalized into the quantum realm [18, 50]: A classical stochastic process $X(t)$ is called Markovian if the conditional probabilites satisfy

$$p\Big(X(t) = x\Big|X(t_n) = x_n, \ldots, X(t_1) = x_1\Big) \;=\; p\Big(X(t) = x\Big|X(t_n) = x_n\Big) \tag{2.13}$$

for all $t > t_n > \cdots > t_1$. Roughly speaking, this means that even though the observable was measured n times, in order to make predictions we only need the latest measurement at time t_n. All other measurements at earlier times $t_1, \ldots, t_{n-1}$ can be discarded and, therefore in this sense, there is clearly no memory. In the quantum case, however, every measurement would disturb the system and therefore $p\big(X(t) = x\big|X(t_n) = x_n, \ldots, X(t_1) = x_1\big)$ would not only depend on the dynamics, but also on the choice of measurement process.

One way to proceed is to focus on the classical one-point probabilities $p(X(t) = x)$ instead [18]. These are "propagated" via stochastic transition matrices $T(x, t|x_0, t_0)$ such that $p(X(t) = x) = \sum_{x_0} T(x, t|x_0, t_0)p(X(t_0) = x_0)$. For the special case of a classical Markov process these transition matrices satisfy

$$T(x, t|x_0, t_0) = \sum_{x_1} T(x, t|x_1, s)T(x_1, s|x_0, t_0) \quad \text{for all} \quad t \geq s \geq t_0. \tag{2.14}$$

In the most straightforward generalization to the quantum case one can say that if

$$\Pi(t - t_0) = \Pi(t - s)\Pi(s - t_0) \quad \text{for all} \quad t \geq s \geq t_0 \tag{2.15}$$

then the dynamics is called *semigroup Markovian*. The functional relation (2.15) is uniquely solved by exponentials with some time-independent generator $\tilde{\mathcal{G}}$:

$$\Pi(t - t_0) = e^{-i(t-t_0)\tilde{\mathcal{G}}}. \tag{2.16}$$

It is well known that (2.16) is physical (CPTP) if and only if the generator $\tilde{\mathcal{G}}$ has the GKSL form (2.12) with time-constant jump operators J_k and Hamiltonian H and time-constant non-negative jump rates $j_k \geq 0$ [118, 119]. This is called a semigroup because one can associatively compose propagators of the form (2.16) via multiplication, but by taking the inverse we leave the set of physical propagators (even though the inverse mathematically exists, it is known never to be CP unless Π is unitary).

Clearly, the exact propagator of an open quantum system, either expressed using the memory kernel [Eq. (2.8)] or the time-local generator [Eq. (2.10)], is not typically

of the semigroup form (2.16). It might, however, be well approximated by a simple exponential $e^{-i(t-t_0)\tilde{\mathcal{G}}}$ in certain time intervals. Therefore it is an important issue how a suitable $\tilde{\mathcal{G}}$ can be constructed. Within the time-local approach one argues that non-Markovian behaviour typically occurs at short times, because $\mathcal{G}(t-t_0)$ is converging quickly towards its stationary value $\mathcal{G}(\infty)$. Hence the idea of the Markov approximation is to replace $\mathcal{G}(t-t_0) \to \mathcal{G}(\infty)$ from the start:

$$\dot{\rho}(t) \approx -i\mathcal{G}(\infty)\rho(t). \tag{2.17}$$

In the time-nonlocal approach one typically identifies Markovianity with a fast decay of the memory kernel $\mathcal{K}(t)$. In this case extending the lower integration bound in (2.3) to $t_0 \to -\infty$ gives a negligible error. Additionally one replaces $\rho(s) \to \rho(t)$ under the integral, arguing that $\mathcal{K}(t-s) \approx 0$ if $t-s$ exceeds some short "memory time" set by $\mathcal{K}$:

$$\dot{\rho}(t) \approx -i\int_{-\infty}^{t} ds\mathcal{K}(t-s)\rho(t) \tag{2.18a}$$

$$= -i\hat{\mathcal{K}}(0)\rho(t). \tag{2.18b}$$

Thus in this approach the *zero-frequency* memory kernel $\hat{\mathcal{K}}(0)$ is taken as the semigroup generator. From this point of view it is often argued that any approximation involving finite frequencies must account for "non-Markovian" behaviour [31, 41, 42, 123, 124].

Based on the typical language used, which talks about performing "the" Markov approximation as if this was a unique procedure, one may get the impression that the two canonical semigroup generators $\mathcal{G}(\infty)$ and $\hat{\mathcal{K}}(0)$ should obviously coincide. Indeed, both objects are physically well-motivated and seem to encode similar ideas just in a different formulation. We will get back to this question and the relation between "memory", either understood as a Markovian semigroup or as retardation/frequency dependence of the memory kernel, in Sec. 3.2.1.

2.2.2 | Markovianity as divisibility

The issue of Markovianity, however, is even more complex. Even though the semigroup dynamics (2.16) introduced long ago certainly represent the strongest form of Markovianity, it was only recently argued that this constraint is perhaps *too strong* – many evolutions that are not semigroups seem to "behave Markovian" anyway [16–18, 43–45]. One extension of the concept of semigroup Markovianity focuses on *divisibility*, a view which we will adopt in this thesis. From here on we say that $\Pi(t,t_0)$ is *quantum Markovian* if and only if there exists a physically legitimate (CPTP) divisor $\Pi(t,s|t_0)$ such that

$$\Pi(t,t_0) = \Pi(t,s|t_0)\Pi(s,t_0) \quad \text{for all} \quad t \geq s \geq t_0. \tag{2.19}$$

This condition is referred to as CP divisibility and also reduces to (2.14) in the classical case [18]. The divisor maps states $\rho(s) = \Pi(s, t_0)\rho_0$ from intermediate times s to later times $t > s$, $\rho(t) = \Pi(t, s|t_0)\rho(s)$. Importantly, the divisor can always be defined as

$$\Pi(t, s|t_0) \coloneqq \Pi(t, t_0)\Pi^{-1}(s, t_0), \tag{2.20}$$

but it is not always CP (since Π^{-1} is not).

From the somewhat abstract definition of quantum Markovianity as divisibility it is not immediately clear in which sense the dynamics is memoryless. This however becomes clear in the following ways:

- Due to Stinespring's theorem [125] a CP divisor can be considered to arise from a unitary U'_{tot} applied to the product state[2] $\bullet \otimes \rho_{R'}$,

$$\Pi(t, s|t_0)\bullet = \text{Tr}_{R'}\left\{U'_{\text{tot}}(t, s|t_0)\bullet \otimes \rho_{R'} {U'_{\text{tot}}}^{\dagger}(t, s|t_0)\right\}, \tag{2.21}$$

  where $U'_{\text{tot}}(t, s|t_0)$ and $\rho_{R'}$ are in general different from $U_{\text{tot}}(t, t_0)$ and ρ_R in Eq. (2.1). This means that even though during the evolution correlations are building between system and environment, at *any* time s one can effectively "interrupt" the dynamics discarding all the correlations, and then restart from the product state $\rho(s) \otimes \rho_{R'}$ using the divisor evolution producing the state $\rho(t)$ at time t as if nothing happened. According to this precise operational specification, correlations caused by past system-environment interactions can be "forgotten" and the evolution is "memoryless". Differently put, it is possible to simulate the dynamics as if there were no time correlations at all.

- There is an instructive equivalent perspective from the quite different vantage point of quantum estimation. Assume that with probability p the system S was prepared in a state $\rho_0^{(1)}$, and with probability $1 - p$ in the state $\rho_0^{(2)}$. We take into account that mixed states of $\mathcal{S}$ can always be prepared using an entangled system P of the same size, which is not evolving by itself, such that $\rho_0^{(i)} = \text{Tr}_P \rho_{SP}^{(i)}$. Thus SP is described by $\rho_{SP}^{(i)}(t) \coloneqq \Pi(t, t_0) \otimes \mathcal{I}_P \rho_{SP}^{(i)}$. At time t we perform a measurement to find out which initial state on SP was prepared (this is called a one-shot, two-state discrimination problem). One can show [18] that using the best possible measurement the probability to successfully determine the state is given by $(1 + \|\Delta(t)\|_1)/2$, where

$$\Delta(t) = p\rho_{SP}^{(1)}(t) - (1 - p)\rho_{SP}^{(2)}(t) \tag{2.22}$$

[2] Stinespring's theorem allows to chose a pure state $\rho_{R'}$. Since all pure states on R' are related to each other by unitaries, we can actually chose an arbitrary pure $\rho_{R'}$ independent of s and t_0 and redefine $U'_{\text{tot}}(t, s|t_0)$ accordingly.

denotes the Helstrom matrix [126] and $\|A\|_1 := \mathrm{Tr}\sqrt{A^\dagger A}$ the trace norm. Here $\|\Delta(t)\|_1$ gives the probability bias towards one of the states, and is thus a measure of the information in SP understood as distinguishability. If $\|\Delta(t)\|_1$ decreases as a function of time, we interpret this as information flowing from the system SP into the environment, since we loose the ability to distinguish in SP. If $\|\Delta(t)\|_1$ instead increases then information must be flowing from the environment back into the system SP. This is another well-defined memory effect and motivates calling the dynamics non-Markovian. The precise equivalence to the notion of divisibility was worked out in Refs. [95, 127], where it was shown that $\|\Delta(t)\|_1$ decreases monotonically for arbitrary pairs of initial states $\rho_{SP}^{1,2}$ if and only if the dynamics is CP divisible[3].

Whether an evolution is CP divisible or not turns out to be straightforwardly encoded into the generator: the divisor is CPTP, and thus the evolution is quantum Markovian, if and only if all time-dependent GKSL jump rates in Eq. (2.12) are non-negative, $j_k(t, t_0) \geq 0$ for all t [43]. Despite this important advance of understanding the properties of quantum evolutions, it is still not known what conditions on the more accessible *memory kernel* are equivalent to CP divisibility. This provides another key motivation for investigating the connection between the memory kernel and the generator.

2.3 | Beyond semigroup Markov approximations

Even though GKSL semigroups (2.16) are often used in phenomenological constructions because of their mathematical simplicity and guaranteed physicality, we will see explicitly in the models considered in Sec. 3.4–3.5 that they only arise in rather extreme limits when deriving dynamics microscopically. In this case one can typically not find exact solutions for the more complex models of interest and is therefore forced to rely on approximations. Here we want to introduce the ideas of some commonly used approximation strategies for going beyond semigroups which are explored in this thesis.

2.3.1 | Initial slip corrections

A very simple procedure aiming to improve semigroup Markov approximations is the so-called slippage of the initial condition [128–131], in which one tries to find a semigroup

[3] In Ref. [127] the technical assumption of invertible propagators Π for all times t was needed. In Ref. [95] the discussion was extended to the mathematically more involved case of non-invertible propagators.

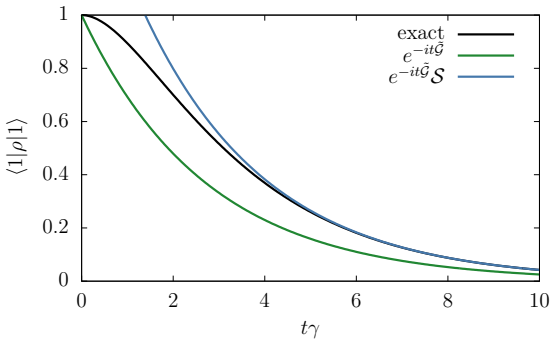

FIGURE 2.1. Comparison between the exact decay if the occupation $\langle 1|\rho(t)|1\rangle$ (black) and a semigroup approximation with (blue) and without (green) initial slip correction in the Jaynes-Cummings model (see Sec. 3.4) with $\Gamma = 0.3\gamma$.

generator $\tilde{\mathcal{G}}$ and an initial slip superoperator $\mathcal{S}$, which need not be a CP map, such that

$$\Pi(t - t_0) \approx e^{-i(t-t_0)\tilde{\mathcal{G}}}\mathcal{S}. \tag{2.23}$$

The idea behind this approximation is that often long-time dynamics are well-described by a semigroup, and non-semigroup corrections only contribute significantly at short times. Thus one tries to capture more of the fast early dynamics by slipping the initial condition $\rho_0 \to \mathcal{S}\rho_0$. Clearly this ansatz may violate complete positivity at short times (since $\Pi(t_0) = \mathcal{S} \neq \mathcal{I}$) and one can therefore merely hope to lower the time-scale at which the semigroup becomes accurate.

The striking impact that a slip correction can have on a semigroup approximation is illustrated in Fig. 2.1: Here we show the decay of an excited atom into the ground state as described by the Jaynes-Cummings model, which is introduced in detail in Sec. 3.4. For the chosen parameters, the dynamics is quantum Markovian but not well-described by a semigroup except at very long times. Although the slip-corrected semigroup also fails to describe the short-time behaviour, even violating positivity until $t\gamma \approx 2$, it already lies on top of the exact solution at intermediate times $t\gamma \approx 4$. The semigroup achieves the same error only much later at $t\gamma \approx 10.5$.

Interestingly, these slip-corrected semigroups, typical for the time-local approach, can be naturally constructed by making use of the time-nonlocal structure of the solution (2.8b), which we explored in more detail in a separate publication [3]: starting from the eigendecomposition $\mathcal{K}(\omega) = \sum_i k_i(\omega)|k_i(\omega))(\bar{k}_i(\omega)|$ we select d^2 fixed-point frequencies ω_p satisfying $k_{i_{\omega_p}}(\omega_p) = \omega_p$ [Eq. (2.7)] and label the corresponding right eigenvectors for simplicity as $|\omega_p) \equiv |k_{i_{\omega_p}}(\omega_p))$ (d denotes the dimension of the Hilbert space). This selection of poles $\{\omega_p\}$ has to be made such that (i) it contains zero (to guarantee

the existence of a stationary state) (ii) it is symmetric with respect to the imaginary axis (to guarantee hermicity preservation of the approximation) and (iii) the set of right eigenvectors $\{|\omega_p)\}$ are linearly independent. The last assumption allows one to construct a dual basis $\{(\bar{\omega}_p|\}$ satisfying $(\bar{\omega}_p|\omega_{p'}) = \delta_{pp'}$ via biorthonormalization, which will be different from the set of left eigenvectors $\{(\bar{k}_{i_{\omega_p}}(\omega_p)|\}$ of the memory kernel. Assuming for simplicity that all the selected poles ω_p are of first order and neglecting all the non-selected poles and branch cut contributions in Eq. (2.8b), we obtain the approximation

$$\Pi(t-t_0) \approx \sum_{\omega_p} \frac{e^{-i\omega_p(t-t_0)}}{1-\frac{\partial k_{i_{\omega_p}}}{\partial\omega}\Big|_{\omega_p}} |\omega_p)(\bar{k}_{i_{\omega_p}}(\omega_p)| \tag{2.24a}$$

$$= \left[\sum_{\omega_p} e^{-i\omega_p(t-t_0)}|\omega_p)(\bar{\omega}_p|\right]\left[\sum_{\omega_p}\frac{1}{1-\frac{\partial k_{i_{\omega_p}}}{\partial\omega}\Big|_{\omega_p}}|\omega_p)(\bar{k}_{i_{\omega_p}}(\omega_p)|\right] \tag{2.24b}$$

$$= e^{-i(t-t_0)\tilde{\mathcal{G}}}\mathcal{S}. \tag{2.24c}$$

with the semigroup generator $\tilde{\mathcal{G}} := \sum_{\omega_p}\omega_p|\omega_p)(\bar{\omega}_p|$ and the initial slip superoperator

$$\mathcal{S} = \sum_{\omega_p}\frac{1}{1-\frac{\partial k_{i_{\omega_p}}}{\partial\omega}\Big|_{\omega_p}}|\omega_p)(\bar{k}_{i_{\omega_p}}(\omega_p)|. \tag{2.25}$$

Thus, an important insight is that finite frequency contributions from $\hat{\mathcal{K}}$ enter into the construction of $\tilde{\mathcal{G}}$ and $\mathcal{S}$. However, it is at this point completely unclear whether $\tilde{\mathcal{G}}$ is connected in a simple way to the stationary generator $\mathcal{G}(\infty)$ or the low-frequency kernel $\hat{\mathcal{K}}(0)$ [Eqs. (2.17)–(2.18)]. Also, the selection of poles even with the above mentioned constraints seems to leave a lot of freedom. The results presented in Sec. 3.2.2 will completely resolve all these points.

2.3.2 | Perturbation theories

A standard approach to obtain systematic approximations to the dynamics is to compute a perturbative expansion in (an ideally small) parameter. Semigroups then often arise in leading order, combined with special limits of physical parameters (high temperature, high voltage, etc.). One thus needs to go beyond semigroup approximations whenever higher-order corrections cannot be neglected or parameters are not fine-tuned to these special limits. In the context of QMEs describing transport, one typically expands in the tunnel coupling Γ between quantum dot and environment. This is in contrast to Green's function techniques, where one instead expands in the Coulomb interaction U

of a quantum dot. Using perturbative QMEs it is thus possible to treat all parameters of the local system's Hamiltonian non-perturbatively, which is important, for example, in typical quantum dot systems where the Coulomb interaction can be large.

A straightforward way to derive series expansions of Π, $\mathcal{K}$ or $\mathcal{G}$ is the Nakajima-Zwanzig projection operator technique [110, 111]. This was first applied to derive expressions for the propagator Π and the memory kernel $\mathcal{K}$ and later extended to the time-local generator $\mathcal{G}$ [34–36]. In Chap. 4–5 of this thesis we will instead use an equivalent diagrammatic approach, which originated in the study of quantum transport [23, 132–134] and is based on Wick's theorem. In this approach the memory kernel $\mathcal{K}$ naturally appears as the sum over all connected diagrams, but it has remained unclear how the generator $\mathcal{G}$ can be expressed using the same building blocks. Importantly, the traditional derivation of $\mathcal{G}$ [34–36] does not allow to pin this down. The diagrammatic language turns out to be vital for more advanced schemes going beyond the simple bare perturbation theory. For example, a renormalized perturbative memory kernel expansion valid for a large class of fermionic models was derived in Refs. [135, 136], where one expands around the high-temperature limit $T \to \infty$ instead of the decoupled limit $\Gamma \to 0$, and thereby already includes dissipative behavior into the reference solution. This in turn led to the discovery of the non-perturbative fermionic duality [137, 138], an exact "dissipative symmetry" cross-relating different eigenvalues and -vectors of the exact, finite T memory kernel and propagator in a simple fashion.

An important fact that is often overlooked is that perturbative series for Π, $\mathcal{K}$ and $\mathcal{G}$ are *not equivalent*. Computing the n-th order approximations $\Pi^{(n)}$, $\mathcal{K}^{(n)}$ and $\mathcal{G}^{(n)}$ in the same parameter and subsequently solving the corresponding master equations

$$\dot{\Pi}^{(n)}_{\mathcal{K}}(t,t_0) = -i\int_{t_0}^{t} ds \mathcal{K}^{(n)}(t,s)\Pi^{(n)}_{\mathcal{K}}(s,t_0), \tag{2.26a}$$

$$\dot{\Pi}^{(n)}_{\mathcal{G}}(t,t_0) = -i\mathcal{G}^{(n)}(t,t_0)\Pi^{(n)}_{\mathcal{G}}(t,t_0), \tag{2.26b}$$

one finds that the approximate solutions generally differ, $\Pi^{(n)} \neq \Pi^{(n)}_{\mathcal{K}} \neq \Pi^{(n)}_{\mathcal{G}}$. As a result, it is difficult to compare results obtained in different research communities which exclusively use either one or the other approach. The solutions can even be qualitatively different. As a trivial example, the directly computed propagator $\Pi^{(n)}$ often suffers from unphysical secular terms growing as $\mathcal{O}(\Gamma^n t^n)$, which typically do not appear in $\Pi^{(n)}_{\mathcal{K}}$ or $\Pi^{(n)}_{\mathcal{G}}$. We will address the highly non-trivial comparison between $\Pi^{(n)}_{\mathcal{K}}$ and $\Pi^{(n)}_{\mathcal{G}}$ in Chap. 4 and advance the understanding of the pros and cons of these expansions by deriving the representation of $\mathcal{G}$ within the *same* diagrammatic language as for $\mathcal{K}$.

3

Generators as fixed points of memory kernel functionals

As we have seen in Chap. 2, there are two exact but distinct quantum master equation approaches to the dynamics of an open quantum system: the first uses a *time-nonlocal* memory kernel $\mathcal{K}$, whereas the second produces the same evolution using a *time-local* generator $\mathcal{G}$. As discussed, the memory kernel $\mathcal{K}$ is advantageous for advanced approximation schemes, whereas the time-local generator $\mathcal{G}$ provides more subtle insights, e.g., about the Markovianity (divisibility) of an evolution.

In this chapter we are concerned with the general relationship between $\mathcal{K}$ and $\mathcal{G}$, which has already been investigated for time-translation invariant systems in the stationary limit $t_0 \to -\infty$. Refs. [31, 41, 42] discussed this relation using a memory expansion, i.e., a gradient / Moyal expansion [139–141] in the time-domain applied to the density operator. Similar expansions are well developed [142, 143], e.g., for Wigner- and Green-functions [140, 141]. The mentioned works indicated that the naive physical intuition, that the long-time limit of QME (2.9) is equivalent to the low-frequency approximation to QME (2.3), is wrong: The stationary generator $\mathcal{G}(\infty)$ does *not* coincide with the zero-frequency limit $\hat{\mathcal{K}}(0)$ of the (Laplace-transformed) memory kernel. As a result, "natural" Markovian semigroup approximations set up within approach (2.3) or (2.9), using the *exact* $\hat{\mathcal{K}}(0)$ or $\mathcal{G}(\infty)$ respectively, turn out to be *distinct*. This difference has proven to be important in perturbative studies beyond weak coupling [31, 41, 42], and is even crucial for measurement backaction [123, 124]. From these studies the difference between $\hat{\mathcal{K}}(0)$ and $\mathcal{G}(\infty)$ appears to be very complicated. Pinning down this relation also ties in with the much broader [122] discussion of non-Markovianity, where the interesting connection between divisibility, statistical discrimination [16, 19, 144] and information flow [17–19, 120, 145–147] continues to be developed [22, 148].

A further important step in clarifying this issue was provided by the proof in Ref. [39]

that $\hat{\mathcal{K}}(0)$ and $\mathcal{G}(\infty)$, despite their difference, both have the *exact* stationary state as a right zero eigenvector. However, this work was restricted to master equations for probabilities (not including coherences) and also left unanswered the relation between the full eigenspectra of $\mathcal{G}(\infty)$ and $\hat{\mathcal{K}}(\omega)$, which is one of several results established in this chapter. Such relations are of interest since these eigenspectra enter as input into advanced calculations of their dynamics [27, 29, 30] and provide insight into the time-evolution [149], just as the eigenspectra of Hamiltonians do for the evolution of closed systems. Similar exact relations among the eigenvectors of the memory kernel $\mathcal{K}$ proved to be very useful for simplifying the complicated calculations for strongly coupled, strongly interacting quantum dots far out of equilibrium [3, 135, 137].

Thus, it is a pressing question how the time-local generator is related to the time-nonlocal memory kernel for a general finite-dimensional open quantum system. The central result of this chapter established in Sec. 3.1 is that this relation takes the surprisingly simple form of a *functional fixed-point equation* $\mathcal{G}(t,t_0) = \hat{\mathcal{K}}[\mathcal{G}](t,t_0)$. Importantly, it applies to transient dynamics and allows for arbitrary driving. In Sec. 3.2 we explore the implications for time-translation invariant systems in the long time limit, where the stationary generator becomes the fixed point of a simpler *function* of superoperators, $\mathcal{G}(\infty) = \hat{\mathcal{K}}(\mathcal{G}(\infty))$. This leads to the key insight that $\mathcal{G}(\infty)$ "samples" the memory kernel $\hat{\mathcal{K}}(\omega)$ at a finite number of frequencies. This *completely defines* $\mathcal{G}(\infty)$ and significantly simplifies the connection between the mentioned distinct semigroup Markov approximations. The sampled frequencies are shown to be exact time-evolution poles of the Laplace space propagator $\hat{\Pi}(\omega)$, well-known from the time-nonlocal approach [Eq. (2.6)]. The transformation connecting eigenvectors of $\mathcal{G}(\infty)$ and $\hat{\mathcal{K}}(\omega)$ is found to be related to the initial-slip correction procedures introduced in Sec. 2.3.1. Furthermore, we show that both the stationary and the transient fixed-point equation are self-consistent expressions for the solution of the memory expansion discussed in Refs. [31, 41, 42] by explicitly constructing and summing this series. In other words, by computing all corrections accounting for "memory" in one approach, one obtains the "memoryless" approximation of the other, underlining the need for our quantitative connection.

In Sec. 3.3 we show that the fixed-point equation can be turned into two separate iterative numerical approaches for obtaining the transient and the stationary generator, respectively, from a given memory kernel. This provides a new starting point for hybrid approaches in which the results of advanced time-nonlocal calculations [24–27] can be plugged into the time-local formalisms *directly*, bypassing the solution $\Pi(t,t_0)$ that ties Eqs. (2.3) and (2.9) together. Ref. [26] numerically addressed the converse problem of extracting $\mathcal{K}$ from an evolution generated by $\mathcal{G}$, which analytically seems to be more complicated.

Finally we explicitly illustrate the derived relations between $\mathcal{K}$ and $\mathcal{G}$ on two *nonperturbative* examples. First, we address the exactly solvable dissipative Jaynes-Cummings model [20, 93, 150, 151] in Sec. 3.4 and show how the developed iteration schemes deal with nontrivial singularities of $\mathcal{G}(t,t_0)$ in time. Second, the fermionic resonant level model with its richer time-dependent algebraic structure is discussed in Sec. 3.5 and further showcases the nontrivial connection between a time-local and nonlocal description.

3.1 | Functional fixed-point relation

By definition the generator $\mathcal{G}(t,t_0)$ and the memory kernel $\mathcal{K}(t,s)$ are related by the fact that they produce the same dynamics $\Pi(t,t_0)$ [Eq. (2.1)]. To derive a *direct* relation we start from the time-local QME for the propagator (2.9), from which the generator can be obtained as

$$-i\mathcal{G}(t,t_0) = \dot{\Pi}(t,t_0)\Pi(t,t_0)^{-1}. \tag{3.1}$$

As mentioned in Sec. 2.1.2 there may be singular time points, which we will encounter in the model considered in Sec. 3.4. Inserting the equivalent time-nonlocal QME (2.3) into equation (3.1) gives

$$\mathcal{G}(t,t_0) = \int_{t_0}^{t} ds\, \mathcal{K}(t,s)\Pi(s,t_0)\Pi(t,t_0)^{-1}. \tag{3.2}$$

The key step to connect these two approaches is to recognize the expression for the *divisor* [Eq. (2.20)], which we encoutered when discussing quantum Markovianity. The divisor obeys the *same* time-local QME as the propagator, $d\Pi(t,s|t_0)/dt = -i\mathcal{G}(t,t_0)\Pi(t,s|t_0)$, with *different* initial condition $\Pi(s,s|t_0) = \mathcal{I}$ for all $s \in [t_0,t]$. The inverse of its formal solution,

$$[\Pi(t,s|t_0)]^{-1} = \mathcal{T}_{\rightarrow} e^{i\int_s^t d\tau \mathcal{G}(\tau,t_0)} \quad \text{for} \quad t_0 \leq s \leq t, \tag{3.3}$$

involves anti-time-ordering denoted by $\mathcal{T}_{\rightarrow}$. Inserted into Eq. (3.2) we find the key result

$$\mathcal{G}(t,t_0) = \hat{\mathcal{K}}[\mathcal{G}](t,t_0). \tag{3.4}$$

The time-local generator is a *fixed point of a functional* which maps a superoperator function of time $X(t,t_0)$ to another such function:

$$\hat{\mathcal{K}}[X](t,t_0) := \int_{t_0}^{t} ds\, \mathcal{K}(t,s)\mathcal{T}_{\rightarrow} e^{i\int_s^t d\tau X(\tau,t_0)}. \tag{3.5}$$

This functional is closely related to the ordinary Laplace transform (2.5) of the memory kernel $\mathcal{K}(t-s)$, to which it reduces for constant c-number functions of time $X = \omega\mathcal{I}$ in the limit $t_0 \to -\infty$ for time translational systems. We already note that the functional $\hat{\mathcal{K}}[X]$ may have fixed points *other* than $X = \mathcal{G}$. The nonuniqueness and stability of fixed points are further discussed in Sec. 3.4–3.5 for two specific models.

In Fig. 3.1 we graphically outline this derivation. This highlights that time-local propagation with $\mathcal{G}$ needs to be consistent with time-locally evolving backward with $\mathcal{G}$ and *time-nonlocally* propagating forward with the memory kernel. We stress that Eq. (3.4) is a transformation between two complementary descriptions of the same dynamics. It thus also applies to *approximate* dynamics Π' generated equivalently by some $\mathcal{K}'$ and $\mathcal{G}'$, and thus has broad applicability.

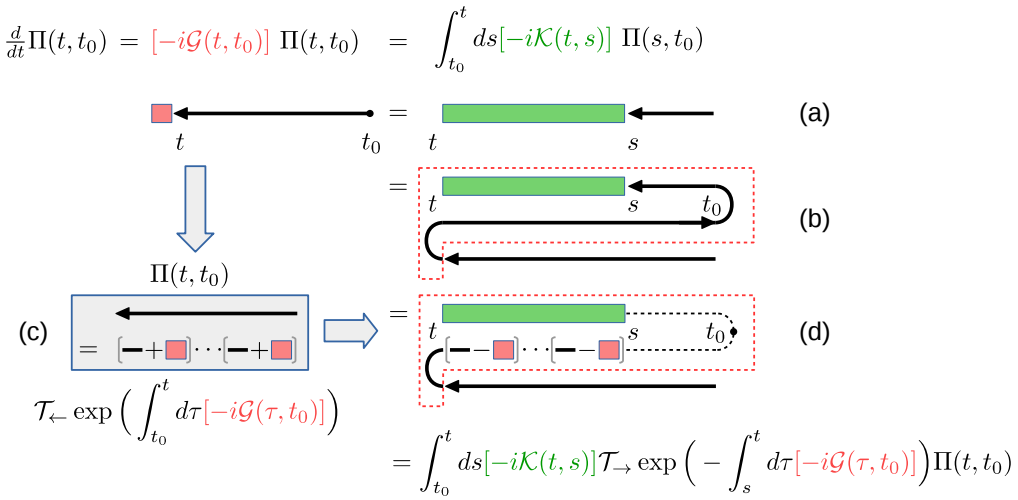

Figure 3.1. Graphical representation of the derivation of the functional fixed-point equation (3.4). (a) Equivalent expressions for $\dot{\Pi}(t,t_0)$ as given by the two QMEs. (b) Insertion of canceling backward and forward propagation to *initial time* t_0. (c) Evolution $\mathcal{T}_{\leftarrow} \exp\left(\int_{t_0}^{t} d\tau[-i\mathcal{G}(\tau,t_0)]\right) = \lim_{N\to\infty}(\mathcal{I} - i\mathcal{G}(t_1)\Delta t_1)\ldots(\mathcal{I} - i\mathcal{G}(t_N)\Delta t_N)$ expressed as product of infinitesimal steps for the sake of illustration. (d) Backward propagation to memory-time s expressed in terms of $\mathcal{G}$ using the divisor. The self-consistency expressed by the functional fixed-point equation (3.4) arises from the backward propagation needed to enforce the time-local structure of QME (2.9) onto the QME (2.3).

Equation (3.4) is explicitly consistent with trace-preservation, a fundamental property of the dynamics. Due to the ordering in Eq. (3.5), where the kernel $\mathcal{K}$ stands to the left of the exponential, the trace-preservation property of the kernel, $\mathrm{Tr}\,\mathcal{K}(t,s)\bullet = 0$, implies the corresponding property of the generator, $\mathrm{Tr}\,\mathcal{G}(t,t_0)\bullet = 0$. In fact, for *any*

superoperator function $X(t, t_0)$ one has

$$\operatorname{Tr} \hat{\mathcal{K}}[X](t, t_0) = 0. \tag{3.6}$$

Moreover, the connection between the hermicity-preservation property of the kernel and the generator can also be easily checked: Since $-i\mathcal{K}(t)A = [-i\mathcal{K}(t)A^\dagger]^\dagger = \mathcal{H}[-i\mathcal{K}(t)]\mathcal{H}A$ for any operator A, where $\mathcal{H}A := A^\dagger$ is an antilinear superoperator, we have

$$\mathcal{H}\{-i\hat{\mathcal{K}}[X](t, t_0)\}\mathcal{H} = -i\hat{\mathcal{K}}[-\mathcal{H}X\mathcal{H}](t, t_0). \tag{3.7}$$

3.2 | Stationary fixed-point relation

We now focus on the implications for time-translational systems in the stationary limit and consider the case where the generator converges to a constant superoperator $\mathcal{G}(\infty) = \lim_{t_0 \to -\infty} \mathcal{G}(t - t_0)$. Using the fixed point relation (3.4) we find

$$\mathcal{G}(\infty) = \lim_{t_0 \to -\infty} \int_{t_0}^{t} ds\, \mathcal{K}(t - s) \mathcal{T}_{\rightarrow} e^{i \int_s^t d\tau \mathcal{G}(\tau - t_0)} \tag{3.8a}$$

$$= \int_{-\infty}^{t} ds\, \mathcal{K}(t - s) e^{i(t-s)\mathcal{G}(\infty)} \tag{3.8b}$$

We don't prove rigorously the mathematically non-trivial convergence of (3.8a) to the limit (3.8b), which is instead physically motivated by the observation that typically either the generator has already become stationary, $\mathcal{G}(\tau - t_0) \approx \mathcal{G}(\infty)$ ($\tau \geq s \gg t_0$), or the memory kernel has already decayed ($t \gg s$), thus suppressing the expression. Hence we obtain the *stationary* fixed-point equation

$$\mathcal{G}(\infty) = \hat{\mathcal{K}}(\mathcal{G}(\infty)). \tag{3.9}$$

Compared to (3.5) the right hand side features the much simpler extension of the Laplace transform (2.5) with frequency ω replaced by the time-constant superoperator X:

$$\hat{\mathcal{K}}(X) := \int_0^\infty ds\, \mathcal{K}(s) e^{isX}. \tag{3.10}$$

In contrast to the ordinary Laplace transform (2.5) it is crucial that the exponential appears to the right of the memory kernel, since in general $[\mathcal{K}(s), e^{isX}] \neq 0$.

3.2.1 | Exact sampling relation between spectral decompositions

The stationary fixed-point equation (3.9) immediately makes clear that in general the stationary generator $\mathcal{G}(\infty)$ is *not* the low-frequency limit of the memory kernel, $\hat{\mathcal{K}}(0)$. We now make precise *which* parts of the frequency dependence of the memory kernel $\hat{\mathcal{K}}(\omega)$ matter in the stationary limit. To this end, assume that one can diagonalize the stationary generator $\mathcal{G}(\infty) = \sum_i g_i |g_i)(\bar{g}_i|$, and denote the distinct left and right eigenvectors to the same eigenvalue g_i by $(\bar{g}_i|$ and $|g_i)$ respectively, which satisfy the Hilbert-Schmidt biorthogonality relation $(\bar{g}_i|g_{i'}) = \delta_{ii'}$. Insertion into Eq. (3.9) gives $\mathcal{G}(\infty) = \sum_i \hat{\mathcal{K}}(g_i)|g_i)(\bar{g}_i|$ with the ordinary Laplace transform (2.5) evaluated at $\omega = g_i$. Focusing on nondegenerate eigenvalues we therefore have

$$\hat{\mathcal{K}}(g_i)|g_i) = \mathcal{G}(\infty)|g_i) = g_i|g_i). \tag{3.11}$$

Diagonalizing the kernel *after* Laplace transforming, $\hat{\mathcal{K}}(\omega) = \sum_j k_j(\omega)|k_j(\omega))(\bar{k}_j(\omega)|$, this implies that at designated frequencies $\omega = g_i$ *one* of its eigenvalues, labeled $j = f_i$, must coincide with an eigenvalue g_i of the stationary generator $\mathcal{G}(\infty)$:

$$k_{f_i}(g_i) = g_i. \tag{3.12}$$

The right eigenvectors can then be normalized to coincide

$$|k_{f_i}(g_i)) = |g_i). \tag{3.13}$$

Importantly the eigenvectors of the kernel $|k_j(\omega))$ can also contain poles, which have an important impact on the evolution as illustrated explicitly in Sec. 3.5. However, since $\mathcal{G}(\infty)$ was assumed to be finite it can not sample any of these eigen*vector* poles of the kernel.

We note that the left eigenvectors $(\bar{g}_i|$ and $(\bar{k}_{f_i}(g_i)|$ in general *differ* with one important exception, labeled by $i = 0$: From the trace-preservation property of the dynamics [see Eq. (3.6)] it follows that both $\mathcal{G}(\infty)$ and $\hat{\mathcal{K}}(\omega)$ at every frequency ω have the *left* zero eigenvector $(\mathbb{1}| = \mathrm{Tr}\,\bullet$, the trace functional. The corresponding zero eigenvalue is denoted by $g_0 = k_0(\omega) = 0$ for all ω labeling $f_0 = 0$. Thus, a nontrivial consequence of Eq. (3.11) is that the associated *right* zero eigenvectors of $\mathcal{G}(\infty)$ and $\hat{\mathcal{K}}(0)$, respectively, coincide with the stationary state:

$$|g_0) = |k_0(0)) = |\rho(\infty)). \tag{3.14}$$

This generalizes the result of Ref. [39], which proved this statement for probability vectors evolving with a time-local master equation (i.e. for probabilities only).

We summarize the key result of this section: For Hilbert-space dimension d the stationary time-local generator, with its finite set of eigenvalues $g_0, \ldots, g_{d^2-1}$, can be written as

$$\mathcal{G}(\infty) = \sum_i k_{f_i}(g_i)|k_{f_i}(g_i))(\bar{g}_i|. \tag{3.15a}$$

It "samples" *one* term of the Laplace-transformed memory kernel at *each* of the frequencies $\omega = g_0, \ldots, g_{d^2-1}$:

$$\hat{\mathcal{K}}(g_i) = k_{f_i}(g_i)|k_{f_i}(g_i))(\bar{k}_{f_i}(g_i)| + \sum_{j \neq f_i} k_j(g_i)|k_j(g_i))(\bar{k}_j(g_i)|. \tag{3.15b}$$

From each sampled frequency only a single right eigenvector $|k_{f_i}(g_i))$ for one specific eigenvalue satisfying $k_{f_i}(g_i) = g_i$ is needed to construct $\mathcal{G}(\infty)$. Importantly, its left eigenvectors $(\bar{g}_i|$ are determined by the right ones through the biorthogonality constraint.

We already note that some intuitive ideas turn out to be incorrect: First, the sampling formula shows that in general *nonzero* frequencies of $\hat{\mathcal{K}}(\omega)$ may matter at stationarity. This makes precise that "memory", often understood as retardation or frequency dependence of the kernel [31, 41, 42, 123, 124], is in general *not* the same as "memory" defined by a *Markovian semigroup* [17, 18, 43, 118, 119], in which $\mathcal{G}(\infty)$ naturally appears. Second, the sampled frequencies g_i need *not* be the eigenvalues with the smallest decay rates $[-\mathrm{Im}k_j(\omega_p)]$, which we will see in the examples discussed later.

The sampling formula (3.15) implies that the analytical calculation of the typically more complicated quantity $\mathcal{G}(\infty)$ can in principle be reduced to the calculation of $\hat{\mathcal{K}}(\omega)$ at just d^2 specific frequencies. We will show in Sec. 3.3 how $\mathcal{G}(\infty)$ can be iteratively computed from $\hat{\mathcal{K}}(\omega)$, thus determining which frequencies are actually sampled. It is therefore not necessary to compute the transient generator $\mathcal{G}(t)$ in order to compute $\mathcal{G}(\infty)$. This is a significant advance since $\hat{\mathcal{K}}$ can be approximated accurately for complicated many-body dynamics using well-developed techniques [23, 24, 27, 29, 30]. As mentioned, our relations remain valid when dealing with such approximate kernels: they are simply a way to change from a time-nonlocal to a time-local representation.

3.2.2 | Exact time-evolution poles

We now compare the sampling relations (3.15) with the formal exact solution (2.8) for time-translational systems obtained by the resolvent method: As we have seen in Sec. 2.1.1 each eigenvalue of $\hat{\mathcal{K}}$ satisfying $\omega_p = k_j(\omega_p)$ for some ω_p represents a pole of $\hat{\Pi}(\omega)$. Hence by our result (3.12) the eigenvalues of $\mathcal{G}(\infty)$ are guaranteed to be included among these *eigenvalue* poles of $\hat{\Pi}(\omega)$. Thus, our stationary fixed-point equation (3.9)

reveals how the time-local approach keeps track of these characteristic frequencies of the evolution, which are explicit in the time-nonlocal approach.

In other words, for time-translational systems the relation $\mathcal{G}(\infty) = \hat{\mathcal{K}}(\mathcal{G}(\infty))$ establishes that the time-local generator $\mathcal{G}(\infty)$ is a superoperator-valued characteristic "frequency" of the evolution. To be sure, there are further contributions from non-sampled poles and branch cuts, which can be infinitely many and may also involve the eigenvectors [24]. These are encoded in the transient fixed-point equation (3.4) through the anti-time-ordered integration (3.5). Thus, the eigenvalues of $\mathcal{G}(\infty)$ generally do not exhaust all the eigenvalue poles of $\hat{\Pi}(\omega)$. *Which* of the eigenvalues of $\hat{\mathcal{K}}(\omega)$ satisfying $\omega_p = k_j(\omega_p)$ are eigenvalues of $\mathcal{G}(\infty)$ is not *apriori* clear.

Our result (3.15a) now reveals that the first contribution to the exact dynamics (2.8a) actually contains a Markovian semigroup generated by $\mathcal{G}(\infty)$, which is however already corrected by a slippage $\mathcal{S}$:

$$\Pi(t - t_0) = e^{-i(t-t_0)\mathcal{G}(\infty)}\mathcal{S} + \dots \tag{3.16}$$

Here $\dots$ denotes the above mentioned non-sampled contributions and $\mathcal{S}$ is constructed as in Eq. (2.25) using all the eigenvalues of $\mathcal{G}(\infty)$:

$$\mathcal{S} = \sum_i \frac{1}{1 - \frac{\partial k_{f_i}}{\partial \omega}\Big|_{g_i}} |g_i)(\bar{k}_{f_i}(g_i)|. \tag{3.17}$$

3.2.3 | Nonperturbative semigroup approximations

We can now address the puzzling issue regarding the more basic approximation strategies that we mentioned in the introduction [Sec. 2.2.1]: The *equivalent* QMEs (2.3) and (2.9) "naturally" lead to semigroup approximations which *differ*, even when constructed from the *exact* $\mathcal{G}$ and $\mathcal{K}$.

(i) *Stationary generator* $\mathcal{G}(\infty)$: Assuming that the generator converges to a stationary value $\mathcal{G}(\infty)$ we can try to approximate the time-local QME as a semigroup as in Eq. (2.17). This idea underlies Refs. [41, 42] and motivated the direct calculation of $\mathcal{G}(\infty)$ by a series expansion in the coupling in Ref. [39]. The resulting approximate dynamics has an interesting feature: There are many evolutions for which the *asymptotic* generator $\mathcal{G}(\infty)$ has a GKSL form [118, 119] with nonnegative jump rates, which guarantees that the approximation is completely positive in addition to trace preserving. Nonperturbative approximations preserving *both* these properties are notoriously difficult to construct, especially starting from microscopic models [47, 152–154]. Here the class of evolutions

goes beyond semigroups by including all CP-divisible evolutions, but also allowing for certain *non* CP-divisible ones[1].

Our sampling result (3.15) furthermore shows that the exact solution as obtained using the time non-local approach naturally contains the semigroup generated by $\mathcal{G}(\infty)$ together with an initial-slip correction $\mathcal{S}$. Due to the automatic inclusion of $\mathcal{S}$, the first term of Eq. (3.16) is neither a semigroup nor a CP map around the initial time t_0. This may give faster convergence but also fail dramatically [3]. In contrast, the semigroup approximation (2.17) does not suffer from such problems.

(ii) *Low-frequency memory kernel* $\hat{\mathcal{K}}(0)$. Starting instead from the time-nonlocal Eq. (2.3) one obtains a semigroup generated by $\hat{\mathcal{K}}(0)$ [Eq. (2.18b)]. This approximation is equivalent to neglecting all frequency dependence of the memory kernel, $\hat{\Pi}(\omega) \approx i/(\omega - \hat{\mathcal{K}}(0))$, leaving only d^2 eigenvalue poles $\omega_j = k_j(0)$. In contrast to $\mathcal{G}(\infty)$, we know of no general conditions that guarantee that $\hat{\mathcal{K}}(0)$ generates a completely positive evolution for some broad class of nontrivial models. Even when it is known that $\mathcal{G}(\infty)$ has nonnegative GKSL coefficients – ensuring that $e^{-i(t-t_0)\mathcal{G}(\infty)}$ is completely positive – one *still* has to explicitly check that the same holds for $\hat{\mathcal{K}}(0)$. Although both approximations (2.17) and (2.18b) nonperturbatively account for oscillation frequencies and decay rates in a different way, it follows from the sampling result (3.13) that *both* converge to the *exact* stationary state. Note, however, that $\mathcal{G}(\infty) = \hat{\mathcal{K}}(0)$ is possible also for a non-semigroup evolution, see Sec. 3.5.

3.2.4 | Summing the memory expansion

Whereas the argument leading to the semigroup $\Pi \approx e^{-i(t-t_0)\hat{\mathcal{K}}(0)}$ may be justified in the weak coupling limit, it has been noted that when computing $\hat{\mathcal{K}}$ to higher order in the system-environment coupling this becomes inconsistent [40–42, 156]. It was argued that one should instead use a *memory expansion*, where not only the kernel $\mathcal{K}(t-s)$ is expanded in the memory-time s relative to the current time t, but simultaneously the propagator $\Pi(s,t_0) = \Pi(t,t_0) - (t-s)\partial\Pi(t,t_0)/\partial t + \ldots$ under the memory integral before taking the stationary limit. This way Ref. [41] obtained a semigroup with an approximate generator

$$\hat{\mathcal{K}}(0) + \frac{\partial\hat{\mathcal{K}}}{\partial\omega}(0)\,\hat{\mathcal{K}}(0). \tag{3.18}$$

[1] Recall that Π is CP-divisible if $\mathcal{G}$ has nonnegative GKSL coefficients for *all* times t [Sec. 2.2.2]. By contrast, Eq. (2.17) generates CP dynamics even if negative coefficients at *finite* times occur. Models where the evolution has negative asymptotic GKSL coefficients have also been studied recently [22, 45, 155]

When computing $\hat{\mathcal{K}}(0)$ to second order in, e.g., a tunnel coupling, the first order contributions to the second term are comparable [41] and may lead to cancellations that are necessary to respect complete positivity [123, 124]. In Ref. [42] the approximation (3.18) was generalized to higher orders by applying partial integrations of the time-nonlocal QME (2.9), which can be shown to be equivalent to further continuing the memory expansion of Ref. [41]. Thus, starting from the time-nonlocal QME one is led to a *time-local* QME by the memory expansion.

Another key result of this chapter is that this memory expansion can in fact be summed up to all orders [App. A]. One finds that the constant generator that accounts for *all* memory terms is precisely the stationary time-local generator obeying $\mathcal{G}(\infty) = \hat{\mathcal{K}}(\mathcal{G}(\infty))$, our stationary fixed-point equation (3.9). This means that our sampling formula (3.15a) is the nonperturbative result of this series: The infinite sum of memory terms – featuring all derivatives of $\hat{\mathcal{K}}(\omega)$ at *zero* frequency – can be condensed into a finite sum of contributions of $\hat{\mathcal{K}}(\omega)$ at just d^2 finite frequencies $\omega = g_i$.

One may roughly understand the equation $\mathcal{G}(\infty) \approx \hat{\mathcal{K}}(0) + \frac{\partial \hat{\mathcal{K}}}{\partial \omega}(0)\,\hat{\mathcal{K}}(0)$ as follows: to obtain $\mathcal{G}(\infty)$ one linearizes the frequency dependence of the memory kernel $\hat{\mathcal{K}}(\omega) \approx \hat{\mathcal{K}}(0) + [\partial\hat{\mathcal{K}}/\partial\omega(0)]\omega$ and evaluates it at the characteristic "frequency" $\omega = \mathcal{G}(\infty) \approx \hat{\mathcal{K}}(0)$ of the system, which in first approximation is the low-frequency kernel itself. This tentative picture is made rigorous by our fixed-point equation (3.9), where the frequency is likewise replaced by a superoperator, but in a self-consistent way.

Furthermore, the memory expansion can not only be resummed in the stationary limit $t_0 \to -\infty$, but also for the full transient dynamics, thereby recovering the functional fixed point equation (3.4) [App. A]. By making use of the divisor we can give a closed formula for terms of arbitrary order [Eqs. (A.5), (A.8)]. We show how this expansion can be expressed in Moyal brackets [139, 157] with respect to time similar to that used in Green's function techniques [140, 141] in App. B. Altogether, this shows that equations (3.4) and (3.9) are very useful for generating gradient expansions in time when given a memory kernel $\mathcal{K}$.

3.3 | Iterative construction of the generator

In this section we show how the stationary and transient fixed-point equations [Eqs. (3.9) and (3.4) respectively] may be turned into computational tools to obtain $\mathcal{G}$ from a given memory kernel $\mathcal{K}$. We focus on time-translational systems – setting $t_0 = 0$ – and the ideal situation where $\mathcal{K}$ has been computed accurately using a method of choice or is even available exactly.

3.3.1 | Iteration for the stationary generator

The simplest scenario is where one iteratively solves Eq. (3.9) to find $\mathcal{G}(\infty)$ *directly* from $\mathcal{K}(t)$ or $\hat{\mathcal{K}}(\omega)$, i.e., without considering the transient evolution $\Pi(t)$ or the transient generator $\mathcal{G}(t)$. Using the converged result one may then set up the nonperturbative semigroup $e^{-it\mathcal{G}(\infty)}$ to approximate the full evolution $\Pi(t)$.

First, consider the low-frequency kernel as an initial approximation to the generator, $\mathcal{G}^{(0)}(\infty) = \hat{\mathcal{K}}(0)$, as in Eq. (3.18). If the exact dynamics is a semigroup, $\mathcal{K}(t) = \hat{\mathcal{K}}(0)\bar{\delta}(t)$ and $\mathcal{G}(t) = \hat{\mathcal{K}}(0)$, then this already is the fixed point since $\mathcal{G}^{(1)}(\infty) = \hat{\mathcal{K}}(\hat{\mathcal{K}}(0)) = \hat{\mathcal{K}}(0)$. This may *also* happen for non-semigroup evolutions (see Sec. 3.5). In general, further approximations are obtained by n-fold iteration, $\mathcal{G}^{(n)}(\infty) = \hat{\mathcal{K}}\big(\ldots\hat{\mathcal{K}}(\hat{\mathcal{K}}(0))\big)$. Inspecting the first iteration,

$$\mathcal{G}^{(1)}(\infty) = \hat{\mathcal{K}}(\hat{\mathcal{K}}(0)) = \sum_{j\neq 0} \hat{\mathcal{K}}(k_j(0))|k_j(0))(\bar{k}_j(0)|, \tag{3.19}$$

we see that the stationary state $|k_0(0))$ remains unaffected (trace-preservation), but in general all $j \neq 0$ contributions are altered by the memory kernel evaluated at *finite* frequencies, thus generating a difference between $\hat{\mathcal{K}}(0)$ and $\mathcal{G}(\infty)$.

The convergence of this procedure with n is certainly not obvious, but our first applications in Sec. 3.4–3.5 are encouraging. Indeed, one can consider starting the iteration from *any* initial superoperator $\mathcal{G}^{(0)}(\infty) = X$. In this case, property (3.6) guarantees that the iteration trajectory $\mathcal{G}^{(n)}(\infty) = \hat{\mathcal{K}}\big(\ldots\hat{\mathcal{K}}(X)\big)$ is confined to the linear space of trace-preserving superoperators irrespective of X. If iX is hermicity-preserving, then the trajectory will additionally be confined to such superoperators by property (3.7).

3.3.2 | Iteration for the transient generator

We next describe the more complicated iteration of the functional equation (3.4). Here the aim is to construct the full transient generator $\mathcal{G}(t)$ starting from the memory kernel $\mathcal{K}(t)$. As a preparation we decompose the kernel into its time-local ($\bar{\delta}$-singular) part $\mathcal{K}_L$ and a remaining time-nonlocal part $\mathcal{K}_N$ as in Eq. (2.4). In addition to the system Liouvillian L, the part $\mathcal{K}_L$ may contain an environment-induced contribution (as for fermionic wide-band models [135–137] as studied in Sec. 3.5), but this need not be the case (as in the model studied in Sec. 3.4). Inserting Eq. (2.4) into the functional (3.5) we obtain

$$\mathcal{G}^{(n+1)}(t) = \mathcal{K}_L + \int_0^t ds\, \mathcal{K}_N(t-s)\mathcal{T}_{\rightarrow} e^{i\int_s^t d\tau \mathcal{G}^{(n)}(\tau)}. \tag{3.20}$$

Iterating this equation starting from the constant function $\mathcal{G}^{(0)}(t) = \hat{\mathcal{K}}(0)$ gives approximations $\mathcal{G}^{(n)}(t)$ which generate evolutions with two important properties *at every iteration*:

First, each approximation is accurate at long times, provided $\mathcal{G}(t)$ has a stationary limit and Eq. (3.4) converges to Eq. (3.9). Our choice of starting point ensures by Eq. (3.14) that $\mathcal{G}^{(n)}(t)|\rho(\infty)) = 0$ holds initially for $n = 0$, implying that the generated evolution goes to the exact stationary state for $t \to \infty$. This also holds for the next iteration, $\mathcal{G}^{(n+1)}(\infty)|\rho(\infty)) = \lim_{t\to\infty}[\mathcal{K}_L + \int_0^t ds\, \mathcal{K}_N(t-s)]|\rho(\infty)) = \hat{\mathcal{K}}(0)|\rho(\infty)) = 0$, using a similar argument as in Eq. (3.8). This applies also for the starting point $\mathcal{G}^{(0)}(t) = \mathcal{G}(\infty)$ [Eq. (3.14)] or any starting point X for which $X|\rho(\infty)) = 0$. However, starting from the memory kernel formalism, $\hat{\mathcal{K}}(0)$ is already available.

Second, each generated approximation is also accurate at short times. To see this, note that at the initial time the generator is given by the time-local part of the kernel

$$\mathcal{G}(0) = \mathcal{K}_L, \tag{3.21}$$

which we split off from the generator,

$$\mathcal{G}(t) = \mathcal{K}_L + \mathcal{G}_N(t), \qquad \mathcal{G}_N(0) = 0. \tag{3.22}$$

The second term incorporates all effects due to the time-nonlocal part of the kernel $\mathcal{K}_N(t)$. For the first iteration we have

$$\mathcal{G}^{(1)}(t) = \mathcal{K}_L + \int_0^t ds\, \mathcal{K}_N(t-s) e^{i\hat{\mathcal{K}}(0)(t-s)} \tag{3.23a}$$

$$\approx \mathcal{K}_L + t\, \mathcal{K}_N(0) + \ldots \tag{3.23b}$$

as dictated by the short-time limit of the *time-nonlocal* part of the memory kernel. This implies that in the exponential of the next iteration we similarly have at short times $\int_s^t d\tau \mathcal{G}^{(1)}(\tau) \approx (t-s)\mathcal{K}_L$, giving the same leading behavior. Thus, each iteration $n \geq 1$ coincides with the exact initial generator (3.21) including the *linear* order, $\mathcal{G}^{(n)}(t) = \mathcal{K}_L + t\, \mathcal{K}_N(0) + \ldots$. Clearly, no semigroup approximation can achieve this.

The convergence of this iteration is again not evident and an analysis of the local stability is complicated due to the time-nonlocality of the superoperator equations. Remarkably, we numerically find for several models that this procedure can be made to work, even when the generator is time-singular [Sec. 3.4] or has time-dependent algebraic structure [Sec. 3.5].

3.4 | Application: Atomic decay in a radiation field

We first illustrate our findings for the dissipative Jaynes-Cummings model [20, 93, 150, 151], which is algebraically simple but can show challenging time-singularities in the generator. This exactly solvable model describes a two-level atom with transition frequency ε ($H = \varepsilon d^\dagger d$ with $\{d, d^\dagger\} = \mathbb{1}$) interacting with a continuous bosonic reservoir ($H_R = \int d\omega \omega b_\omega^\dagger b_\omega$ with $[b_\omega, b_{\omega'}^\dagger] = \delta(\omega - \omega')\mathbb{1}$) initially in a vacuum state $|0\rangle$. The coupling is bilinear,

$$H_T = \int d\omega \sqrt{\frac{\Gamma(\omega)}{2\pi}} \left(d^\dagger b_\omega + b_\omega^\dagger d \right), \tag{3.24}$$

with real amplitudes set by a spectral density $\Gamma(\omega)$. The occupation numbers of reservoir modes are either 0 or 1 due to a dynamical constraint: the coupling (3.24) conserves the total excitation number $d^\dagger d + \int d\omega b_\omega^\dagger b_\omega$. Here we study the effects of energy-dependent coupling $\Gamma(\omega)$ without initial reservoir statistics ($T = 0$): We assume a Lorentzian profile of width γ whose maximum value $\Gamma \equiv \Gamma(\varepsilon)$ lies precisely at the atomic resonance:

$$\Gamma(\omega) = \Gamma \frac{\gamma^2}{(\varepsilon - \omega)^2 + \gamma^2}. \tag{3.25}$$

Although this model has been studied in detail [20, 21, 150, 151] and features in text books [93] the remarkable relation between its generator $\mathcal{G}$ and memory kernel $\mathcal{K}$ has not been noted, but see Ref. [158]. All results below can be generalized to any profile $\Gamma(\omega)$.

From the solution [93] of the total-system state $|\psi_{\text{tot}}(t)\rangle$, with $|\psi_{\text{tot}}(0)\rangle = |\psi(0)\rangle \otimes |0\rangle$, we extract the propagator $\text{Tr}_R\{|\psi_{\text{tot}}(t)\rangle\langle\psi_{\text{tot}}(t)|\} = \Pi(t)|\psi(0)\rangle\langle\psi(0)|$ working in the Schrödinger picture and setting $t_0 = 0$. It has the form of an amplitude damping channel [12] with spectral decomposition[2]

$$\begin{aligned}\Pi(t) =& |00)\Big[(00| + (11|\Big] + |\pi(t)|^2\Big[|11) - |00)\Big](11| \\ &+ \pi(t)\,|10)(10| + \pi(t)^*|01)(01|,\end{aligned} \tag{3.26}$$

using $|\nu\nu') = |\nu\rangle\langle\nu'|$ and $(\nu\nu'| = \langle\nu| \bullet |\nu'\rangle$, where $|\nu\rangle$ denotes the atomic state $\nu = 0, 1$. The time-dependent parameter reads

$$\pi(t) = e^{-i\varepsilon t} e^{-\gamma t/2} \left[\cosh\left(\frac{\gamma' t}{2}\right) + \frac{\gamma}{\gamma'} \sinh\left(\frac{\gamma' t}{2}\right) \right] \tag{3.27}$$

[2] In Ref. [2] the coherence blocks of Π, $\mathcal{G}$ and $\mathcal{K}$ inadvertently swapped $|01) \leftrightarrow |10)$, without impact on the discussions or plots. This has been corrected here.

where $\gamma' := \sqrt{\gamma(\gamma - 2\Gamma)}$. Thus, an initially excited state evolves with probability $\langle 1|\rho(t)|1\rangle = |\pi(t)|^2$. In the frequency domain we have

$$\begin{aligned}\hat{\Pi}(\omega) =& \frac{i}{\omega}|00)\Big[(00| + (11|\Big] + \widehat{|\pi|^2}(\omega)\Big[|11) - |00)\Big](11| \\ &+ \hat{\pi}(\omega)|10)(10| + \widehat{\pi^*}(\omega)|01)(01|. \end{aligned} \tag{3.28}$$

The Laplace transforms

$$\widehat{|\pi|^2}(\omega) = \frac{1}{4}\frac{(\gamma/\gamma' - 1)^2}{\gamma + \gamma' - i\omega} + \frac{1}{4}\frac{(\gamma/\gamma' + 1)^2}{\gamma - \gamma' - i\omega} - \frac{1}{2}\frac{\gamma^2/\gamma'^2 - 1}{\gamma - i\omega}, \tag{3.29}$$

$$\hat{\pi}(\omega) = \frac{\gamma/\gamma' + 1}{\gamma - \gamma' - 2i(\omega - \varepsilon)} - \frac{\gamma/\gamma' - 1}{\gamma + \gamma' - 2i(\omega - \varepsilon)}, \tag{3.30}$$

and $\widehat{\pi^*}(\omega) = [\hat{\pi}(-\omega^*)]^*$ determine the finite number of poles of the propagator $\hat{\Pi}(\omega)$ listed in Table 3.1.

It is now straightforward [20, 21] to determine the generator $\mathcal{G}(t) = i\dot{\Pi}(t)\Pi^{-1}(t)$ and the kernel $\hat{\mathcal{K}}(\omega) = \omega\mathcal{I} - i\hat{\Pi}^{-1}(\omega)$ whose relation has our interest. The spectral decomposition for the generator reads

$$\mathcal{G}(t) = 2i\,\mathrm{Re}\left(\frac{\dot{\pi}(t)}{\pi(t)}\right)\Big[|11) - |00)\Big](11| + i\frac{\dot{\pi}(t)}{\pi(t)}|10)(10| + i\left(\frac{\dot{\pi}(t)}{\pi(t)}\right)^*|01)(01|, \tag{3.31}$$

whereas for the kernel in the frequency domain it is

$$\begin{aligned}\hat{\mathcal{K}}(\omega) =& \Big(\omega - \frac{i}{\widehat{|\pi|^2}(\omega)}\Big)\Big[|11) - |00)\Big](11| \\ &+ \Big(\omega - \frac{i}{\hat{\pi}(\omega)}\Big)|10)(10| + \Big(\omega - \frac{i}{\widehat{\pi^*}(\omega)}\Big)|01)(01|. \end{aligned} \tag{3.32}$$

The eigenvalues of $\hat{\mathcal{K}}$ satisfying $k_j(\omega_p) = \omega_p$ for some j correspond to the poles of $\hat{\Pi}(\omega)$ in Table 3.1.

3.4.1 | Overdamped dynamics ($\gamma \geq 2\Gamma$)

Even with all explicit expressions in hand, it is by no means obvious that this model obeys our sampling result (3.15) in the stationary limit $t \to \infty$. We now first verify this noting that our assumption that $\mathcal{G}(\infty)$ exists holds only for broad spectral densities such that $\gamma \geq 2\Gamma$. In this case the real quantity $\gamma' = \sqrt{\gamma(\gamma - 2\Gamma)} \leq \gamma$ represents a suppression/enhancement of the decay rates $-\mathrm{Im}\,\omega_p$ relative to the value γ in Table 3.1. In this overdamped regime $\lim_{t\to\infty} \dot{\pi}(t)/\pi(t) = -i\varepsilon - \frac{1}{2}(\gamma - \gamma')$ converges and the dynamics is CP-divisible[3], but not semigroup Markovian (except for $\gamma \to \infty$).

[3]The generator can be written in time-dependent GKSL form with jump rate $j(t) = -2\mathrm{Re}[\dot{\pi}(t)/\pi(t)]$. For $\gamma \geq 2\Gamma$ we have $j > 0$ by $\dot{\pi}(t)/\pi(t) = -i\varepsilon - \frac{1}{2}\gamma + \frac{1}{2}\gamma' \tanh(\frac{1}{2}\gamma' t + \mathrm{arctanh}\frac{\gamma}{\gamma'})$ which implies CP divisibility.

Table 3.1 shows that the resulting four *eigenvalues* of $\mathcal{G}(\infty)$ indeed coincide with four of the eight *poles* of $\hat{\Pi}(\omega)$ as predicted by Eq. (3.12). Interestingly, $\mathcal{G}(\infty)$ does *not always* sample the "slowest" part of the evolution, i.e., the poles with the smallest decay rates, even in this simple model. Whereas this happens for sufficiently large broadening $\gamma > \frac{9}{4}\Gamma$, just before entering the underdamped regime there is a range $2\Gamma < \gamma < \frac{9}{4}\Gamma$, where two non-sampled poles $\omega_{4,5}$ have smaller decay rates than the sampled pole ω_3, see Table 3.1. Thus, $\mathcal{G}(\infty)$ is completely determined by the sampling of $\hat{\mathcal{K}}(\omega)$ as dictated by Eq. (3.15a). This does not illustrate the full complexity of the sampling since the right eigenvectors of $\hat{\mathcal{K}}(\omega)$ are frequency independent and thus trivially provide the right eigenvectors (3.13) of $\mathcal{G}(\infty)$.

Poles $\hat{\Pi}(\omega)$		Eigenvalues $\mathcal{G}(\infty)$
$\omega_0 = 0$		$g_0 = 0$
$\omega_1 = +\varepsilon - i\frac{1}{2}(\gamma - \gamma')$		$g_1 = +\varepsilon - i\frac{1}{2}(\gamma - \gamma')$
$\omega_2 = -\varepsilon - i\frac{1}{2}(\gamma - \gamma')$		$g_2 = -\varepsilon - i\frac{1}{2}(\gamma - \gamma')$
$\omega_3 = -i(\gamma - \gamma')$		$g_3 = -i(\gamma - \gamma')$
$\omega_4 = +\varepsilon - i\frac{1}{2}(\gamma + \gamma')$	$\longleftarrow$	*Possibly closer to real axis*
$\omega_5 = -\varepsilon - i\frac{1}{2}(\gamma + \gamma')$	$\longleftarrow$	*than ω_3!*
$\omega_6 = -i\gamma$		
$\omega_7 = -i(\gamma + \gamma')$		

Table 3.1. Jaynes-Cummings model: Poles of $\hat{\Pi}(\omega)$ and eigenvalues of $\mathcal{G}(\infty)$ using the abbreviation $\gamma' = \sqrt{\gamma(\gamma - 2\Gamma)}$.

Numerical implementation of the stationary iteration described in Sec. 3.3.1 converges in a few steps to the exact stationary generator, which explicitly reads

$$-i\mathcal{G}(\infty) = -\frac{2\Gamma}{1+\sqrt{1-2\Gamma/\gamma}}\Big[|11) - |00)\Big](11| + \Big(-i\varepsilon - \frac{\Gamma}{1+\sqrt{1-2\Gamma/\gamma}}\Big)|10)(10| + \Big(i\varepsilon - \frac{\Gamma}{1+\sqrt{1-2\Gamma/\gamma}}\Big)|01)(01|. \tag{3.33}$$

Importantly, we numerically observe this convergence starting from *random* initial superoperators X, suggesting that it is a unique stable fixed point. Other fixed points of Eq. (3.10) can be constructed analytically[4], but these seem to be unstable since they are not found in the numerical iteration. Due to this remarkable fact, the iterative solution

[4](i) Select any four poles $\omega_{s_1}, \ldots, \omega_{s_4}$ from Table 3.1 that have *linearly independent* right eigenvectors. These are eigenvectors from *different* superoperators $\hat{\mathcal{K}}(\omega_i')$ and thus need not be linearly independent. (ii) From this basis $|k_{s_1}), \ldots, |k_{s_4})$ construct a corresponding dual basis $(\bar{k}_{s_1}|, \ldots, (\bar{k}_{s_4}|$. (iii) Construct a fixed point as $\mathcal{G}_{s_1 \ldots s_4} = \sum_{i=1}^{4} \omega_{s_i} |k_{s_i})(\bar{k}_{s_i}|$.

allows one to infer which of the poles are sampled by $\mathcal{G}(\infty)$. As mentioned earlier this can be used to assist the identification of the sampled poles in analytical calculations, which aim to exploit Eq. (3.15).

Given the kernel $\hat{\mathcal{K}}(\omega)$, one can thus find $\mathcal{G}(\infty)$ by iteration *directly* at stationarity, avoiding the transient time-dependence of $\mathcal{G}(t)$. We plot the resulting semigroup approximation in Fig. 3.2(b) and the *different* semigroup, generated by the exact low-frequency kernel

$$-i\hat{\mathcal{K}}(0) = -\frac{\Gamma}{1+\Gamma/(2\gamma)}\Big[|11) - |00)\Big](11| + \left(-i\varepsilon - \frac{\gamma\Gamma}{2(\gamma+i\varepsilon)}\right)|10)(10| + \left(i\varepsilon - \frac{\gamma\Gamma}{2(\gamma-i\varepsilon)}\right)|01)(01|, \tag{3.34}$$

in Fig. 3.2 (a). The $\hat{\mathcal{K}}(0)$ semigroup crosses the exact solution already at intermediate times to approach it from above, whereas the $\mathcal{G}(\infty)$ semigroup approaches it from below. Indeed, in the overdamped regime the occupation decay rate of Eq. (3.33) is always larger than that of Eq. (3.34). As expected, both semigroups have problems with the initial nonlinear time-dependence on the scale γ^{-1} set by the reservoir bandwidth (3.25). Only in the wide-band limit $\gamma \to \infty$ the exact evolution is a semigroup, which in this case is generated by $\mathcal{G}(\infty) = \hat{\mathcal{K}}(0)$.

The slip-corrected semigroup $\Pi(t) \approx e^{-it\mathcal{G}(\infty)}\mathcal{S}$ is shown in Fig. 2.1 in comparison to the ordinary semigroup $e^{-it\mathcal{G}(\infty)}$. Here the slip superoperator is given by

$$\mathcal{S} = |00)\Big[(00| + (11|\Big] + \frac{(\gamma+\gamma')^2}{4\gamma^2}\Big[|11) - |00)\Big](11| + \frac{1}{1-\frac{2\gamma\Gamma}{(\gamma+\gamma')^2}}\Big[|10)(10| + |01)(01|\Big]. \tag{3.35}$$

This slip correction improves the approximation starting from intermediate times as discussed in Sec. 2.3.1, but violates positivity at short-times.

We have also implemented the functional iteration $\mathcal{G}^{(n)}(t)$ for the transient generator explained in Sec. 3.3.2, using Eq. (3.20) with $\mathcal{K}_L = -i[H, \bullet]$ and $H = \varepsilon d^\dagger d$. In Fig. 3.2 (a) and (b) we additionally show the evolutions generated by the approximate $\mathcal{G}^{(n)}(t)$ starting from the initial function $\mathcal{G}^{(0)}(t) = \hat{\mathcal{K}}(0)$ and $\mathcal{G}(\infty)$, respectively. Like the semigroups, each approximation approaches the exact stationary state at large times. However, contrary to the semigroups, each iteration is also very accurate at short times, see Eq. (3.23b). These two constraints enforce rapid convergence at intermediate times throughout the overdamped parameter regime: in Fig. 3.2 (a) and (b) we did not plot the $n = 2$ and $n = 3$ approximations, respectively, since they are hard to distinguish from the exact solution. Thus, Fig. 3.2 (a) shows that Eq. (3.23a), based solely on one

iteration of the *time-nonlocal* memory kernel, already provides a remarkably accurate representation of the *time-local* generator.

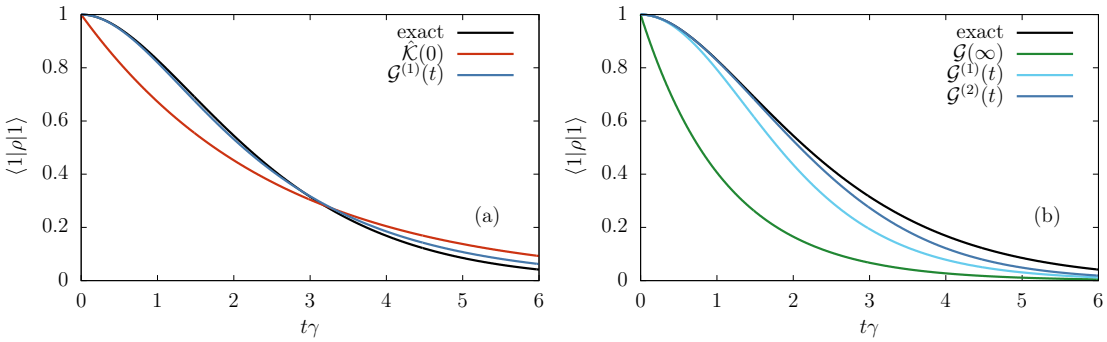

Figure 3.2. Jaynes-Cummings model, overdamped regime $\Gamma/\gamma = 0.495$ ($\gamma'/\gamma = 0.1$): Decay of the probability $\langle 1|\rho(t)|1\rangle$ for the excited state when it is initially occupied, $\rho(0) = |1\rangle\langle 1|$. **(a)** Solutions obtained from the Markovian approximation $\dot{\rho}(t) \approx -i\hat{\mathcal{K}}(0)\rho(t)$ (red) together with the first iteration $\mathcal{G}^{(1)}$ (cyan) of the transient fixed-point equation (3.20) starting from $\mathcal{G}^{(0)} = \hat{\mathcal{K}}(0)$. The exact solution is shown in black. **(b)** Solutions obtained from the Markovian approximation $\dot{\rho}(t) \approx -i\mathcal{G}(\infty)\rho(t)$ (blue) together with two iterations of the transient fixed-point equation, $\mathcal{G}^{(1)}$ (cyan) and $\mathcal{G}^{(2)}$ (green), when started from $\mathcal{G}^{(0)} = \mathcal{G}(\infty)$ and exact solution (black).

3.4.2 | Underdamped dynamics ($\gamma < 2\Gamma$)

For narrow spectral density, $\gamma < 2\Gamma$, the evolution becomes underdamped and non-divisible. The function

$$\pi(t) = e^{-i\varepsilon t}e^{-\gamma t/2}\Big[\cos\Big(\frac{\Omega t}{2}\Big) + \frac{\gamma}{\Omega}\sin\Big(\frac{\Omega t}{2}\Big)\Big] \tag{3.36}$$

now oscillates with frequency $\Omega \equiv -i\gamma' = \sqrt{\gamma(2\Gamma - \gamma)}$ with roots located at

$$t_n = \tfrac{2\pi}{\Omega}\big(n - \tfrac{1}{\pi}\arctan\frac{\Omega}{\gamma}\big) \tag{3.37}$$

This qualitative change of $\pi(t)$ has two consequences.

First, the time-local generator $\mathcal{G}(t)$ exhibits singularities as function of time for every $t = t_n$ [Eq. (3.31)]. As discussed in Sec. 2.1.2 these singularities are physical by restricting the allowed subspace of $\rho(t_n)$ irrespective of the initial state ρ_0. Here the allowed subspace at any t_n contains only the groundstate $|00)$, which makes $\Pi(t_n) = |00)(\mathbb{1}| = |0\rangle\langle 0|\,\mathrm{Tr}\,\bullet$ an entanglement breaking map [114–117].

A second consequence is that the stationary limit of $\mathcal{G}(t)$ does not exist, even though the stationary propagator does converge, $\lim_{t\to\infty}\Pi(t) = |00)(\mathbb{1}|$, and the low-frequency

memory kernel $\hat{\mathcal{K}}(0)$ is well defined. Irrespective of how generic both these complications are, they present perhaps the most crucial challenge to *any* time-local approach. It is well known, for example, that perturbative calculations of $\mathcal{G}(t)$ cannot venture beyond the first singularity on the time axis [37, 93]. In this sense the model presents a worst-case test for both variants of the fixed point iteration.

The stationary iteration [Sec. 3.3.1] is simply expected to fail since it relies on the convergence of $\mathcal{G}(t)$ for $t \to \infty$. Nevertheless, it is interesting to explore what happens. Indeed, the stationary iteration for $\mathcal{G}^{(n)}(\infty)$ does not converge anymore with n. However, $\mathcal{G}$ is always block diagonal and we observe that the iterations for the generator on the occupation subspace $|00), |11)$ converge to

$$\lim_{n\to\infty} \mathcal{G}_o^{(n)}(\infty) = -i\gamma\big[|11) - |00)\big](11|, \tag{3.38}$$

whereas the generator $\mathcal{G}_c^{(n)}$ on the subspace $|01), |10)$ of the coherences oscillates indefinitely with n. In Fig. 3.3a we plot the time-evolution of occupations obtained from the semigroup approximation constructed from Eq. (3.38). In contrast to the semigroup generated by the well-defined $\hat{\mathcal{K}}(0)$, it gives an accurate envelope to the decay of the excited state, even in the strongly underdamped limit, $\gamma \ll \Gamma$ where $\Omega \approx \sqrt{2\Gamma\gamma} \gg \gamma$.

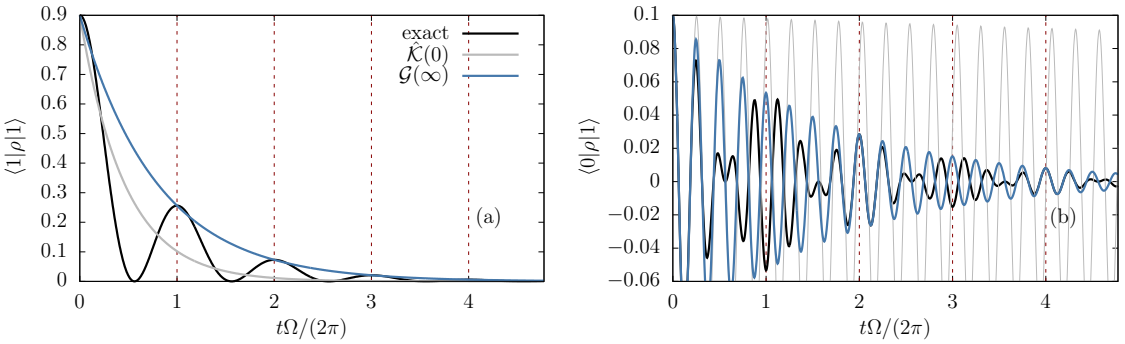

Figure 3.3. Jaynes-Cummings model, underdamped regime $\Gamma/\gamma = 13$ ($\Omega/\gamma = 5$) and $\varepsilon = 20$: **(a)** Decay of the excited state occupation $\langle 1|\rho(t)|1\rangle$ and **(b)** decay of the real part of the coherence $\langle 0|\rho(t)|1\rangle$. The initial state is $\rho(0) = 0.1\big[|00) + |01) + |10)\big] + 0.9|11)$. Shown are the solution for the Markovian approximations $\dot{\rho}(t) \approx -i\mathcal{G}(\infty)\rho(t)$ [blue] with generator obtained by iteration of the stationary fixed point equation (3.9), and $\dot{\rho}(t) \approx -i\hat{\mathcal{K}}(0)\rho(t)$ [gray]. The exact solution is shown in black.

The converged part of the iteration can in fact be related to a regularization of $\lim_{t\to\infty} \mathcal{G}(t)$. Noting that

$$\frac{\dot{\pi}(t)}{\pi(t)} = -i\varepsilon - \tfrac{1}{2}\gamma - \tfrac{1}{2}\Omega \tan\left(\tfrac{1}{2}\Omega t - \arctan\frac{\gamma}{\Omega}\right) \tag{3.39}$$

we see that replacing $\frac{\pi(t)}{\pi(t)} \to -i\varepsilon - \frac{1}{2}\gamma$ amounts to a principal-value time-average over one period. This gives a regularized stationary limit for the generator,

$$\mathcal{G}(\infty)_{\text{reg}} = -i\gamma\big[|11) - |00)\big](11| + (\varepsilon - \tfrac{1}{2}i\gamma)|10)(10| + (-\varepsilon - \tfrac{1}{2}i\gamma)|01)(01|. \quad (3.40)$$

which coincides with the numerically converged block (3.38) of the iteration. The value of the coherence block exposes a key complication of the exact evolution of this model. In Fig. 3.3b, we show that the semigroup constructed from $\mathcal{G}(\infty)_{\text{reg}}$ describes the decay *and* oscillation of the coherences accurately in the center of every *even* time interval. However, it is *also* accurate up to the *sign* in every *odd* interval. The intermediate π-phase jumps occurring in the exact solution are caused by the divergences of the generator at times t_n. The stationary fixed-point iteration may thus still be useful beyond the limitations we assumed in the present paper.

Finally, we consider how the transient fixed-point iteration [Sec. 3.3.2] deals with the time-singularities in this model. In Fig. 3.4 we show how the occupations, starting from the semigroup approximation generated by $\hat{\mathcal{K}}(0)$, converge to the exact solution. The first two iterations only improve the solution before the first singularity and even become unphysical at larger times. However, the following iterations also converge beyond the first singularity. The fifth iteration (not shown) is indistinguishable from the exact solution in the shown time interval. More iterations are required to converge the solution in a larger time interval also including the second singularity. The success of our iteration strategy starting from the memory kernel $\mathcal{K}$ highlights its difference to perturbation theory, which always fails in capturing dynamics beyond a singularity [93]. Thus even time-singular generators can be locally stable fixed points of the functional $\hat{\mathcal{K}}$.

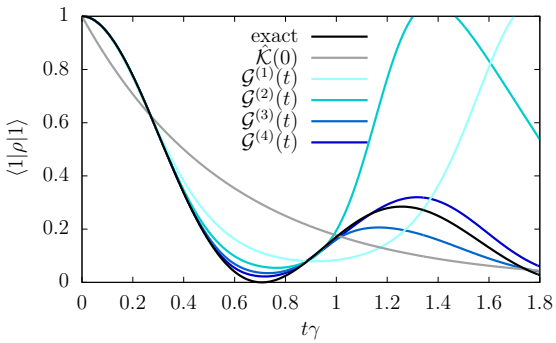

Figure 3.4. Jaynes-Cummings model, underdamped regime: Decay of the probability $\langle 1|\rho(t)|1\rangle$ obtained from generators of the transient iteration for $\Gamma/\gamma = 13$ and $\varepsilon = 20$ using the starting point $\hat{\mathcal{K}}(0)$.

3.5 | Application: Non-interacting quantum dot coupled to an electrode

We complement the above by an analysis of the fermionic resonant level model (RLM). Although its generator has no time-singularities, its time-dependent algebraic structure provides a challenge complementary to the previous model. The Hamiltonian is formally identical to that of the Jaynes-Cummings model except that the reservoir operators are fermionic, $\{b_\omega, b^\dagger_{\omega'}\} = \delta(\omega-\omega')\mathbb{1}$. Also, we consider the reservoir at temperature T and chemical potential μ coupled with an energy independent spectral density $\Gamma = \text{const}$. This is the most basic model of transient electron tunneling from a localized state. Even though it ignores interaction effects, its propagator is feature rich. This was noted in recent work [1], but the nontrivial relations between $\mathcal{K}$ and $\mathcal{G}$ and their spectra noted below were overlooked. The diagonal representation of Π reads (Ref. [1], Eq. (E1))

$$\begin{aligned}\Pi(t) =& \tfrac{1}{2}\Big[|\mathbb{1}) + \mathsf{p}(t)|(-\mathbb{1})^N)\Big]\,(\mathbb{1}| + e^{-\Gamma t}\tfrac{1}{2}|(-\mathbb{1})^N)\,\Big[((-\mathbb{1})^N| - \mathsf{p}(t)(\mathbb{1}|\Big] \\ &+ \sum_{\eta=\pm} e^{(i\eta\varepsilon-\frac{1}{2}\Gamma)t}|d^\dagger_\eta)(d^\dagger_\eta|\end{aligned} \tag{3.41}$$

where $d_+ \equiv d^\dagger$, $d_- \equiv d$. In contrast to the Jaynes-Cummings model its eigenvectors depend on time through the function

$$\mathsf{p}(t) = \sum_{\eta=\pm}\eta\,\mathrm{Im}\Big[\frac{e^{-(\pi T+i\epsilon)t}}{\pi\sinh(\Gamma t/2)}\Phi(e^{-2\pi Tt},1,\tfrac{1}{2}+\tfrac{i\epsilon+\eta\Gamma/2}{2\pi T}) + \frac{e^{\eta\Gamma t/2}}{\pi\sinh(\Gamma t/2)}\Psi(\tfrac{1}{2}+\tfrac{i\epsilon+\eta\Gamma/2}{2\pi T})\Big] \tag{3.42}$$

involving Lerch (Φ) and digamma (Ψ) functions with $\epsilon = \varepsilon - \mu$. This richer structure is also reflected by the analytic properties of the propagator (Ref. [1], App. D)

$$\begin{aligned}\hat\Pi(\omega) =& \sum_{\eta=\pm}\frac{i}{\omega+\eta\varepsilon+i\frac{\Gamma}{2}}|d^\dagger_\eta)(d^\dagger_\eta| + \frac{i}{\omega}\tfrac{1}{2}\Big[|\mathbb{1}) + \hat{\mathsf{k}}\left(\omega+i\tfrac{\Gamma}{2}\right)|(-\mathbb{1})^N)\Big]\,(\mathbb{1}| \\ &+ \frac{i}{\omega+i\Gamma}\tfrac{1}{2}|(-\mathbb{1})^N)\,\Big[((-\mathbb{1})^N| - \hat{\mathsf{k}}\left(\omega+i\tfrac{\Gamma}{2}\right)(\mathbb{1}|\Big]\end{aligned} \tag{3.43}$$

expressed in the Laplace transform $\hat{\mathsf{k}}(\omega)$ of $\mathsf{k}(t) \equiv 2T\sin[(\varepsilon-\mu)t]/\sinh[\pi Tt]$. Its poles, see Table 3.2, include two infinite series for $T > 0$ merging into branch cuts as $T \to 0$.

The generator $\mathcal{G}(t) = i\dot\Pi(t)\Pi^{-1}(t)$ (Ref. [1], Eq. (B14))

$$\mathcal{G}(t) = \sum_{\eta=\pm}\big(-\eta\varepsilon - i\tfrac{1}{2}\Gamma\big)|d^\dagger_\eta)(d^\dagger_\eta| - i\Gamma\tfrac{1}{2}|(-\mathbb{1})^N)\Big[((-\mathbb{1})^N| - \mathsf{g}(t)(\mathbb{1}|\Big] \tag{3.44}$$

Poles $\hat{\Pi}(\omega)$		Eigenvalues $\mathcal{G}(\infty)$
$\omega_0 = 0$		$g_0 = 0$
$\omega_1 = +(\varepsilon-\mu) - i\frac{1}{2}\Gamma$		$g_1 = +(\varepsilon-\mu) - i\frac{1}{2}\Gamma$
$\omega_2 = -(\varepsilon-\mu) - i\frac{1}{2}\Gamma$		$g_2 = -(\varepsilon-\mu) - i\frac{1}{2}\Gamma$
$\omega_3 = -\Gamma$		$g_3 = -\Gamma$
$\omega_{4+2n} = \omega_1 - i\pi T(2n+1)$	$\leftarrow$	*Possibly closer to real axis*
$\omega_{5+2n} = \omega_2 - i\pi T(2n+1)$	$\leftarrow$	*than ω_3!*

TABLE 3.2. RLM: Poles of $\hat{\Pi}(\omega)$ ($n = 0, 1, 2, \ldots$) and eigenvalues of $\mathcal{G}(\infty)$.

is obtained with $\mathsf{g}(t) = \int_0^t ds e^{-\frac{1}{2}\Gamma s}\mathsf{k}(s)$. The evolution changes its Markovian character from CP divisible ($|\mathsf{g}(t)| \leq 1$) close to resonance to non-divisible sufficiently far from resonance. The kernel $\hat{\mathcal{K}}(\omega) = \omega\mathcal{I} - i\hat{\Pi}^{-1}(\omega)$ can be expressed as (Ref. [1], (D13))

$$\hat{\mathcal{K}}(\omega) = \sum_{\eta=\pm}\big(-\eta\varepsilon - i\tfrac{1}{2}\Gamma\big)|d_\eta^\dagger)(d_\eta^\dagger| - i\Gamma\tfrac{1}{2}|(-\mathbb{1})^N)\Big[((-\mathbb{1})^N| - \hat{\mathsf{k}}\big(\omega + i\tfrac{1}{2}\Gamma\big)(\mathbb{1}|\Big]. \quad (3.45)$$

Unlike the Jaynes-Cummings model, none of these superoperators commute with themselves at different time/frequency/parameter values (on which their eigen*vectors* depend) nor with each other (since $\mathsf{p}(t), \mathsf{k}(t), \mathsf{g}(t)$ all differ). We now show that, nevertheless, the sampling relation (3.15) explicitly holds.

Table 3.2 shows that the four eigenvalues of $\mathcal{G}(\infty)$ indeed coincide with four of the poles of $\hat{\Pi}(\omega)$, which coincide with the four frequency-independent eigenvalues of $\hat{\mathcal{K}}(\omega)$. However, the propagator $\hat{\Pi}(\omega)$ has infinitely many more poles $\{\omega_n\}_{n\geq 4}$ which arise from the function $\hat{\mathsf{k}}\big(\omega + i\frac{1}{2}\Gamma\big)$ located in the eigenvectors of $\hat{\mathcal{K}}(\omega)$. These are not sampled as explained after Eq. (3.13). For $T \leq \Gamma/(2\pi)$ some of these non-sampled poles lie *in between* the sampled poles ω_1, ω_2 and ω_3 and form branch cuts as $T \to 0$.

In Table 3.3 we illustrate how $\mathcal{G}(\infty)$ also nontrivially samples the eigen*vectors* of $\hat{\mathcal{K}}(\omega)$ as follows: (i) We collect one right eigenvector from each of the four *different* superoperators $\hat{\mathcal{K}}(0)$, $\hat{\mathcal{K}}(\pm\varepsilon - i\frac{1}{2}\Gamma)$ and $\hat{\mathcal{K}}(-i\Gamma)$. (ii) This gives four right vectors $|\hat{k}_{j_i}(g_i)) = |g_i)$. (iii) From this set one *algebraically* constructs a set of biorthonormal covectors $(g_i'|$. This way we remarkably obtain the left and right eigenvectors of $\mathcal{G}(\infty)$ as given by Eq. (3.44) using the *analytic* property $\mathsf{g}(\infty) = \hat{\mathsf{k}}(i\frac{1}{2}\Gamma)$. Note in particular that one would *not* obtain the correct *left* eigenvectors of $\mathcal{G}(\infty)$ by naively sampling the left pole-eigenvectors of the kernels. For eigenvalue $g_3 = -i\Gamma$ a difference arises as indicated by the two arrows in Table 3.3.

We observe that for the RLM each eigenvalue-pole is sampled precisely once by $\mathcal{G}(\infty)$. Combined with the mere assumption that $\mathcal{G}(\infty)$ is diagonalizable the sampling

(iv) Don't copy these!	$\hat{\mathcal{K}}(g_i)$	*(i) Copy these*	*(iii) Biorthogonalize*	$\mathcal{G}(\infty)$	*(ii) Collect here*
$(\hat{k}'_{j_i}(g_i)\|$	$\hat{k}_{j_i}(g_i)$	$\|\hat{k}_{j_i}(g_i))$	$(g'_i\|$	g_i	$\|g_i)$
$(\mathbb{1}\|$	0	$\frac{1}{2}\big[\|\mathbb{1}) + \hat{\mathsf{k}}(i\frac{\Gamma}{2})\|(-\mathbb{1})^N)\big]$	$(\mathbb{1}\|$	0	$\frac{1}{2}\big[\|\mathbb{1}) + \hat{\mathsf{k}}(i\frac{\Gamma}{2})\|(-\mathbb{1})^N)\big]$
$\downarrow \quad (d^\dagger_\eta\|$	$-\eta\varepsilon - i\frac{1}{2}\Gamma$	$\|d^\dagger_\eta)$	$\downarrow \quad (d^\dagger_\eta\|$	$-\eta\varepsilon - i\frac{1}{2}\Gamma$	$\|d^\dagger_\eta)$
$\frac{1}{2}\big[((-\mathbb{1})^N\| - \hat{\mathsf{k}}(-i\frac{\Gamma}{2})(\mathbb{1}\|\big]$	$-i\Gamma$	$\|(-\mathbb{1})^N)$	$\frac{1}{2}\big[((-\mathbb{1})^N\| - \hat{\mathsf{k}}(i\frac{\Gamma}{2})(\mathbb{1}\|\big]$	$-i\Gamma$	$\|(-\mathbb{1})^N)$

TABLE 3.3. RLM: Sampling of memory kernel $\hat{\mathcal{K}}(\omega)$ by the stationary generator $\mathcal{G}(\infty)$ [Eq. (3.15)]. Left columns: for each *different* superoperator $\hat{\mathcal{K}}(g_i)$ we list *one* pole-eigenvalue with its left and right eigenvector. Right columns: collecting the right eigenvectors from $\hat{\mathcal{K}}(g_i)$ and biorthonormalizing we construct the left eigenvectors $(g'_i|$. Row $i = 1, 2$ corresponds to $\eta = \pm$.

relation (3.15) thus completely determines this superoperator, because it exhausts the number of eigenvalue-poles ($d^2 = 4$).

For the RLM the numerical stationary iteration [Sec. 3.3.1] starting from any initial $\mathcal{G}^{(0)}(\infty)$ also converges to the exact stationary generator. This holds for *all* parameters of the model. Strikingly, using $\mathcal{G}^{(0)}(\infty) = \hat{\mathcal{K}}(0)$ as a starting point the iteration terminates right away at the *zeroth* iteration, implying an exact relation[5]

$$\mathcal{G}(\infty) = \hat{\mathcal{K}}(0). \tag{3.46}$$

Using $\mathsf{g}(\infty) = \hat{\mathsf{k}}(i\frac{1}{2}\Gamma)$ one verifies Eq. (3.46) comparing Eqs. (3.45) and (3.44).

The transient iteration [Sec. 3.3.2] starting from the constant ansatz $\mathcal{G}^{(0)}(t) = \hat{\mathcal{K}}(0)$ does not terminate immediately, because the evolution is not a semigroup (except for $T \to \infty$ or $\varepsilon - \mu \to \infty$ or $\varepsilon = \mu$) [1]. However, for this ansatz the *first* transient iteration $\mathcal{G}^{(1)}(t) = \int_0^t ds \mathcal{K}(t-s) e^{i\hat{\mathcal{K}}(0)(t-s)} = \mathcal{G}(t)$ does give the exact solution, again for all parameters of the model. This reflects an exact relation [Ref. [1], Eqs. (52a), (D15)]

$$\mathcal{G}(t) = \int_0^t ds \mathcal{K}(t-s), \tag{3.47}$$

which for $t \to \infty$ again implies Eq. (3.46). In Fig. 3.5 we show the time-dependence of the occupations for the zeroth and first iteration. Unlike the Jaynes-Cummings model, the level can initially actually fill up more before decaying to the empty stationary state, an effect caused by time-dependence of eigenvectors of $\Pi(t)$ [Eq. (3.41)]. This reentrant behavior is completely produced in one step by $\mathcal{G}^{(1)}(t)$ from the Markov semigroup

[5] This relation should not be misunderstood as saying that "$\mathcal{G}(\infty)$ only samples $\mathcal{K}(\omega)$ at $\omega = 0$" and that there is something trivial about the sampling: keeping only $\omega = 0$ in Eq. (3.15) would give $\mathcal{G}(\infty) = 0$. Instead, this relation is a nontrivial statement about the memory kernel of this model: sampling $\hat{\mathcal{K}}(\omega)$ according to Eq. (3.15) at eigenvalue-poles – including ones at *nonzero* frequencies and *ignoring* eigenvector poles / branch cuts – exactly reproduces the *zero*-frequency kernel $\hat{\mathcal{K}}(0)$.

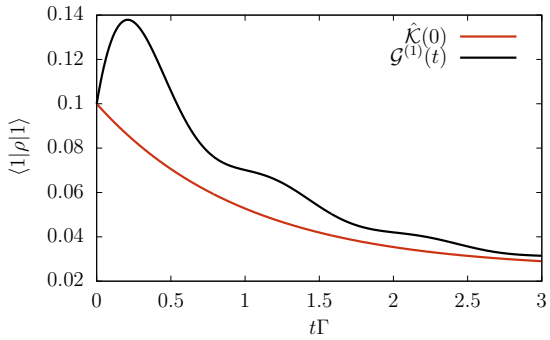

Figure 3.5. Decay of the occupation $\langle 1|\rho(t)|1\rangle$ in the RLM for $\varepsilon - \mu = 2\pi\Gamma$, $T = 0.1 \cdot \Gamma/(2\pi)$ obtained from $\mathcal{G}^{(0)}(t) = \hat{\mathcal{K}}(0)$ and $\mathcal{G}^{(1)}(t) = \mathcal{G}(t)$. The former corresponds to a Markov semigroup approximation using $\hat{\mathcal{K}}(0)$, which is never able to describe the initial growth of the occupation *away* from the stationary value. When used as initial guess in the transient iteration the exact solution is recovered by the fixed-point equation (3.4) after a single step.

approximation $\mathcal{G}^{(0)} = \hat{\mathcal{K}}(0) = \mathcal{G}(\infty)$, which can never capture an initial growth in the "wrong direction".

In fact, any trace-preserving constant ansatz $\mathcal{G}^{(0)}(t) = X$ gives the exact solution after one iteration, $\mathcal{G}^{(1)}(t) = \mathcal{G}(t)$ as shown in App. C. Furthermore, starting from an arbitrary time-constant superoperator, $\mathcal{G}^{(0)} = X \neq 0$, the *second* transient iteration always reaches the fixed point, because the first iteration $\mathcal{G}^{(1)}(t)$ produces a trace-preserving generator [Eq. (3.6)]. That two iterations suffice for *all* parameters of the model is remarkable since this includes the extended parameter regime where the level is sufficiently off-resonant and the evolution is not CP-divisible [1, 3]. For comparison, in the underdamped regime where the Jaynes-Cummings model is non-CP-divisible many iterations are required [Fig. 3.3]. The termination of the fixed-point iteration is closely related to truncations of (renormalized) coupling expansions for $\mathcal{K}(t)$ and $\Pi(t)$ for fermionic models, which occur in the absence of *interactions* and for energy independent coupling, see Sec. 4.3.2. This indicates that the number of iterations is related to dynamically generated many-body effects.

3.6 | Summary

We have found the general connection between two canonical approaches to the dynamics of open quantum systems, the time-local and time-nonlocal quantum master equation. This relation extends the response function of an open system – the frequency-domain memory kernel $\hat{\mathcal{K}}(\omega)$ – to a functional mapping of *superoperator-functions of time*

of which the generator is a *fixed point*: $\mathcal{G}(t,t_0) = \hat{\mathcal{K}}[\mathcal{G}](t,t_0)$. The fixed-point property expresses that the generator is a characteristic "frequency" of the evolution produced by the memory kernel. This is very similar to how pole frequencies characterize the response of linear systems in physical sciences and engineering [159]. In our general quantum setting, we showed how the fixed-point equation provides a self-consistent solution of the complicated gradient expansion [Eq. (3.18) and (B.7)]. Interestingly, this also revealed a connection of the time-convolutionless approach to a Moyal formulation of quantum theory of *open* systems [Eq. (B.5)].

We obtained several general insights into the role of the frequency dependence of the memory kernel. We precisely determined how the stationary generator $\mathcal{G}(\infty)$ samples the *right* eigenvectors and eigenvalues of the memory kernel $\hat{\mathcal{K}}(\omega)$ at zero *and nonzero* characteristic frequencies of the evolution. The sampled frequencies form a finite subset of the exact poles of the frequency-domain evolution as obtained by the Laplace-resolvent method in the time-nonlocal approach. Remarkably, knowing only the location of these poles in the complex plane in principle suffices to *completely construct* the stationary generator $\mathcal{G}(\infty)$ from the memory kernel. This can be exploited to significantly simplify analytical calculations. This generator may also be obtained numerically by iterating the stationary fixed-point equation (3.9).

Similarly, the full transient generator may be obtained from the memory kernel by iterating the functional fixed-point equation (3.4). At each iteration the approximate generator is both initially *and* asymptotically accurate. We have shown that even time-singular generators can be locally stable and also showcased an evolution with time-dependent eigenvectors whose generator is exactly found after at most two iterations. The apparent success of this iteration strategy raises several interesting questions:

- The convergence of the (transient and stationary) functional iteration formally relies on the stability of the fixed points in the space of generators, raising the question how this stability is encoded into $\hat{\mathcal{K}}$. For scalar functions $k(x)$ (with $x \in \mathbb{R}$) it is well known that a fixed point $x_* = k(x_*)$ is stable if $|k'(x_*)| < 1$. We expect that by generalizing this stability condition to the functionals $\hat{\mathcal{K}}(\bullet)$ and $\hat{\mathcal{K}}[\bullet]$ that there exists a stability equation of the schematic form "$|\partial\hat{\mathcal{K}}/\partial\mathcal{G}| < 1$". This might expose further unexplored non-perturbative relations connecting the time-local and time-nonlocal approaches.

- A related fundamental question concerns the uniqueness of the fixed points. For the stationary functional $\hat{\mathcal{K}}(\bullet)$ we already found that additional fixed points $\tilde{\mathcal{G}}(\infty) \neq \mathcal{G}(\infty)$ can exist [Sec. 3.4.1]. However, this does not imply that the transient functional $\hat{\mathcal{K}}[\bullet]$ must also have fixed points other than $\mathcal{G}(t)$. For example, if there

were some $\tilde{\mathcal{G}}(t)$ obeying $\hat{\mathcal{K}}[\tilde{\mathcal{G}}(t)] = \tilde{\mathcal{G}}(t) + e^{-\lambda t}$, then $\tilde{\mathcal{G}}(t)$ would not be a fixed point of the transient functional, but $\tilde{\mathcal{G}}(\infty)$ would be a fixed point of the stationary functional. Thus the uniqueness of the fixed point warrants additional study to lend further support to the iterative method and to physically understand what guarantees the uniqueness observed in practice.

- We have seen [Sec. 3.4] that starting from a semigroup approximation, each iteration of the transient functional incorporates more of the "memory" integral over $\mathcal{K}$ into $\mathcal{G}$ in a stepwise fashion. This defines a discrete flow in the functional superoperator space and is reminiscent of a renormalization group flow. The range of attraction around the fixed point must somehow be related to physical retardation properties of the open system. It is an intriguing question whether the nature of the flow could be used to classify open systems in some way, similar to the way RG fixed points are used to characterize field theories and critical systems.

Since our results apply quite generally and can be tailored to both numerical [25, 26] and analytical [23, 24, 27] applications, they seem relevant to the challenging problems of strongly interacting open quantum systems dominated by nonperturbative dissipation and memory effects. Altogether, this provides new starting points for combining well-developed memory kernel formalisms to access the advantages of a time-local description.

4

The connection between time-local and time-nonlocal series expansions

In the last chapter we found that the time-local generator $\mathcal{G}$ is a fixed point of the Laplace-like transformation functional (3.5) induced by the time-nonlocal memory kernel $\mathcal{K}$. Besides revealing surprising exact relations between spectral properties of $\mathcal{G}$, $\mathcal{K}$ and Π [Sec. 3.2], we explained how to iteratively construct from a given $\mathcal{K}$ an equivalent $\mathcal{G}$, guaranteeing that both produce the *exact same* dynamics [Sec. 3.3]. In this chapter we instead explore how the fixed-point relation can be used to translate $\mathcal{K}$-methods into $\mathcal{G}$-methods, giving *different* approximations. Specifically, we will show how a series expansion for $\mathcal{K}$ can be transformed into a corresponding series for $\mathcal{G}$. The precise connection between such corresponding series was an open problem even for the well understood bare perturbation theories in the coupling to the environment, which were independently developed for $\mathcal{K}$ and $\mathcal{G}$.

This transformation of methods from $\mathcal{K}$ to $\mathcal{G}$ is of interest because several techniques have been developed to compute $\mathcal{K}$ for complicated models featuring strong interaction and memory effects [23–27, 29, 30, 133, 134, 160–162]. By contrast, the computation of the time-local generator is much more challenging, but nevertheless has been approached from various angles [38, 39, 42, 163, 164]. As discussed in Sec. 1.2 this is motivated, for example, by the fact that $\mathcal{G}$ is the quantity of choice for understanding (non-)Markovianity by its connection to divisibility [Sec. 2.2], which seems practically impossible to achieve with a description of the dynamics based on $\mathcal{K}$ [48, 49, 53].

The main result presented in Sec. 4.1 is that the fixed-point equation (3.5) reveals a *recursive* relation between perturbative expansions of $\mathcal{K}$ and $\mathcal{G}$, allowing a series for the kernel $\mathcal{K}$ to be translated directly into a corresponding series for the more complicated generator $\mathcal{G}$. As discussed in Sec. 2.3.2, approximations to $\mathcal{K}$ and $\mathcal{G}$ computed to the *same* order using the *same* perturbative scheme give *different* approximate evolutions Π due to

the *difference in time (non-)locality*. This raises the intriguing but delicate question which of the two expansions does "better", an issue calling for a general way to meaningfully compare such expansions. In Sec. 4.3 we illustrate how this can be done for the example of the interacting Anderson quantum dot by calculating both $\mathcal{K}$ and $\mathcal{G}$ in bare perturbation theory. We do this using a particular diagrammatic language [23, 136], but we stress that this technique is not at all essential to our central result. The same result is obtained, for instance, using the Nakajima-Zwanzig projection technique instead. We also explore a more powerful *renormalized* perturbation theory for $\mathcal{K}$, which was initially developed as a first stage of a continuous RG-flow method for open quantum systems [23, 165], to deal with strong dissipative coupling and non-equilibrium. It was later studied on its own merits [1, 135–137] and revealed powerful exact relations [3, 137]. However, applications of this renormalized series to the *transient* time-evolution of interacting systems analyzed here were not yet explored.

4.1 | Recursive expansion of the generator in terms of the memory kernel

Given a memory kernel $\mathcal{K}$ (or an approximation to it), we ask the question how to construct a corresponding (approximation to the) generator $\mathcal{G}$. Whereas in Sec. 3.3.2 we explained how to do this using a fixed point iteration of the functional (3.5), here we instead focus on useful formal implications of the fixed-point equation (3.4), in particular, how it leads to a natural reorganization of perturbation expansions *when the time-(non)locality* of the quantum master equation is *altered*.

Thus, the goal is to find a perturbative expansion for $\mathcal{G}$ based on a corresponding expansion for $\mathcal{K}$. By "corresponding" we mean that both series count powers of the same formal expansion parameter. We start by decomposing $\mathcal{K}$ as in Eq. (2.4) into a time-local contribution $\mathcal{K}_L$, which is at first taken to be the uncoupled system Liouvillian, and a time-nonlocal contribution $\mathcal{K}_N$ denoting the remaining environment part due to non-zero coupling. The kernel $\mathcal{K}^{(0)}(t,s) := \mathcal{K}_L\bar{\delta}(t-s)$ producing semigroup dynamics $\Pi^{(0)} := e^{-i\mathcal{K}_L t}$ via Eq. (2.3) will be the reference point of the perturbation theory. Importantly, we will also allow for a renormalized expansion, in which a *further* time-local contribution – which was still contained in $\mathcal{K}_N$ – is included in $\mathcal{K}_L$, making the reference evolution $\Pi^{(0)}$ *dissipative*, see details below. In either case we assume for simplicity that $\mathcal{K}_L$ is time-independent, but this is not a limiting assumption.

Decomposing $\mathcal{G}(t,t_0) = \mathcal{K}_L + \mathcal{G}_N(t,t_0)$ analogously, the fixed point equation (3.4)

implies that $\mathcal{G}_N$ obeys

$$\mathcal{G}_N(t,t_0) = \int_{t_0}^{t} ds\, \mathcal{K}_N(t,s)\mathcal{T}_{\rightarrow} e^{i\int_s^t d\tau[\mathcal{K}_L+\mathcal{G}_N(\tau,t_0)]}. \tag{4.1}$$

We correspondingly use $\mathcal{G}^{(0)} = \mathcal{K}_L$ as a reference for the expansion of $\mathcal{G}$. Assuming that the nonlocal part of the memory kernel is given by a series in some formal parameter, $\mathcal{K}_N = \mathcal{K}^{(1)} + \mathcal{K}^{(2)} + \ldots$, we can derive the *corresponding* series for $\mathcal{G}_N = \mathcal{G}^{(1)} + \mathcal{G}^{(2)} + \ldots$ in the *same* parameter by first expanding the anti-time-ordered exponential in Eq. (4.1) and then matching orders. The first two terms explicitly read

$$\mathcal{G}^{(1)}(t,t_0) = \int_{t_0}^{t} ds\, \mathcal{K}^{(1)}(t,s)e^{-i\mathcal{K}_L(s-t)}, \tag{4.2}$$

$$\begin{aligned}\mathcal{G}^{(2)}(t,t_0) = &\int_{t_0}^{t} ds\, \mathcal{K}^{(2)}(t,s)e^{-i\mathcal{K}_L(s-t)} \\ &+ i\int_{t_0}^{t} ds \int_{s}^{t} d\tau\, \mathcal{K}^{(1)}(t,s)e^{-i\mathcal{K}_L(s-\tau)}\mathcal{G}^{(1)}(\tau,t_0)e^{-i\mathcal{K}_L(\tau-t)}.\end{aligned} \tag{4.3}$$

The general n-th order $\mathcal{G}^{(n)}$ is similarly given by

$$\mathcal{G}^{(n)}(t) = \sum_{l=0}^{n-1} i^l \sum_{\Sigma_i m_i = n} \int_{t_0<\tau_0<\cdots<\tau_l<t} d\tau_0 \ldots d\tau_l \mathcal{K}^{(m_0)}(t,\tau_0)e^{-i\mathcal{K}_L(\tau_0-\tau_1)}\mathcal{G}^{(m_1)}(\tau_1)\cdots\mathcal{G}^{(m_l)}(\tau_l)e^{-i\mathcal{K}_L(\tau_l-t)}, \tag{4.4}$$

where the second sum runs over $m_0, \ldots, m_l > 0$. We thus see that the fixed-point equation automatically organizes the series expansion of $\mathcal{G}_N$ into a *recursive* form. It is well known that when computing the memory kernel $\mathcal{K}$, for example using standard projection operator or diagrammatic techniques, one obtains only time ordered contributions (convolutions), whereas the generator $\mathcal{G}$ has a more complicated structure involving combinations of non-time ordered integrations. The recursive reorganization implied by the fixed-point relation completely disentangles this nontrivial structure: Eq. (4.4) reveals that collecting all *time-ordered* contributions one obtains precisely the various memory kernel components $\mathcal{K}^{(n)}$ – obtainable by well-developed *standard* techniques – and that the remaining integrations are exclusively anti-time-ordered. In the remainder of the paper we will exploit this insight using the diagrammatic approach, noting that one may equivalently use the projection operator technique.

So far we refrained from making use of the propagator. However, if the orders of Π are formally known this can be useful. By similarly expanding $\Pi = \Pi^{(0)} + \Pi^{(1)} + \ldots$ and inserting into $\mathcal{G}_N\Pi = \mathcal{K}_N * \Pi$, written as $\mathcal{G}_N = \left[\mathcal{K}_N * \Pi - \mathcal{G}_N\left(\Pi - e^{-i\mathcal{K}_L t}\right)\right] e^{i\mathcal{K}_L t}$, one obtains a useful reorganization, expressing the n-th order of $\mathcal{G}$ in terms of its lower

orders with the help of both the memory kernel $\mathcal{K}$ and the propagator up to order n,

$$\mathcal{G}^{(n)} = \mathcal{K}^{(n)} * \Pi^{(0)} e^{i\mathcal{K}_L t} + \sum_{j=1}^{n-1} \left[\mathcal{K}^{(n-j)} * \Pi^{(j)} - \mathcal{G}^{(n-j)} \cdot \Pi^{(j)} \right] e^{i\mathcal{K}_L t}. \tag{4.5}$$

The above relations are key results because they apply generally to open quantum system.

Since the fixed-point equation is flexible and can be exploited in various ways, it is important to keep a point in mind that we already touched on in Sec. 2.3.2: We are interested in comparing different solutions generated by corresponding perturbative expansions, the difference arising from their time-(non)locality. We want to explore whether summing up partial contributions in a time-local framework leads to better results in some sense than when doing the corresponding sum in the time-nonlocal framework. Given, for example, a second order approximation to the kernel, $\mathcal{K}_{\text{pert}} = \mathcal{K}_L \bar{\delta} + \mathcal{K}^{(1)} + \mathcal{K}^{(2)}$, it is only meaningful to compare the evolution it produces via Eq. (2.3) with the evolution produced via Eq. (2.9) by the *perturbative* $\mathcal{G}_{\text{pert}} \approx \mathcal{K}_L + \mathcal{G}^{(1)} + \mathcal{G}^{(2)}$, where we in both cases expand in the same parameter. When taking $\mathcal{K}_L = L := [H, \bullet]$, this corresponds to contrasting the well-established bare perturbation expansions of $\mathcal{K}$ [133, 134, 166] and $\mathcal{G}$ [34–36, 38, 93, 112, 113] whose traditional derivations are very difficult to compare. Since we are able to treat both expansions in the same, standard way a comparison becomes possible.

This perturbative generator $\mathcal{G}_{\text{pert}}$ has to be contrasted with the approximate *self-consistent* generator $\mathcal{G}_{\text{sc}}$, which produces exactly the *same* evolution via Eq. (2.9) as the perturbative $\mathcal{K}_{\text{pert}}$ does via Eq. (2.3). In other words, it satisfies the fixed-point equation $\mathcal{G}_{\text{sc}} = \hat{\mathcal{K}}_{\text{pert}}[\mathcal{G}_{\text{sc}}]$ being self-consistent relative to the kernel approximation. This approximate but self-consistent generator *differs* from $\mathcal{G}_{\text{pert}}$ considered in this chapter, $\mathcal{G}_{\text{sc}} \neq \mathcal{G}_{\text{pert}}$. One should realize that when using $\mathcal{G}_{\text{sc}}$ one essentially gives up calculating the generator directly but formulates all approximations using $\mathcal{K}$ and afterwards produces the *equivalent* generator (as opposed to *corresponding*).

4.2 | Comparing approximations

Before we start investigating different approximations, we note that one obvious comparison to consider is the difference of the approximate state evolution with the exact one. In the following we will quantify the difference between two density operators ρ and σ using the trace distance

$$D(\rho, \sigma) := \frac{1}{2} \|\rho - \sigma\|_1, \tag{4.6}$$

featuring on the right hand side the trace norm we already encountered in the discussion of Markovianity in Sec. 2.2.2. This is a metric on the space of density operators with a physical meaning: it determines the optimal probability [126] of distinguishing ρ and σ drawn from an unbiased ensemble. Also, given any observable A it can be shown that the trace distance bounds the difference of its expectation value using either ρ or σ relative to the largest singular value $\|A\|_\infty$ (Schatten ∞-norm [167]):

$$\left|\langle A\rangle_\rho - \langle A\rangle_\sigma\right| / \|A\|_\infty \leq 2D(\rho,\sigma). \tag{4.7}$$

Of course, for problems of actual interest the exact solution needed for this comparison is not available. Then the most basic thing to check is whether the approximation stays *physical*, for which two criteria need to be fulfilled. First, the trace needs to be preserved. This is automatically guaranteed in Eqs. (4.20a)–(4.20c) below term by term, because on the left there is always a creation superfermion $G^+_{\eta\sigma}$, which has the trace functional as a left zero eigenvector [136]. Second, an evolution needs to be CP. It is well known how to check this based on the *solution* for the *propagator* $\Pi(t)$ by checking the positivity of the so-called Choi operator [167], but frequently this is not discussed in studies of advanced approximation strategies which go beyond the applicability of the GKSL theorem [118, 119]. One should note that CP can *not* be determined by looking at a trajectory $\rho(t) = \Pi(t)\rho_0$ starting from some specific initial state ρ_0, see Ref. [1] for details and examples. Moreover, an evolution $\Pi(t)$ may even produce valid quantum states $\rho(t)$ for any valid input state ρ_0, i.e., be positivity preserving, but *still fail* to be completely positive. This is not a rare situation and such unphysical maps are well known from their mathematical application to the detection of entanglement [168].

4.3 | Application: Interacting quantum dot

As an example, we consider a single orbital quantum dot with spin described by

$$H = \epsilon(n_\uparrow + n_\downarrow) + U n_\uparrow n_\downarrow. \tag{4.8}$$

Here ϵ is the energy of the orbital, $n_\sigma = d^\dagger_\sigma d_\sigma$ the number operator for spin σ and U is the Coulomb interaction. This quantum dot is connected to several free electron reservoirs

$$H_R = \sum_{r\sigma} \int d\omega(\omega + \mu_r) a^\dagger_{r\sigma}(\omega) a_{r\sigma}(\omega). \tag{4.9}$$

We allow that the reservoirs labeled by r are initially in thermal equilibrium at different temperatures T_r and chemical potentials μ_r, but in illustrations we focus on $T_r = T$. The

tunnel junctions are modeled with the Hamiltonian

$$H_T = \sum_{r\sigma} \int d\omega \sqrt{\frac{\Gamma_{r\sigma}}{2\pi}} \left(a^\dagger_{r\sigma}(\omega) d_\sigma + d^\dagger_\sigma a_{r\sigma}(\omega) \right), \tag{4.10}$$

where $\Gamma_{r\sigma}$ is the real-valued, spin-dependent spectral density of reservoir r assumed to be energy independent (wideband limit). Thus the total Hamiltonian is

$$H_{\text{tot}} = H + H_R + H_T. \tag{4.11}$$

The open system dynamics is calculated by tracing out the reservoirs obtaining an exact description of the evolution of the density operator of the quantum dot. For this effective description a formalism based on superoperators is convenient. Here we use the superfermion approach to Liouville space introduced in Ref. [23] using the later formulation of Ref. [136], where details and comparison with other constructions can be found. Defining first the shorthand notation

$$d_{\eta\sigma} \coloneqq \begin{cases} d^\dagger_\sigma & \text{for} \quad \eta = + \\ d_\sigma & \text{for} \quad \eta = - \end{cases}, \tag{4.12}$$

the superfermions are superoperators defined as

$$G^p_{\eta\sigma} \bullet \coloneqq \frac{1}{\sqrt{2}} \left[d_{\eta\sigma} \bullet + p(-\mathbb{1})^n \bullet (-\mathbb{1})^n d_{\eta\sigma} \right], \tag{4.13}$$

where $p = +$ gives a creation and $p = -$ an annihilation superoperator and

$$(-\mathbb{1})^n \coloneqq (\mathbb{1} - 2n_\uparrow)(\mathbb{1} - 2n_\downarrow) \tag{4.14}$$

denotes the fermion parity operator. The superfermions act in the Liouville-Fock space analogously to the way that ordinary creation/annihilation operators act in the Hilbert-Fock space. The *supervacuum* state $|0)$ corresponding to Eq. (4.13) is given by the infinite-temperature stationary state $|0) \coloneqq \frac{1}{2}\mathbb{1}$ considered as a supervector. From this a complete basis for the Liouville-Fock space is generated by the superfermionic creation operators ($G^+_{\eta\sigma}$) in the usual way [135]. This choice of fields and vacuum is particularly well-adapted to the perturbation expansion, as we will see [Eq. (4.26)]. Furthermore, the superfermions anticommute,

$$\left\{ G^{p_1}_{\eta_1\sigma_1}, G^{p_2}_{\eta_2\sigma_2} \right\} = \delta_{p_1\bar{p}_2} \delta_{\eta_1\bar{\eta}_2} \delta_{\sigma_1\sigma_2}, \tag{4.15}$$

where $\bar{x} \coloneqq -x$, and they satisfy a super-Pauli principle, which states that it is formally impossible to create or destroy two identical superfermions

$$\left(G^p_{\eta\sigma} \right)^2 = 0. \tag{4.16}$$

This implies that the maximally filled state in Liouville space holds four superfermions and any term with five or more G^+ in a row must vanish algebraically. In the same fashion as ordinary operators are written down as strings of creation/annihilation field operators this can also be done for superoperators. For example, the local Liouvillian, $L\bullet := [H, \bullet]$, is given by [136]

$$L = \sum_{\eta\sigma} \left[\bar{\eta} \left(\epsilon + \tfrac{1}{2}U \right) G^+_{\bar{\eta}\sigma} G^-_{\eta\sigma} + \tfrac{1}{2}U \left(G^+_{\bar{\eta}\sigma} G^-_{\eta\sigma} G^-_{\bar{\eta}\bar{\sigma}} G^-_{\eta\bar{\sigma}} + G^+_{\bar{\eta}\bar{\sigma}} G^+_{\eta\bar{\sigma}} G^+_{\bar{\eta}\sigma} G^-_{\eta\sigma} \right) \right]. \tag{4.17}$$

4.3.1 | Bare expansions – Success of the time-local approach

Bare perturbation theory for the memory kernel $\mathcal{K}$

One systematic way of computing $\mathcal{K}$ is by a bare perturbation expansion in the coupling to the environment. This is substantially simplified [135, 169–171] by combining diagrammatic [134, 161] and Liouville-Fock space techniques [23, 24, 137] and exploiting the wideband limit from the very beginning. We refer the reader to Ref. [136] for further details. The crucial underlying assumption for this is that the reservoirs are *non-interacting*: in this case all multi-particle correlation functions of the reservoirs – determining the time-nonlocal backaction of the system via the memory kernel – factorize into one-particle functions (Wick-theorem).

Because the total Hamiltonian H_{tot} is time-independent, the kernel only depends on the difference of its time arguments, $\mathcal{K}(t,s) = \mathcal{K}(t-s)$. Using the decomposition (2.4) we have $\mathcal{K}_L = L$ and the goal is to compute the nonlocal part $\mathcal{K}_N = \mathcal{K}^{(1)} + \mathcal{K}^{(2)} + \ldots$, where each term $\mathcal{K}^{(n)}$ contains n tunneling contributions [Eq. (4.10)]. Because of the bilinear structure of H_T it follows that all odd orders vanish. The first two nonvanishing orders are then diagrammatically represented by

$-i\mathcal{K}^{(2)}(t) =$  , (4.18)

$-i\mathcal{K}^{(4)}(t) =$  . (4.19)

The diagrams are specifically given by

$$= -\sum_{p\eta\sigma} \gamma^{p}_{\eta\sigma}(t) G^{+}_{\eta\sigma} e^{-iLt} G^{\bar{p}}_{\bar{\eta}\sigma}, \tag{4.20a}$$

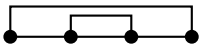

$$= \sum_{p_1\eta_1\sigma_1} \sum_{p_2\eta_2\sigma_2} \int_0^t dt_1 \int_0^{t_1} dt_2 \gamma^{p_1}_{\eta_1\sigma_1}(t) \gamma^{p_2}_{\eta_2\sigma_2}(t_1 - t_2) \times G^{+}_{\eta_1\sigma_1} e^{-iL(t-t_1)} G^{+}_{\eta_2\sigma_2} e^{-iL(t_1-t_2)} G^{\bar{p}_2}_{\bar{\eta}_2\sigma_2} e^{-iLt_2} G^{\bar{p}_1}_{\bar{\eta}_1\sigma_1}, \tag{4.20b}$$

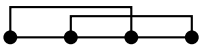

$$= -\sum_{p_1\eta_1\sigma_1} \sum_{p_2\eta_2\sigma_2} \int_0^t dt_1 \int_0^{t_1} dt_2 \gamma^{p_1}_{\eta_1\sigma_1}(t - t_2) \gamma^{p_2}_{\eta_2\sigma_2}(t_1) \times G^{+}_{\eta_1\sigma_1} e^{-iL(t-t_1)} G^{+}_{\eta_2\sigma_2} e^{-iL(t_1-t_2)} G^{\bar{p}_1}_{\bar{\eta}_1\sigma_1} e^{-iLt_2} G^{\bar{p}_2}_{\bar{\eta}_2\sigma_2}. \tag{4.20c}$$

Here the two possible contraction functions read $\gamma^{p}_{\eta\sigma}(t) = \sum_r \gamma^{p}_{\eta\sigma r}(t)$ with

$$\gamma^{+}_{\eta\sigma r}(t) = \tfrac{1}{2}\Gamma_{r\sigma}\bar{\delta}(t) \qquad (p = +), \tag{4.21a}$$

$$\gamma^{-}_{\eta\sigma r}(t) = -i\frac{\Gamma_{r\sigma} T_r}{\sinh(\pi t T_r)} e^{i\bar{\eta}\mu_r t} \quad (p = -). \tag{4.21b}$$

These are essentially the retarded and Keldysh reservoir correlation functions [1, 135], respectively. The $\bar{\delta}$ distribution in the time-local $\gamma^{+}_{\eta\sigma}$ contraction arises due to the wide-band limit, which was already incorporated into the definition of the Hamiltonians. As another consequence of this, the time-nonlocal $\gamma^{-}_{\eta\sigma}$ contractions contains a singularity at $t = 0$. Importantly, in App. D we show that the special algebra of the superfermions elegantly ensures that all shown diagrams stay finite nevertheless. There it is explained how the contributions combine to yield convergent time integrals, which can be straightforwardly implemented.

We illustrate the above for a generic set of parameters in Fig. 4.1(a–b). There we solve the time-nonlocal equation (2.3) using the numerically computed second and fourth order kernels. Referring to the solutions as $\rho^{(2)}_{\mathcal{K},\mathrm{bare}}(t)$ and $\rho^{(4)}_{\mathcal{K},\mathrm{bare}}(t)$ respectively, we plot their trace distance to the exact solution $\rho_{\mathrm{exact}}(t)$ for the noninteracting case $U = 0$ as function of time t and temperature T. As expected, the quality of each approximation is improved with higher temperature and the fourth order solution $\rho^{(4)}_{\mathcal{K},\mathrm{bare}}(t)$ has a larger range of validity than $\rho^{(2)}_{\mathcal{K},\mathrm{bare}}(t)$. At small temperatures the approximations work well only for short times $t\Gamma \lesssim 1$ where the infinite-temperature contributions dominate the dynamics. This is also reflected by the more basic check of the complete positivity (CP) of the *propagator* $\Pi(t)$, which is violated in the black and gray areas. It can be seen that $\rho^{(2)}_{\mathcal{K},\mathrm{bare}}(t)$ suffers from unphysical regimes, which become smaller when going to the next order $\rho^{(4)}_{\mathcal{K},\mathrm{bare}}(t)$. Importantly, when only checking whether the specific output *state* $\rho(t) = \Pi(t)\rho_0$ is unphysical (non-positive), which is the case in the gray areas, one misses that in the black areas the approximation has *already* failed, because the *propagator* does

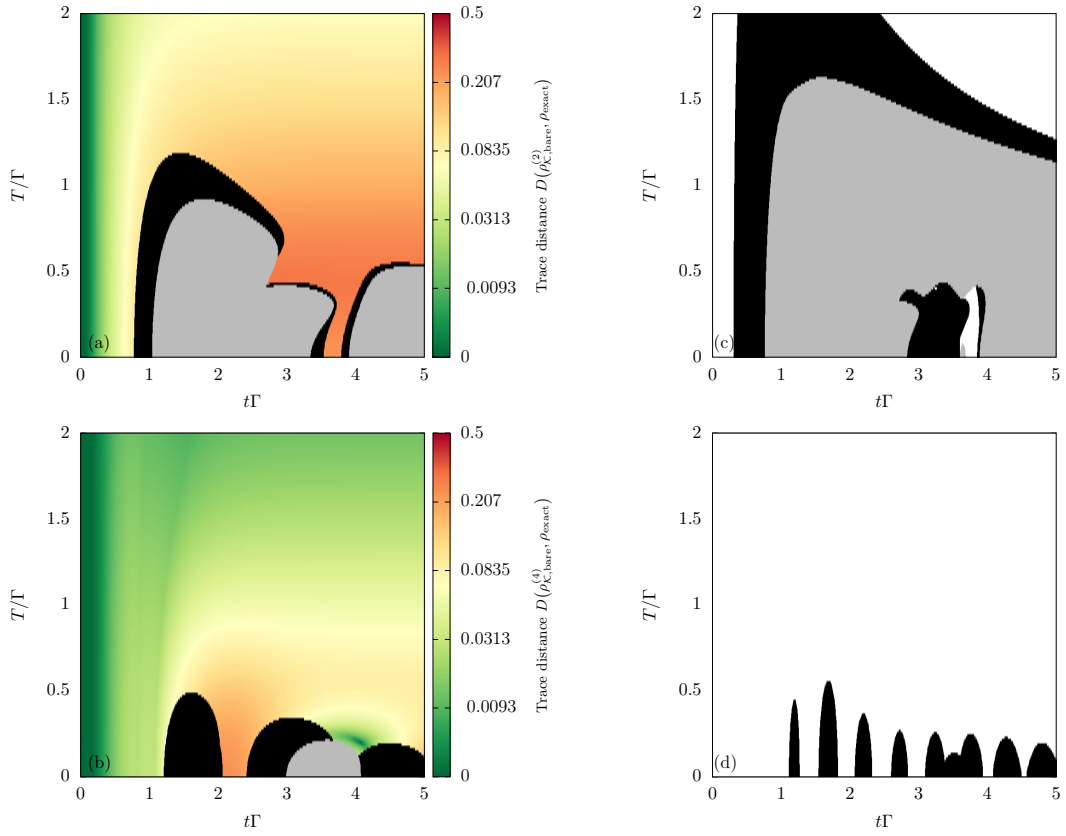

Figure 4.1. Transient evolution of an initially unoccupied Anderson dot, $\rho_0 = |0\rangle\langle 0|$, detuned by $\epsilon = 2\Gamma$ connected to a left and right reservoir at the same temperatures $T_L = T_R = T$ and biased chemical potentials $\mu_L = 0$, $\mu_R = -0.2\Gamma$. Regions in which the approximated state is not positive are shown in gray. Regions in which the approximated state is positive, but the propagator is not completely positive are shown in black. **(a)** Non-interacting case: Trace distance $D(\rho^{(2)}_{\mathcal{K},\text{bare}}(t), \rho_{\text{exact}}(t))$ between the second-order bare time-nonlocal solution $\rho^{(2)}_{\mathcal{K},\text{bare}}(t)$ and the exact solution. **(b)** Non-interacting case: Trace distance $D(\rho^{(4)}_{\mathcal{K},\text{bare}}(t), \rho_{\text{exact}}(t))$. **(c)-(d)** Interacting case $U = 10\Gamma$: regions of (complete) positivity for (c) $\rho^{(2)}_{\mathcal{K},\text{bare}}$ and (d) for $\rho^{(4)}_{\mathcal{K},\text{bare}}$.

not handle entanglement correctly (non-CP). These latter regimes are thus especially dangerous in practice.

Finally, in Fig. 4.1(c–d) we show that when turning on the interaction U the unphysical area of the second order solution $\rho^{(2)}_{\mathcal{K},\text{bare}}(t)$ increases. This is different for $\rho^{(4)}_{\mathcal{K},\text{bare}}(t)$ for the chosen parameters: whereas the detailed shape of the unphysical areas do change with interaction, the overall size does not significantly increase.

Bare perturbation theory for the time-local generator $\mathcal{G}$

With the orders of the kernel $\mathcal{K}$ in hand and decomposing $\mathcal{G} = \mathcal{K}_L + \mathcal{G}^{(1)} + \mathcal{G}^{(2)} + \ldots$ as before our key results (4.2)–(4.3) make it straightforward to compute the orders of $\mathcal{G}$ taking $\mathcal{K}_L = L$. Using our recursive relation (4.5) it is furthermore straightforward to infer a diagrammatic representation for $\mathcal{G}$ using only standard diagrams of $\mathcal{K}$ and Π and the shorthand $\Pi_0 = e^{-iLt}$:

$-i\mathcal{G}^{(2)}(t) =$ 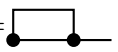 $\cdot\, \Pi_0^\dagger,$ (4.22)

$-i\mathcal{G}^{(4)}(t) =$ 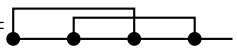 $\cdot\, \Pi_0^\dagger +$ 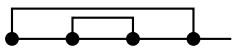 $\cdot\, \Pi_0^\dagger$

$+$ 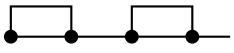 $\cdot\, \Pi_0^\dagger -$ 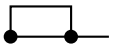 $\cdot\, \Pi_0^\dagger \cdot$ 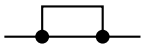 $\cdot\, \Pi_0^\dagger,$ (4.23)

Thus, no new technique and no new diagrammatic representation are required. We see that the general structure consists of *backward* bare propagations $\Pi_0^\dagger$, followed by blocks of $\mathcal{K}$ and Π, which only propagate forward. This is not unexpected: by the definition of the generator, $\mathcal{G} = i\dot{\Pi}\,\Pi^{-1}$, *any* expansion for $\mathcal{G}$ will contain both propagations forward (from $\dot{\Pi}$) and backward (from Π^{-1}). This is precisely what makes the expansion of $\mathcal{G}$ more complicated than that of $\mathcal{K}$ [Eqs. (4.18)–(4.19)].

In Fig. 4.2 we analyze the trace distance of the time-local approximations to the exact solution in the noninteracting case $U = 0$. We emphasize again that the second and

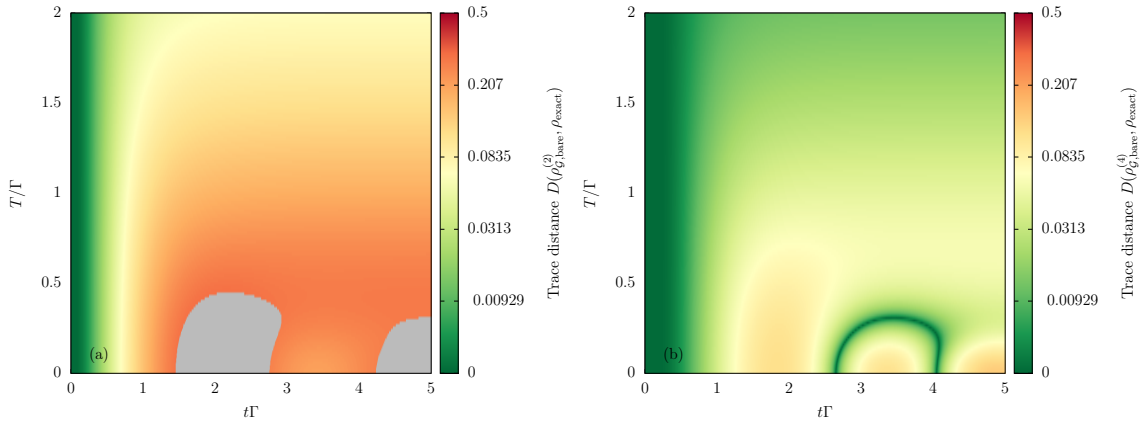

Figure 4.2. Transient evolution of an initially empty Anderson dot, $\rho_0 = |0\rangle\langle 0|$, with the same parameters as in Fig. 4.1 and $U = 0$. **(a)** Trace distance $D(\rho^{(2)}_{\mathcal{G},\mathrm{bare}}(t), \rho_{\mathrm{exact}}(t))$ between the second order bare time-local solution and the exact solution. **(b)** Trace distance $D(\rho^{(4)}_{\mathcal{G},\mathrm{bare}}(t), \rho_{\mathrm{exact}}(t))$ between the fourth order bare time-local solution and the exact solution. Areas in which the approximate state is not positive are shown in gray. In this case there are no areas where the approximated state is positive, but the propagator is not completely positive.

fourth order time-local solutions, $\rho^{(2)}_{\mathcal{G},\text{bare}}(t)$ and $\rho^{(4)}_{\mathcal{G},\text{bare}}(t)$ respectively, will be different from the time-nonlocal solutions of the same order: $\rho^{(j)}_{\mathcal{G},\text{bare}}(t) \neq \rho^{(j)}_{\mathcal{K},\text{bare}}(t)$. The general characteristics however stay the same: higher temperature improves the quality of the approximations and $\rho^{(4)}_{\mathcal{G},\text{bare}}(t)$ outperforms $\rho^{(2)}_{\mathcal{G},\text{bare}}(t)$. Compared to the time-nonlocal perturbation theory there are however considerable differences: The area where $\rho^{(2)}_{\mathcal{G},\text{bare}}(t)$ is unphysical is noticeably smaller than for $\rho^{(2)}_{\mathcal{K},\text{bare}}(t)$. Furthermore, $\rho^{(4)}_{\mathcal{G},\text{bare}}(t)$ is even physical everywhere in the plotted parameter regime. Surprisingly this is even true for strong interactions, for example of the order $U \approx 10\Gamma$. Notably, neither $\rho^{(2)}_{\mathcal{G},\text{bare}}(t)$ nor $\rho^{(4)}_{\mathcal{G},\text{bare}}(t)$ shows deceptive regimes where the state is positive, but the propagator is nevertheless not completely positive. These observations suggest in a very basic way that for the Anderson model the bare time-local perturbation theory is superior to the time-nonlocal one, even for the strong interaction.

4.3.2 | Renormalized expansions – Failure of the time-local approach

Renormalized perturbation theory for the memory kernel $\mathcal{K}$

In Eq. (4.21) the occurrence of the time-local $\bar{\delta}$ function in the $\gamma^{+}_{\eta\sigma}$ contraction hints at possible simplifications. The starting point lies in the observation that the $\gamma^{-}_{\eta\sigma}$ contraction vanishes when taking the high-temperature limit for all reservoirs, $\lim_{T_r\to\infty}\gamma^{-}_{\eta\sigma} = 0$. Then the infinite temperature kernel is exactly given by $\lim_{T_r\to\infty}\mathcal{K}_N(t) = \Sigma_\infty\,\bar{\delta}(t)$ with

$$\Sigma_\infty := -\frac{i}{2}\sum_{r\eta\sigma}\Gamma_{r\sigma}G^{+}_{\eta\sigma}G^{-}_{\bar{\eta}\sigma}. \tag{4.24}$$

Thus the time-nonlocal part of the kernel becomes *time-local* in this limit and we thus see that the total time-local Liouvillian

$$L_\infty := L + \Sigma_\infty \tag{4.25}$$

generates the GKSL semigroup dynamics of the model at infinite temperature [136],

$$\Pi_\infty(t) := \lim_{T_r\to\infty}\Pi(t) = e^{-iL_\infty t}. \tag{4.26}$$

Choosing $\mathcal{K}_L = L_\infty$ we want to compute the corresponding nonlocal part denoted by $\mathcal{K}_N = \Sigma$, i.e., the total memory kernel is given by

$$\mathcal{K}(t) = L_\infty\bar{\delta}(t) + \Sigma(t). \tag{4.27}$$

Interestingly all the time-local $\gamma^{+}_{\eta\sigma}$ contractions can be resummed exactly and one obtains a *renormalized* perturbation theory for Σ [23, 136]. To do so the diagrammatic rules have to

be changed as follows: first, only $\gamma^-_{\eta\sigma}$ contrations and superfermionic creation operators $G^+_{\eta\sigma}$ are allowed. Second, all of the intermediate free propagators Π_0 are replaced by infinite temperature propagators Π_∞. Thus the first terms of $-i\Sigma(t)$ are the renormalized versions Eqs. (4.20a)–(4.20c):

$$= -\sum_{\eta\sigma} \gamma^-_{\eta\sigma}(t) G^+_{\eta\sigma} e^{-iL_\infty t} G^+_{\bar{\eta}\sigma}, \tag{4.28a}$$

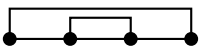

$$= \sum_{\eta_1\sigma_1} \sum_{\eta_2\sigma_2} \int_0^t dt_1 \int_0^{t_1} dt_2 \gamma^-_{\eta_1\sigma_1}(t) \gamma^-_{\eta_2\sigma_2}(t_1 - t_2)$$
$$\times G^+_{\eta_1\sigma_1} e^{-iL_\infty(t-t_1)} G^+_{\eta_2\sigma_2} e^{-iL_\infty(t_1-t_2)} G^+_{\bar{\eta}_2\sigma_2} e^{-iL_\infty t_2} G^+_{\bar{\eta}_1\sigma_1}, \tag{4.28b}$$

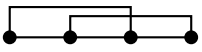

$$= -\sum_{\eta_1\sigma_1} \sum_{\eta_2\sigma_2} \int_0^t dt_1 \int_0^{t_1} dt_2 \gamma^-_{\eta_1\sigma_1}(t - t_2) \gamma^-_{\eta_2\sigma_2}(t_1)$$
$$\times G^+_{\eta_1\sigma_1} e^{-iL_\infty(t-t_1)} G^+_{\eta_2\sigma_2} e^{-iL_\infty(t_1-t_2)} G^+_{\bar{\eta}_1\sigma_1} e^{-iL_\infty t_2} G^+_{\bar{\eta}_2\sigma_2}. \tag{4.28c}$$

Notably, the renormalized perturbation theory is at the same time more powerful *and* simpler than the original one: since γ^+ contractions are no longer allowed, there are considerably fewer terms in the renormalized perturbation theory that need to be computed. Moreover, a finite number of terms of the renormalized series gives the exact solution in three different physical limits: By construction it is exact in the limits of vanishing coupling $\Gamma \to 0$ or infinite temperature $T \to \infty$, but it can be shown that it is additionally exact in the non-interacting limit $U \to 0$ [1, 136] for any Γ and T, which is not the case in any finite order bare perturbation theory in Γ.

Compared to the bare perturbation theory the intermediate propagations between vertices are damped on a timescale of the bare tunnel rate $\sim \Gamma^{-1}$ [Eq. (4.24)], which leads to improved convergence in the time integrations. Since this is the largest rate of decay, the higher order corrections of the renormalized perturbation theory are needed for smaller rates, i.e., they must effectively suppress decay. One thus expects that in the lower orders of this perturbation theory the oscillations described by L are damped.

For the explored parameters, we find that even for strong interactions the renormalized fourth order solution $\rho^{(4)}_{\mathcal{K},\mathrm{ren}}$ always stays physical (same parameters as in Fig. 4.3 (d), data not shown). This is however not the case for the second order renormalized solution $\rho^{(2)}_{\mathcal{K},\mathrm{ren}}$, which becomes unphysical at low temperatures, even for $U = 0$ (data not shown). Larger interaction has a negative impact on the positivity of $\rho^{(2)}_{\mathcal{K},\mathrm{ren}}$.

In Fig. 4.3 (a,e,f) we see that overall compared to the bare $\mathcal{K}$ perturbation theory the renormalized version replaces oscillatory behavior occurring off resonance ($\epsilon \gtrsim \Gamma$) at low $T \lesssim \Gamma$ by a rapid decay to the stationary value. We discuss the details in the next section.

Renormalized perturbation theory for the time-local generator $\mathcal{G}$

We now set up a corrresponding approach for the time-local generator, which to our knowledge has not been explored yet. The renormalized expansion of $\mathcal{K}$ can be translated to the generator $\mathcal{G}$ using the same steps as for the bare $\mathcal{G}$ expansion [Eqs. (4.22)–(4.23)]. Compared to Eqs. (4.22)–(4.23) one now uses the renormalized $\mathcal{K}$ and Π diagrams, where only $G^{+}_{\eta\sigma}$ vertices are allowed and the renormalization $L \to L_\infty = L + \Sigma_\infty$ is made. Importantly, one thus also needs to replace the *backward* evolutions by

$$\Pi_0^\dagger(t) = e^{iLt} \to e^{iL_\infty t} = \Pi_\infty^{-1}(t). \tag{4.29}$$

For the $U = 0$ limit this implies that because the renormalized series for $\mathcal{K}$ terminates at fourth order to give the exact result, the fourth order generator $\mathcal{G} = L_\infty + \mathcal{G}^{(2)}_{\text{ren}} + \mathcal{G}^{(4)}_{\text{ren}}$ is also exact at $U = 0$. Surprisingly however, it turns out that at $U = 0$ the fourth order contribution *also* vanishes, $\mathcal{G}^{(4)}_{\text{ren}} = 0$, which we verify in App. E. Thus, we conclude that the leading-order renormalized generator $\mathcal{G} = L_\infty + \mathcal{G}^{(2)}_{\text{ren}}$ is already exact for $U = 0$, *one order lower* then for the memory kernel $\mathcal{K} = L_\infty\bar{\delta} + \Sigma^{(2)} + \Sigma^{(4)}$.

In Fig. 4.3 we compare the different fourth order methods. In Fig. 4.3(a) we show results at low temperature $T < \Gamma$ and small interaction $U < \Gamma$. We see that the renormalized solutions coincide, but clearly differ from the bare solutions, which are distinct. Initially the bare solutions also coincide (up to $t\Gamma \simeq 1$) and decay like the renormalized ones, but at a smaller rate. They then start to oscillate while their renormalized counterparts have already reached their stationary values. The stationary values are similar for all methods. We focused on the off resonant case $\epsilon > \Gamma > U \simeq T$ since here the fourth order corrections are important, also in the renormalized methods.

In Fig. 4.3(b) we verify that at the symmetry point $\epsilon = -U/2$ the occupations converge to the same stationary value $n_\uparrow = n_\downarrow = \frac{1}{2}$ as they should by symmetry. However, the bare $\mathcal{K}$ solution predicts an oscillation, which is not predicted by the other methods. By contrast, the bare $\mathcal{G}$ method agrees with the renormalized methods showing no oscillations, even though $U = 10\Gamma$ is rather large.

It is thus interesting to consider less constrained parameters with detuning $\epsilon \gtrsim \Gamma$ in the tail of the resonance. For $U > \Gamma$ we find that at high temperature, $T > 5\Gamma$, all methods coincide for these parameters. However, in Fig. 4.3(c) we see that already for $T = 2\Gamma$ the renormalized $\mathcal{G}$ method predicts a *different* stationary occupation.

When lowering the temperature further in Fig. 4.3(d) we see that all methods after the initial rise predict decay ($t\Gamma \gtrsim \frac{1}{2}$), except that the renormalized $\mathcal{G}$ method gives a larger rate. Whereas the renormalized $\mathcal{K}$ method reaches stationarity after this, all other methods show similar overdamped oscillations. Because for the renormalized $\mathcal{G}$

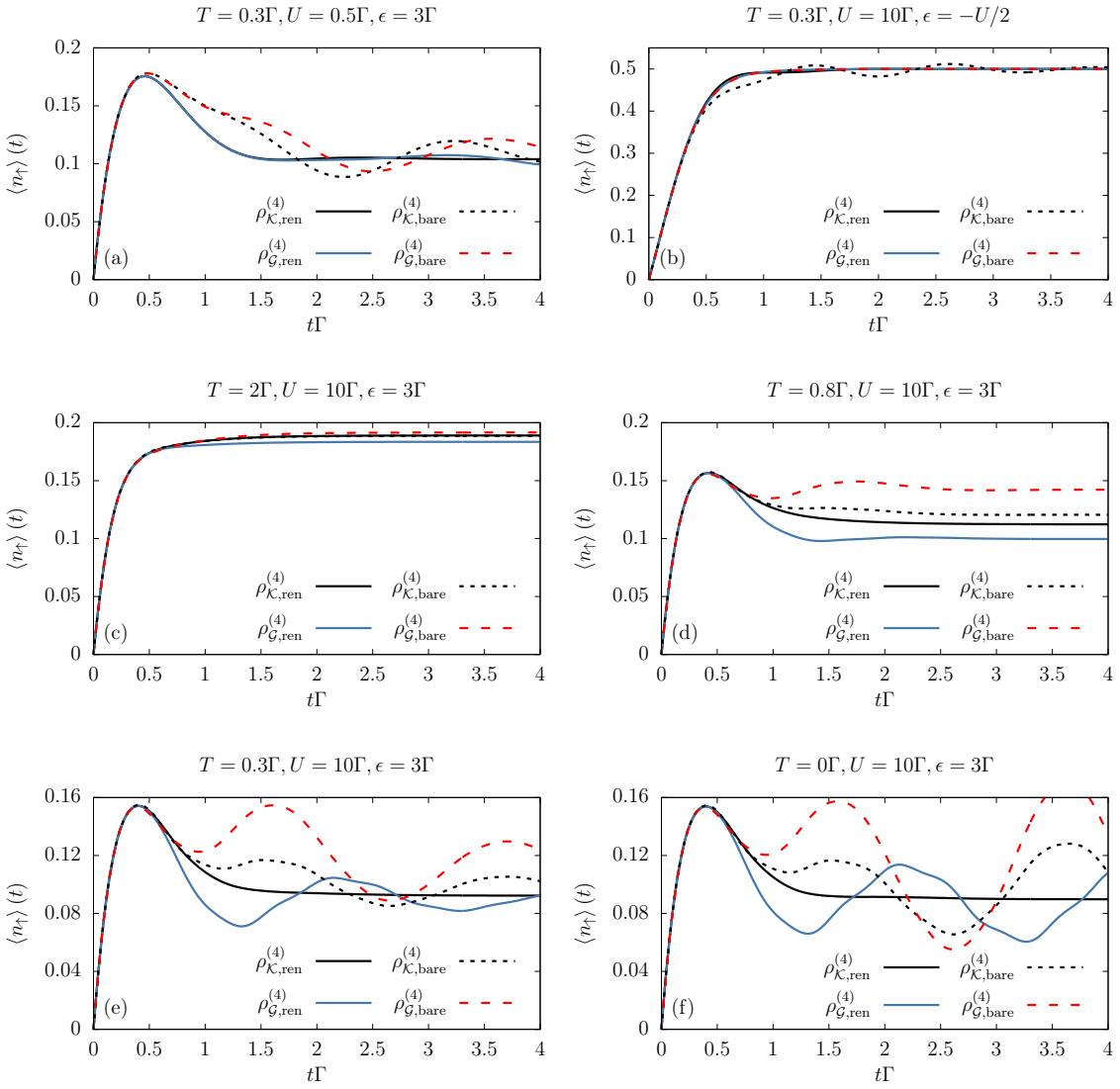

Figure 4.3. Interacting Anderson dot with $\mu_L = \mu_R = 0$: level occupation ($\langle n_\uparrow \rangle = \langle n_\downarrow \rangle$) from the initially unoccupied state $\rho_0 = |0\rangle\langle 0|$. **(a)** Weak interaction, low temperature. **(b)** Strong interaction and low temperature at the symmetry point. **(c)-(f)** Strong interaction with decreasing temperatures off-resonance.

method the initial decay is slower and last longer, this oscillation is out of phase with the other ones. Furthermore, it can be seen that every method predicts a different stationary value.

This picture persists when temperature is lowered further in Fig. 4.3(e)-(f). The above mentioned damped oscillations grow, whereas the renormalized $\mathcal{K}$ method further reduces the stationary value without introducing oscillations. The renormalized $\mathcal{G}$

method instead features pronounced oscillations with a visible second harmonic and an approximately $\frac{\pi}{2}$ phase shift. At $T = 0$ the oscillations of the bare solutions even show negative damping, diverging at long times. This means that one of the complex frequency poles of the propagator has moved into the unphysical part of the complex plane [24] and the stationary state is never reached.

The fact that the oscillations in Fig. 4.3(e)–(f) don't quickly decay for the renormalized $\mathcal{G}$ method may seem surprising at first, since the renormalized propagator Π_∞ [Eq. (4.26)] overdamps oscillatory contributions to the dynamics as mentioned earlier. However, this is counteracted by insisting on a *time-local* formulation of the renormalized approach. This is immidiately clear from our central result Eq. (4.2)–(4.4): in a renormalized expansion with decaying free reference evolution the partial backward time integration will partially undo this decay.

Another way of seeing that time locality is the problem here, is by considering the formal definition of the generator $\mathcal{G} = i\dot{\Pi}\Pi^{-1}$. In order to obtain any perturbative series for $\mathcal{G}$ it is necessary to expand the *inverse* propagator Π^{-1}. For the renormalized expansion Eqs. (4.2)-(4.4) this involves expanding

$$\Pi^{-1} = \left[\Pi_\infty + \Pi^{(2)}_{\text{ren}} + \Pi^{(4)}_{\text{ren}} + \cdots\right]^{-1} \tag{4.30}$$

$$= \Pi_\infty^{-1} - \Pi_\infty^{-1}\Pi^{(2)}_{\text{ren}}\Pi_\infty^{-1} + \cdots . \tag{4.31}$$

Since Π_∞ contains oscillating and decaying contributions (from L and Σ_∞ respectively [Eq. (4.26)]), it follows that Π_∞^{-1} is exponentially increasing in time. However, the geometric series is only guaranteed to converge if

$$\left\|\Pi_\infty^{-1}\left(\Pi^{(2)}_{\text{ren}} + \Pi^{(4)}_{\text{ren}} + \cdots\right)\right\| < 1. \tag{4.32}$$

Because $\Pi^{(2)}_{\text{ren}}(t) + \Pi^{(4)}_{\text{ren}}(t) + \cdots \to \Pi^{(2)}_{\text{ren}}(\infty) + \Pi^{(4)}_{\text{ren}}(\infty) + \cdots$ converges to a stationary (non-zero) value, condition (4.32) is violated after a short time and the time local generator becomes problematic. Note carefully that only for $U = 0$ no problems arise with the renormalized $\mathcal{G}$, because higher order corrections are identically zero by the algebraic structure of the model [App. E] and convergence of $\mathcal{G}$ is not an issue. By contrast, in the bare perturbation theory for $\mathcal{G}$ this problem did not occur, because the unitary reference evolution $\left\|\Pi_0^\dagger\right\|$ is always bounded. This shows that the application of renormalized perturbation expansions is much more subtle in the *time-local* framework than in the time-nonlocal one. This seems to be a generic problem of any perturbative expansion of $\mathcal{G}$ around a reference solution that already incorporates some dissipative/decaying behavior. This is, however, a key idea behind renormalization strategies for open sys-

tem [23, 24, 27, 29, 30], which through their use of the kernel $\mathcal{K}$ suffer no such failure. It remains an intriguing open questions whether similar schemes can be developed for $\mathcal{G}$.

4.4 | Summary

We have shown that the fixed-point relation (3.4) between the memory kernel $\mathcal{K}$ and the generator $\mathcal{G}$ implies a *recursive* relation between time-local and time-nonlocal perturbation series based on the *common* expansion reference $\mathcal{K}_L$. This relation can be exploited to set up calculations of these quantities irrespective of the chosen technique (diagrammatics, projection operators, etc.). Importantly, it allows for an unbiased comparison of the *different* approximations that result when performing the *same* expansion in a time-local or time-nonlocal picture, independent of model specifics. The flexibility in the choice of expansion reference $\mathcal{K}_L$ allows to compare bare expansions with renormalized ones.

For the bare expansion ($\mathcal{K}_L = L = [H, \bullet]$) discussed in Sec. 4.3.1, we developed a diagrammatic technique for computing the time-local generator $\mathcal{G}$, in close analogy to the well-developed technique for the memory kernel $\mathcal{K}$. Judging by the very basic criterion of legitimacy of the approximate propagator (complete positivity), performing the expansion in the time-local formulation leads to a better behaved solution in application to strongly interacting open systems than performing the corresponding expansion in the time-nonlocal one. Combined with its inherent advantages in addressing questions related to non-Markovianity [18, 19, 43, 44, 146] and quantum information, this suggests that the time-local approach, made more accessible here *via* the standard time-nonlocal one, can be a useful alternative to the existing time-local methods [34–36, 38, 93, 112, 113]. We also note that for the time evolution of *transport observables* – measured outside the system – similar memory kernels can be calculated using the same standard techniques that we used [23, 24]. The present paper also provides a starting point for transposing these techniques to the time-local calculation of transport observables.

For the renormalized expansion ($\mathcal{K}_L = L_\infty = L + \Sigma_\infty$) that we additionally developed in Sec. 4.3.2 this advantage of $\mathcal{G}$ over $\mathcal{K}$ at first seems to be confirmed. Expanding about the infinite temperature limit, we found that in the time-local framework the non-interacting Anderson dot is *exactly* solved by the leading order result, *one order lower* than in the time-nonlocal framework. However, in the presence of interaction the unbounded growth of the *dissipative backward* evolution with time leads to problems. We noted that the expansion of the inverse propagator, implicitly required by the expansion of the time-local generator is questionable on times of the order of the inverse decay rate Γ^{-1}.

As explained in Sec. 3.3, the versatile fixed-point equation may provide an additional

route to a renormalized time-local approach: Noting that the renormalized time-nonlocal approach allows to obtain an approximate $\mathcal{K}_{\text{pert}}$, iteration of the fixed-point functional (3.5) can be used to obtain an *equivalent* time-local generator $\mathcal{G}_{\text{sc}}$, which *self-consistently* accounts for the backward evolutions. This provides an approximation different from the truncated renormalized approach to $\mathcal{G}$ explored here following the traditional approach of expanding $\mathcal{G}$ itself. We thus illustrated how the fixed-point relation can be used to transpose standard memory kernel techniques to the interesting but more challenging time-local framework. Overall, our systematic comparison of the time-local and time-nonlocal framework highlighted their complementary merits and limitations.

5

T-flow renormalization group

As we have seen in Chap. 4 the physics of open quantum systems is well understood and characterized in the limits of weak coupling or high temperature: Here the dynamics is memoryless, giving rise to Markovian semigroup dynamics governed by the GKSL quantum master equation [Sec. 2.2.1]. As the temperature is lowered towards the system-reservoir coupling scale, the dynamics is no longer well described by a semigroup. The required non-semigroup corrections are often unproblematic to compute using the well-developed (bare) perturbation expansions of either the memory kernel or the time-local generator [Sec. 4.3.1], as long as the temperature is kept sufficiently high.

In contrast, the description of physics at low temperatures, strong coupling and large interactions remains challenging and is the subject of this chapter. As we saw in Sec. 4.3.2 approximate memory kernel calculations could be improved beyond the standard bare perturbation theory by systematically expanding around the high-temperature limit, which already includes dissipative behavior into the reference solution of the series. Here we pursue this development further and introduce the T-flow method. It allows to compute the memory kernel using the physical temperature T as a renormalization-group flow parameter starting from $T = \infty$, where the evolution is a GKSL-semigroup [135, 136] with simple jump operators [1, 3]. The basic idea is to obtain the low-temperature dynamics by lowering the physical temperature of the system's environment in small steps and systematically computing the memory kernel corrections that this generates. For this task the renormalized perturbation expansion from Sec. 4.3.2 forms the natural starting point. We show how it can be combined with key techniques of the E-flow RG scheme discussed in Sec. 1.3: by simply taking a T derivative (instead of an E derivative) of the full diagrammatic series for the memory kernel and the effective vertices one obtains a self-consistent hierarchy of differential equations, which can be systematically approximated while self-consistently keeping full time-propagators between the

effective vertices.

In contrast to the E-flow RG method, we can formulate everything directly either in the time or frequency domain. Here we focus on numerically solving the T-flow RG equations in time space for the example of an interacting Anderson dot [Sec. 4.3]. Notably, in doing so we automatically generate solutions for all temperatures. One thus works directly in terms of the temperature dependence of relevant time-evolving quantities, which are closely connected to the many-body physics of interest and their experimental signatures. Clearly, this built-in feature of the T-flow is of special interest for thermoelectric calculations which are, however, beyond the scope of the present work.

The chapter is organized as follows. In Sec. 5.1 we connect the time correlations of the environment to the key idea of the T-flow to provide some physical intuition for the later technical developments. We then derive the T-flow equations for the memory kernel in Sec. 5.2 borrowing techniques from the E-flow scheme. The computation of nonlocal observables, in particular particle-currents, is discussed in Sec. 5.3. Our first results are presented in Sec. 5.4, focusing on charge currents, occupations and charge fluctuations after verifying the legitimacy of the computed propagators (complete positivity). We investigate the reliability of our approach by comparison with various other methods and as a first application we investigate the impact of the interaction on the phenomenon of reentrant charge decay, which we predicted in Ref. [1]. We summarize and point out future directions in Sec. 5.5 and discuss relations of our technical results to the broader understanding of memory effects in open quantum systems [122].

5.1 | Temperature as flow parameter: Time correlations

We first consider for simplicity a system in contact with a single environment, the latter initially in equilibrium at temperature T. As mentioned in the introduction, the basic idea of the T-flow is to calculate low-temperature dynamics by literally lowering the temperature of the environment step-by-step. To develop some intuition for this we focus on the environment correlations, similar in spirit to Wilson's RG for critical systems [70] with the key difference that correlations in time – instead of space – are at the focus. In particular, the temperature T sets the inverse correlation time, which is effectively encoded into a single temperature-dependent correlation function $\gamma^-(t,T)$ [Eq. (4.21b)].

Following Wilson's idea we set up a flow from the high-temperature limit where the correlations are short-ranged ($\gamma^- = 0$ for $T \to \infty$) to one with long-ranged power

laws ($\gamma^- \propto 1/t$ for $T \to 0$). Thus, in the low-temperature regime of interest different time scales contribute equally when integrating power law correlations (e.g. $\int_t^{10t} dt'/t' = \ln 10$ independent of t) to compute the dynamics. An important difference with Wilson's RG is that we do not introduce an artificial flow parameter into the description, but instead use a variable that is already part of the problem. This is similar in spirit to the E-flow RG method for open quantum systems [27], which by choosing the Laplace variable E as flow parameter is intrinsically bound to the frequency domain, in the sense that only at the end of the calculation one can go to the conjugate time-domain. By instead choosing the physical environment temperature T we remain flexible to work in either domain.

Whereas at high temperatures the dynamics can be computed via a memory kernel Σ using perturbation theory, this becomes unreliable at low temperatures, because the slowly decaying correlations amplify higher order contributions requiring a more systematic treatment. In the T-flow this is done by integrating out thermal fluctuations in many small steps δT, as opposed to treating the entire correction $T = \infty \to 0$ in one piece. Thus the reduction of thermal fluctuations generates effective higher-order coupling effects. These corrections are controlled by the temperature sensitivity of the correlation function, $\partial_T \gamma^-$. A key observation is that this quantity never behaves as a power law in time and even vanishes at $T = 0$ for all times, in contrast to γ^- itself which is divergent for $t \to 0$ and slowly decaying for $t \to \infty$. In this sense, the computation of the temperature sensitivity of the memory kernel, $\partial_T \Sigma$, is better behaved than that of Σ itself. This is very similar to the calculation the memory kernel in the E-flow method [27].

At this point it is important to note that we do not change temperature as function of time. Instead we consider the entire dynamics – via its memory-kernel – at temperatures T and $T - \delta T$ when we stepwise lower the temperature. Proceeding this way it is by no means obvious that we do not pass through $T = 0$ and continue to negative temperatures. However, the above mentioned properties of the temperature sensitivity of the correlation function ensure that this does not happen: as we will see, the T-flow terminates at the fixed point $T = 0$:

$$\lim_{T \to 0} \frac{\partial \Sigma}{\partial T}(t, T) = 0. \tag{5.1}$$

Finally, before turning to the technical implementation, we highlight that because in our T-flow method temperature itself serves as a flow parameter it does not play the role of a cut off in the technical RG sense (there is no other running energy scale). This should not be confused with the fact explained above that temperature sets the inverse correlation time beyond which time integrations stop contributing, i.e., it does cut off time integrations in the ordinary non-RG sense (time is not a flow parameter).

5.2 | T-flow RG equations for the memory kernel

Reservoirs at the same temperature T

We are now ready to derive the self-consistent T-flow equations for $\partial_T\Sigma$, which allows us to lower the temperature, schematically via $\Sigma(t, T-\delta T) = \Sigma(t,T) - \partial_T\Sigma(t,T)\delta T$, in small steps δT. This is inspired by the derivation of the E-flow method [27], in particular by the definition of the effective vertices and the usage of full propagators between them. For simplicity we first consider the case where all reservoirs have a common temperature $T_r = T$ while allowing for arbitrary applied bias $V = \mu_L - \mu_R$. We are thus considering transient dynamics to a non-equilibrium stationary state.

We start from the diagrammatic representation of the renormalized perturbation series for the memory kernel [see Sec. 4.3.2]:

$-i\Sigma =$ 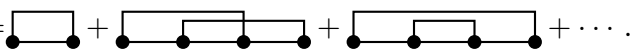 (5.2)

We first bring the renormalized series in self-consistent form by resumming all connected subblocks without uncontracted lines, thereby replacing infinite temperature propagators Π_∞ by full ones represented by double lines, $\Pi \equiv$. We then have

$-i\Sigma =$ 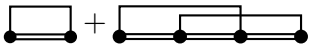 (5.3)

Thus for example, the third term of Eq. (5.2) is already contained within the first term of Eq. (5.3) and so on. Next, we introduce effective n-point supervertices $G_{1\ldots n}$ as sums over all connected diagrams with n uncontracted lines. Specifically we will need

$G_1 \equiv$  (5.4)

$G_{12} \equiv$  (5.5)

Note that the T-dependent effective supervertex G_1 (without superscript) differs from the T- independent superfermion G_1^+ (the first term in (5.4), defined by Eq. (4.13) with $p = +$) by finite-temperature corrections. Some remarks are necessary to make the above definitions more precise and these are given in App. F. Importantly, one can express G_1 using G_{12} and Π in a self-consistent manner as

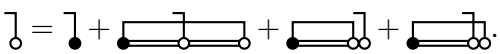 (5.6)

This can be seen in the following way: cutting off the leftmost vertex in each term of Eq. (5.4) from the rest of the diagram (except in the trivial first term), the remaining part on the right will have two uncontracted lines and will either be disconnected or it

will remain connected. In the former case the diagram before cutting will be included in the second term in Eq. (5.6), whereas in the latter case it must belong either to the third or fourth term. By this way of sorting, all diagrams are included without double counting. Combining Eqs. (5.3)–(5.4), we see that the memory kernel can be expressed using effective supervertices as

$$-i\Sigma = \tag{5.7}$$

Note that the resummation to full propagators performed to obtain Eq. (5.3) is crucial for Eqs. (5.7) to hold.

Taking a T derivative of Eq. (5.7), which we diagrammatically represent using a slashed line, we obtain the key relation

$$-i\frac{\partial\Sigma}{\partial T} = + + . \tag{5.8}$$

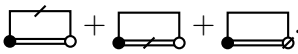

The first term contains the temperature derivative $\partial_T\gamma^-$ (slashed contraction) given by

$$\frac{\partial\gamma^-_{\eta\sigma r}}{\partial T}(t,T) = \frac{i\Gamma_{r\sigma}e^{i\bar{\eta}\mu_r t}}{\sinh(\pi tT)}\left[\frac{\pi tT}{\tanh(\pi tT)} - 1\right] \tag{5.9}$$

$$\sim i\Gamma_{r\sigma}e^{i\bar{\eta}\mu_r t}\pi tTe^{-\pi tT}\begin{cases}\frac{1}{3} & \text{for} \quad t \ll T^{-1}\\ 2 & \text{for} \quad t \gg T^{-1}\end{cases}. \tag{5.10}$$

which is explicitly divergence free. As mentioned in Sec. 5.1, it never behaves as a power law and even vanishes identically as $T \to 0$. The second term of Eq. (5.8) contains the temperature derivative of the propagator $\partial_T\Pi \equiv$. We show in App. G that this is connected to the T derivative of the memory kernel via

$$\frac{\partial\Pi}{\partial T} = -i\Pi * \frac{\partial\Sigma}{\partial T} * \Pi, \tag{5.11}$$

where $*$ denotes time convolution. This turns Eq. (5.8) into a self-consistent equation for $\partial_T\Sigma$. The third term of Eq. (5.8) requires the temperature derivative of the effective supervertex $\partial_T G_1$. It can be obtained by differentiating (5.6). Here the two-point vertex $\partial_T G_{12}$ enters, which can only be expressed in an exact manner using three-point vertices $\partial_T G_{123}$ and so on. This way a hierarchy of self-consistent differential equations is obtained.

Approximations within the above general T-flow scheme consist in truncating this hierarchy. To do so we count the number of bare vertices present in each term, which keep track of the number of contraction functions γ^- in which we are expanding. For example, the first and second term of Eq. (5.3) are counted as $\mathcal{O}(G^{+2})$ and $\mathcal{O}(G^{+4})$, respectively. In this first implementation of the method we will keep all terms in the

vertex equations such that Eq. (5.8) consistently includes all terms of order $\mathcal{O}(G^{+6})$. This means that the T-flow vertex equations are

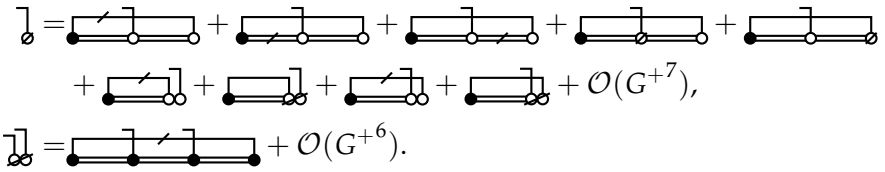

(5.12)

(5.13)

Eq. (5.8) together with Eqs. (5.12)–(5.13) constitute the main result of this chapter. They form a closed set of self-consistent differential equations for the memory kernel Σ and the effective supervertices G_1 and G_{12} as function of temperature T.

The above derived T-flow is started at some high, but finite temperature $T_\infty < \infty$, where initial conditions are obtained straightforwardly using the renormalized perturbation theory: we first compute the next-to-leading order memory kernel $\Sigma(T_\infty)$ [Eqs. (4.28a)–(4.28c)], which is then used to solve the corresponding time-nonlocal quantum master equation giving the propagator $\Pi(T_\infty)$. Inserting $\Pi(T_\infty)$ into the first two terms of Eq. (5.4) gives an initial value for the supervertex $G_1(T_\infty)$. Similarly the first term of Eq. (5.5) is used to compute $G_{12}(T_\infty)$.

Using Eq. (5.9) it is now easy to see that the T-flow reaches a fixed-point at $T = 0$ [Eq. (5.1)]: taking a T derivative of the renormalized perturbation series (5.2) for Σ each summand contains exactly one $\partial_T \gamma^-_{\eta\sigma}$ factor, which vanishes for all times $t \geq 0$ as $T \to 0$ as discussed. This implies that $\lim_{T\to 0} \partial_T \Sigma(t, T)$ vanishes.

Finally, we mention that the $t = 0$ singularity in the contraction γ^- never contributes explicitly in Eq. (5.8). This is because in the first term only a non-singular slashed contraction $\partial_T \gamma^-_{\eta\sigma}$ enters. Furthermore, we show in App. H that in the second and third term the singularity is always compensated. Thus, provided the initial propagator is time-non-singular, it will remain so during the T-flow making the approach well behaved and suitable for numerical calculations. This is indeed the case for Anderson-like models considered here, since the initial propagator is computed using next-to-leading order renormalized perturbation theory, for which the singularity is canceled out by the anticommutation of the superfermions [App. D].

Reservoirs at different temperatures T_r

The T-flow as presented above can be generalized to the case where each reservoir has a different temperature T_r. For this discussion it is useful to collect all temperatures into a single vector $\vec{T} = (T_1, T_2, \ldots, T_n)$. The T-flow is then started at high, but finite temperatures $\vec{T}_\infty = (T_{\infty,1}, T_{\infty,2}, \ldots, T_{\infty,n})$, allowing us to compute an accurate

initial condition using the renormalized perturbation theory. We next chose a path $\vec{T}(\alpha) = (T_1(\alpha), T_2(\alpha), \ldots, T_n(\alpha))$ in this n dimensional temperature space parameterized by $\alpha : 0 \to 1$, passing through the temperature-biased configurations of interest. If we denote by $\vec{T}_0$ the final target configuration of the reservoir temperatures (above $\vec{T}_0 = \vec{0}$) then $\vec{T}(\alpha = 0) = \vec{T}_\infty$ and $\vec{T}(\alpha = 1) = \vec{T}_0$. The case from the main text, where all reservoirs are cooled at the same rate, corresponds to $\vec{T}(\alpha) = \vec{T}_\infty + \alpha(\vec{T}_0 - \vec{T}_\infty)$. Alternatively we could keep $T_2, \ldots, T_n$ fixed while cooling T_1, and afterwards cool T_2 etc..

To generalize the T-flow equations we replace all derivatives

$$\partial_T \to \partial_\alpha = \partial\vec{T}/\partial\alpha \cdot \nabla_{\vec{T}} \tag{5.14}$$

in Eqs. (5.8)–(5.13). For example, slashed contractions now denote

$$\frac{\partial\gamma^-_{\eta\sigma}}{\partial\alpha} = \sum_r \frac{\partial T_r}{\partial\alpha} \frac{i\Gamma_{r\sigma} e^{i\bar{\eta}\mu_r t}}{\sinh(\pi t T_r)} \left[\frac{\pi t T_r}{\tanh(\pi t T_r)} - 1\right]. \tag{5.15}$$

Note that the slashed propagator is now given by the relation

$$\partial_\alpha \Pi = -i\Pi * \partial_\alpha \Sigma * \Pi \tag{5.16}$$

[cf. (5.11)]. With these conventions the same diagrammatic rules apply, which makes the implementation of the T-flow for distinct temperatures straightforward. Finally, we point out that closed temperature loops have no thermodynamic meaning here, because we are not lowering temperature in time (each RG step computes an entire evolution).

5.3 | Computation of the current kernel

Whereas the memory kernel can be used to compute the density operator and thus expectation values of local observables, it is not sufficient to determine expectation values of nonlocal observables such as transport quantities. For these additional observable-kernels are needed [23]. Here we will focus on the particle current flowing out of reservoir r defined by $I_r(t) := -\partial_t \langle N_r \rangle_{\text{tot}}(t)$, which can be obtained using a current kernel $\mathcal{K}_{I_r}$ via

$$I_r(t) = -i \operatorname{Tr} \int_0^t ds \mathcal{K}_{I_r}(t-s)\rho(s). \tag{5.17}$$

Similarly to the the ordinary memory kernel $\mathcal{K}$ [cf. Eq. (4.27)] we can decompose

$$\mathcal{K}_{I_r}(t) = \Sigma_{I_r,\infty}\bar{\delta}(t) + \Sigma_{I_r}(t). \tag{5.18}$$

Here the first term is time-local due to the wideband limit and gives the infinite temperature part of to the current-kernel. This term corresponds to the renormalization (4.25) of the kinetic equation that we performed to obtain the exact result at $T = \infty$. When it is applied to a finite-T state, we obtain a contribution to the current expectation value that probes the deviation of the spin-orbital occupations from half filling,

$$I_{r,\infty}(t) := -i \operatorname{Tr} \Sigma_{I_r,\infty} \rho(t) \tag{5.19}$$

$$= -\frac{1}{4} \eta_1 \Gamma_{r\sigma_1} \operatorname{Tr} G_1^- G_{\bar{1}}^- \rho(t) \tag{5.20}$$

$$= \sum_\sigma \Gamma_{r\sigma} \left(\frac{1}{2} - \langle n_\sigma \rangle(t) \right). \tag{5.21}$$

Note that $\lim_{t\to 0^+} I_r(t) = I_{r,\infty}(0) \neq 0$ in general: the current instantly rises at $t = 0$ (no coupling) to a finite value because we are working in the wideband limit. For large but finite bandwidth D the current approaches our result on the very short timescale $1/D$ [136, 172, 173].

The time-nonlocal current-kernel Σ_{I_r} can be computed using the same diagrammatic series that is used for Σ, except that the leftmost vertex and its contraction need to be replaced [23]. In the superfermionic notation we use here this amounts to replacing the leftmost $G^+_{\eta\sigma} \to \frac{\eta}{2} G^-_{\eta\sigma}$ and $\gamma^-_{\eta\sigma} \to \gamma^-_{\eta\sigma r}$. Given the effective vertex, which we obtain from the T-flow memory kernel computation, we can therefore automatically compute the current kernel as

$-i\Sigma_{I_r} =$  (5.22)

where we use a cross to indicate the replaced vertex. It is therefore not necessary to compute the current kernel in a separate RG flow.

5.4 | Application: Interacting quantum dot

Here we first show explicitly how the T-flow recovers the known exact solution at $U = 0$ [136]. After that we present results obtained by numerical solution of the T-flow equations for non-zero interaction U, whose implementation details are discuss in App. I. We mainly focus on transport observables but emphasize that we have checked that every computed propagator is a completely positive map at each time t, a basic criterion for the physicality of an approximation as explained in Sec. 2.1.

5.4.1 | Exact solution at $U = 0$

Here we show how the T-flow equations (5.8) and (5.11)–(5.13) recover the exact solution for the non-interacting spin-degenerate Anderson dot. The main simplification in this case is that all terms with more than four creation superfermions vanish for algebraic reasons as discussed in Ref. [1, 4, 136]. Therefore the infinite T-flow hierarchy terminates at finite order and is completely contained in the contributions of the main text. In fact they simplify to

$$-i\frac{\partial\Sigma}{\partial T} =$$ 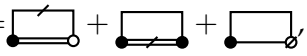 (5.23)

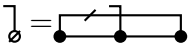 (5.24)

In the second term of Eq. (5.23) we can use a bare vertex (instead of an effective one) and in the third term a bare propagator Π_∞ (instead of a full one) because the corrections to this are of order $\mathcal{O}(G^{+6})$ and vanish algebraically. For the same reason Eq. (5.24) only contains bare vertices and propagators. With the initial condition $G_1(T = \infty, t - \tau, \tau - s) = G_1^+ \bar{\delta}(t - \tau)\bar{\delta}(\tau - s)$ for the supervertex we can immediately integrate (5.24), since only the contraction depends on temperature:

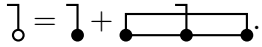 (5.25)

Note that the first term is equal to the initial condition and contains two $\bar{\delta}$ functions of time not indicated diagrammatically. Insertion of G_1 [Eq. (5.25)] and $\partial_T G_1$ [Eq. (5.24)] into the first and last term of (5.23) respectively, gives

$$-i\frac{\partial\Sigma}{\partial T} =$$  (5.26)

$=$ 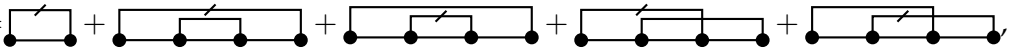 (5.27)

where in the third term of the first line we again replaced a full propagator by a bare one. In the last line we inserted the expansion of the full propagator and its temperature derivative [Eq. (5.11) with (5.23)] using that all orders greater than $\mathcal{O}(G^{+4})$ vanish algebraically. With the initial condition $\Sigma(T = \infty) = 0$ we can integrate the last equation and recover the exact memory kernel for the $U = 0$ Anderson dot

$$-i\Sigma =$$ 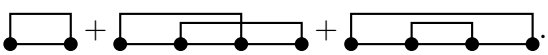 (5.28)

This is the result computed in Ref. [136] [Eq. (123), Sec. 4 and App. F loc. cit.], where the full solution is analyzed in detail, see also Ref. [1].

5.4.2 | Stationary limit – Benchmarks and charge fluctuations

We first consider the stationary limit for the purpose of benchmarking, stressing right away that this is not the limit where a real-time formulation is supposed to be particularly advantageous. For this reason, we need to restrict our attention to bias $V \geq \Gamma$, since for smaller bias the stationary limit is reached only at relatively large times, which is of course challenging when working in the time-domain. We consider the dot at the particle-hole symmetric point $\epsilon = -U/2$ connected to two reservoirs $r \in \{L, R\}$ with temperature $T_L = T_R = T$ under a symmetric bias $\mu_{L/R} = \pm V/2$ with $\Gamma_{r\sigma} \equiv \Gamma$ independent of r and σ. For sufficiently low temperatures the Kondo effect becomes important and renders both bare and renormalized perturbation theory computations unreliable.

In Fig. 5.1(a) we compare the obtained stationary current I_{stat} as function of V for $T = 0$ with results from the functional renormalization group (fRG), time-dependent density matrix renormalization group (tDMRG) and real-time quantum Monte Carlo method (QMC) reported in Refs. [174–176]. We find very good agreement with all four methods for $U = 2\Gamma$ and $U = 4\Gamma$. At $U = 8\Gamma$ we see that the currents predicted by our method are very close to the QMC ones, but slightly higher than the currents of fRG and tDMRG. The agreement with QMC persists for $U = 10\Gamma$ noting that for this value no fRG and tDMRG data were reported in Ref. [176].

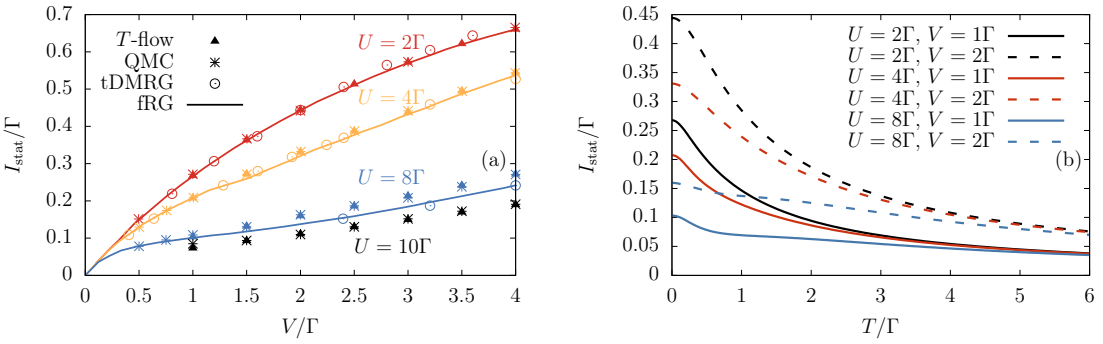

Figure 5.1. Stationary current at the symmetry point $\epsilon = -U/2$. **(a)** Comparison of the stationary current I_{stat} at $T = 0$ as function of bias V between the T-flow method, fRG, tDMRG and QMC. **(b)** Stationary current as function of temperature.

In Fig. 5.1(b) we show the stationary current as function of temperature. Here each curve is efficiently obtained within a *single* T-flow renormalization group trajectory. We find that the current is monotonically increasing as T is lowered. The asymptotic current

for high temperatures is independent of ϵ and U and given by

$$I_{\text{stat}} = \frac{\Gamma V}{4T} \quad \text{if} \quad T \gg \Gamma, \epsilon, U, V, \tag{5.29}$$

which can be derived from a high T expansion of the leading order memory and current kernels (4.28a) and (5.22).

In Fig. 5.2 we show the stationary charge fluctuations $(\Delta n)^2_{\text{stat}} := \langle n^2 \rangle_{\text{stat}} - \langle n \rangle^2_{\text{stat}}$. Because the stationary occupation at the symmetry point equals $\langle n \rangle_{\text{stat}} = 1$, it follows that the stationary charge fluctuations are related to the stationary occupation-correlation as

$$(\Delta n)^2_{\text{stat}} = 2 \langle n_\uparrow n_\downarrow \rangle_{\text{stat}}. \tag{5.30}$$

The behavior for high temperatures can be analytically calculated from Eq. (4.28a) to be

$$(\Delta n)^2_{\text{stat}}(T) = \frac{1}{2}\left(1 - \frac{4\epsilon + 3U}{4T}\right) \quad \text{for} \quad T \gg \Gamma, \epsilon, U, V, \tag{5.31}$$

which we stress also holds if the system is *not* at the particle hole symmetric point. The temperature dependence is shown in Fig. 5.2(a): Whereas the curves for different bias V merge at high T into the limiting curve (5.31) [inset], the fluctuations at small temperatures are suppressed as expected by Coulomb blockade. However, the fluctuations hit a

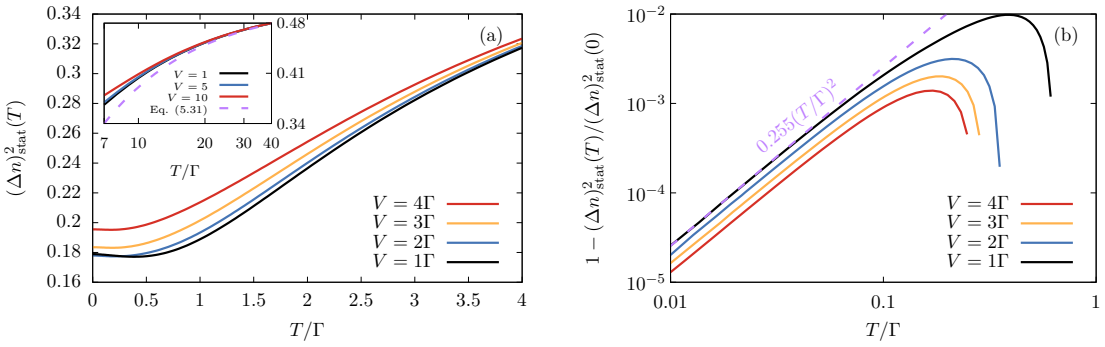

Figure 5.2. Stationary charge fluctuations $(\Delta n)^2_{\text{stat}}$ as function of temperature for $U = 8\Gamma$, $\epsilon = -U/2$ and several bias voltages. **(a)** Low and intermediate temperature regime. Inset: High temperature regime. **(b)** Scaling of the fluctuation for $T \ll \Gamma$.

global minimum at *finite* T, which is especially noticeable for small V, after which they increase again. For the chosen parameters this minimum occurs at $T \approx 0.4\Gamma$ for $V = \Gamma$ and then moves towards lower temperatures with increasing V. We attribute this enhancement of charge fluctuations at small T and V to the onset of the Kondo effect which in the T-flow method requires an account of time-correlations on increasingly larger

time scales as temperature is decreased. Since a large bias suppresses the Kondo effect, the finite temperature minimum of the fluctuations should become less pronounced at larger V, which indeed can be seen. Fig. 5.2(b) shows that for the chosen parameters the fluctuations scale as

$$(\Delta n)^2_{\text{stat}}(T) = (\Delta n)^2_{\text{stat}}(T=0)\left[1 - c\frac{T^2}{\Gamma^2}\right] \quad \text{if} \quad T \ll \Gamma, \tag{5.32}$$

where the constant c depends on U and V. This T^2 scaling is ubiquitous for the Kondo effect in the low temperature Anderson model and appears for example also in the conductance as function of V or T (for $V, T \lesssim T_K$) [27, 177].

5.4.3 | Transient effects – Currents, T-independence and reentrance

We now turn to the transient dynamics. Here we find quite generally that the short time behavior of the propagator is independent of temperature. This contribution stems not just from the leading-order infinite-temperature limit, but additionally from the initial temperature-independent part the memory kernel: For small times δt we have

$$\Pi(\delta t) = \Pi_\infty(\delta t) - \frac{i}{2}\Sigma(t=0)\delta t^2, \tag{5.33}$$

where for conciseness we have not expanded the first term, with the temperature-independent zero-time kernel

$$-i\Sigma(t=0) = \frac{2}{\pi}\Gamma G^+_{\bar{1}} L_\infty G^+_{\bar{1}} + \frac{2}{\pi}\Gamma \sum_{r\sigma} \mu_r G^+_{+\sigma} G^+_{-\sigma}. \tag{5.34}$$

Here the second term does not contribute for symmetric bias $\mu_L = -\mu_R$ considered here. This T-independence means that there is no T-flow of the propagator at short times $\delta t \ll \Gamma^{-1}$. As a consequence all local observables are initially insensitive to temperature as, for example, the occupations

$$\langle n_\sigma\rangle(\delta t) = \frac{1}{2} - e^{-2\Gamma\delta t}\left(\frac{1}{2} - \langle n_\sigma\rangle_{\rho_0}\right) + \left[U\left(\frac{1}{2} - \langle n_{\bar\sigma}\rangle_{\rho_0}\right) - \frac{U+2\epsilon}{2}\right]\frac{\Gamma}{\pi}\delta t^2, \tag{5.35}$$

where again we do not expand the exponential for conciseness. Here the first two terms describe decay to half filling coming from the infinite temperature propagator in (5.33). The third and fourth terms add quadratic corrections depending on the initial deviation of $n_{\bar\sigma}$ from half filling and the level deviation from the symmetry point. This is shown in Fig. 5.3, where the transient occupation $\langle n\rangle(t) = \langle n_\uparrow\rangle(t) + \langle n_\downarrow\rangle(t)$ is plotted for several temperatures. Because the initial evolution is T-independent as explained above and the stationary occupation is fixed by the particle-hole symmetry, temperature can only

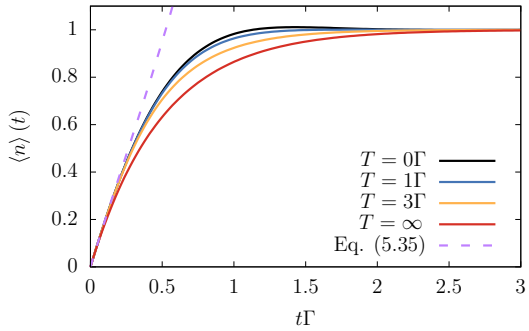

Figure 5.3. Transient occupation $\langle n \rangle(t)$ for $U = 4\Gamma$, $\epsilon = -U/2$, bias $V = \Gamma$ and several temperatures. Initially the dot is empty, $\rho_0 = |0\rangle\langle 0|$. We note that the $\mathcal{O}(\delta t^2)$ contributions of Eq. (5.35) are negligible here, but can play a role, see Fig. 5.5.

affect the intermediate occupations. A noticeable detail of this crossover from weak to strong coupling is that for this moderate value of the interaction the occupation slightly overshoots its stationary value $\langle n \rangle_{\text{stat}} = 1$ for the lowest temperatures, but this effect is lost already for $U = 8\Gamma$ (not shown).

Interestingly, for non-local observables the short-time behavior may also be temperature independent. An example is the particle current plotted in Fig. 5.4. Similar to the decomposition (5.33) there are contributions from both the infinite temperature current and the T-independent zero-time current-kernel, e.g., for the left reservoir:

$$I_L(\delta t) = I_{L,\infty}(\delta t) - i \operatorname{Tr} \Sigma_{I_L}(t=0)\rho_0 \delta t \tag{5.36}$$

$$= (V - U - 2\epsilon)\frac{\Gamma \delta t}{\pi} + (1 - \langle n \rangle_{\rho_0})\Gamma \left[1 + (U - 2\pi\Gamma)\frac{\delta t}{\pi}\right]. \tag{5.37}$$

Again we stress that this result also holds if the system is *not* at the particle hole symmetry point. In Fig. 5.4(a) $I_L(t)$ is shown for large interaction $U = 8\Gamma$ at bias $V = \Gamma$ as the temperature is lowered. As expected the initial onset of the current follows Eq. (5.37). Whereas for $T \gtrsim \Gamma$ the current monotonically converges to its stationary value, at lower temperatures the current after an initial increase first decreases until $t\Gamma \approx 1$ and then turns up again. For $T \lesssim 0.2\Gamma$ the stationary current is significantly higher than the local maxima at $t\Gamma \approx 1/2$. The local minimum at $t\Gamma \approx 1$ becomes less pronounced if U is decreased and eventually vanishes (not shown).

In Fig. 5.4(b) we compare the transient currents obtained by the T-flow with those obtained in Ref. [178] using a two-particle-irreducible effective action (2PI) approach at low temperature $T = 0.1\Gamma$ and intermediate interaction $U = 4\Gamma$. We find overall good agreement. In particular, both predict that the current slightly overshoots its stationary value at large bias. At small bias the stationary current of the 2PI approach is slightly

smaller compared to our T-flow result, which in the stationary benchmarks in Fig. 5.1(a) compared favorably with other methods.

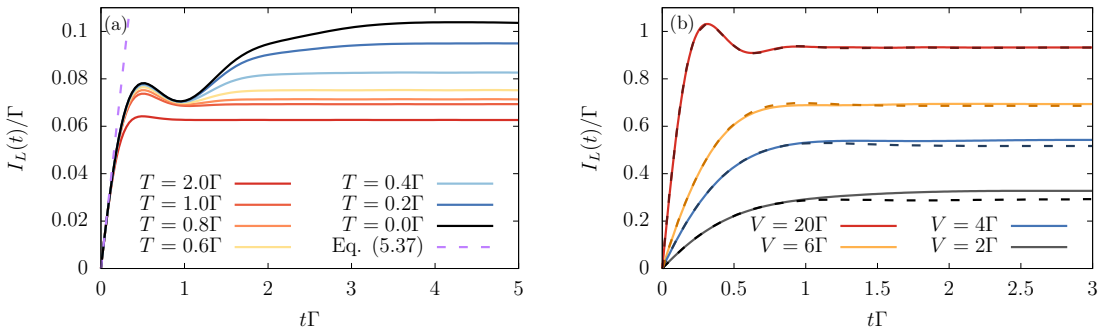

FIGURE 5.4. **(a)** Transient current $I_L(t)$ for $U = 8\Gamma$, $\epsilon = -U/2$, $V = \Gamma$ and several temperatures. Initially the dot is singly occupied, $\rho_0 = |\uparrow\rangle\langle\uparrow|$. **(b)** Transient current $I_L(t)$ for $U = 4\Gamma$, $\epsilon = -U/2$, $T = 0.1\Gamma$ and several bias voltages. Solid lines: T-flow. Dashed lines: 2PI approach from Ref. [178].

Finally, as an application we consider the transient effects of the interaction in the empty-orbital regime $\epsilon \gg \{\Gamma, V\}$, which is characterized by $\langle n\rangle_{\text{stat},T=0} \approx 0$. Perhaps surprisingly, preparing the dot in a state with a higher occupation than its stationary occupation need not lead to a simple decay of the occupation. Instead, it is possible that the dot initially fills up *more* as predicted in Ref. [1] on quite general grounds. How this can happen can be understood specifically from Eq. (5.35), which shows that initially the occupation grows towards half filling – away from the stationary value – as dictated by Π_∞. Indeed, in Fig. 5.5 the occupation initially increases until $t\Gamma \approx 0.3$, after which the naively expected monotonic decay starts. The occupations then reenter their initial value precisely at the reentrant time $t_r = \Gamma^{-1}$. More strongly, for the chosen initial state this reentrance occurs for *any local observable* of the dot, as for example the correlation in Fig. 5.5, implying that the entire reduced density operator returns to its initial value.

This at first puzzling reentrant behavior was already explained in Ref. [1] in general terms showing that it is generically enforced in non-semigroup dynamics by the fundamental property of trace-preservation of the dynamics. In short, for every time t_r the propagator has a fixed point denoted $\rho_1(t_r)$ such that $\Pi(t_r)\rho_1(t_r) = \rho_1(t_r)$, which is moreover a physical state, $\rho_1(t_r) \geq 0$ and $\operatorname{Tr}\rho_1(t_r) = 1$. Thus, all local observables must return to their initial values at time t_r if the initial state $\rho_0 = \rho_1(t_r)$ is prepared. (Note that this argument does not imply reentrant behavior of non-local observables such as currents measured outside the system.) Whereas in Ref. [1] this general effect was predicted, it was illustrated only for the occupation of a non-interacting spinless quantum

dot coupled to a single reservoir, a solvable model. Here we have illustrated that it occurs for more than one observable and shown that it remains clearly visible in the strongly-interacting, low-temperature case under finite bias transport conditions. We highlight that the rationale behind the T-flow method ties in directly with the competition between finite-T and infinite-T dynamics that drives this physical effect.

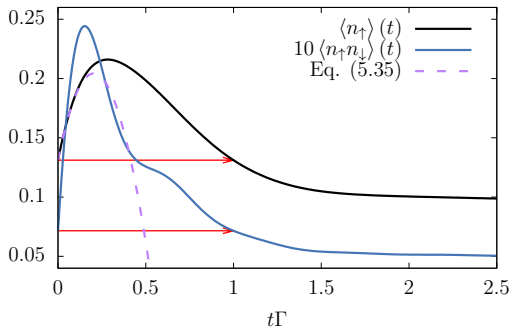

Figure 5.5. Reentrant effect for dot occupation and correlation for parameters $U = 8\Gamma$, $\epsilon = 2.75\Gamma$, $V = \Gamma$ at $T = 0$. The reentrant effect for time $t_r = \Gamma^{-1}$ is realized by the initial state ρ_0 with $\langle n_\uparrow \rangle_{\rho_0} = \langle n_\downarrow \rangle_{\rho_0} \approx 0.131$ and $\langle n_\uparrow n_\downarrow \rangle_{\rho_0} \approx 0.007$.

5.5 | Summary

In this chapter we presented the T-flow renormalization group method, which uses the physical environment temperature to achieve a flow of the density-operator dynamics to its nontrivial low-temperature limit. Starting from the simple high-temperature limit, the temperature is lowered in many small steps using the self-consistent RG equations (5.8)–(5.13). In this way we collect useful information about the physics at *all* traversed finite temperatures, which sets our scheme apart from RG methods using unphysical flow parameters.

We implemented the RG equations directly in time space at the example of an interacting Anderson dot including vertex corrections. For voltages on the order of the coupling or larger, stationarity is reached quickly, allowing us to benchmark our transient method in the stationary regime. We demonstrated quantitative agreement in the current-voltage characteristics, noting in particular that the agreement with accurate quantum Monte Carlo simulations extends up to $U = 10\Gamma$. Comparing transient currents with the 2PI Green's function results we found good agreement as well. Interestingly, we could show analytically that the short time dynamics of both local and nonlocal observables are temperature independent in the wide-band limit considered here, with

important contributions from the short-time memory kernels. The observed collapse of the data onto a T-independent limiting curve may be of interest for experimental studies of transient transport.

As an application we investigated the reentrant effect that we noticed first in Ref. [1] in the analysis of a non-interacting quantum dot model: the charge prepared on a quantum dot, which is destined to decay, can initially show an unexpected further accumulation. We showed that this effect is due to a generic interplay between short-time infinite-T dynamics and long-time finite-T corrections and remains clearly visible even for strong interactions and finite-bias non-equilibrium. Moreover, we illustrated that this effect does not only occur for the occupation but also for the *correlation* of two electrons in agreement with general arguments about non-semigroup dynamics that we put forward in Ref. [1].

For the formulation and application of the method we focused on the case of equal reservoir temperatures and studied the transient approach to non-equilibrium stationary states and transport quantities. However, we also provided the general formulation for distinct temperatures of the reservoirs whose application to thermoelectric transport with strong coupling and interaction is interesting. The additional heat currents of interest in this situation [179, 180] can be computed by straightforward extension of the presented technique for the charge current. Moreover, the presented method can be extended in several further directions: (i) Since the T-flow allows to avoid the frequency domain it is straightforward to include non-periodic driving of bias and gate voltages [$V(t)$ and $\epsilon(t)$] or tunnel barriers [$\Gamma(t)$]. This comes at the numerical price of dealing with double (triple) time-dependence of the contraction functions γ_1^p and the memory kernel $\mathcal{K}$ (the supervertex G_1), but should present no principal problem. (ii) However, it is equally well possible to formulate the T-flow entirely in the Laplace-frequency domain by changing the translation rules of the diagrams as in Ref. [23, 135]. This may provide more direct access to stationary quantities than by converging transient calculations well into the stationary regime, in particular for regimes where $T, V \ll \Gamma$. How this compares with the well-developed E-flow scheme is an interesting open question. (iii) The T-flow can also address systems with bosonic environments provided a renormalized perturbation theory around the infinite temperature and wideband limit is set up analogous to fermionic environments [29, 181], which seems possible.

We emphasized throughout that the presented T-flow scheme is naturally suggested by physical considerations underlying the renormalized perturbation expansion. Nevertheless, further considerations of its physical underpinnings would be of interest. Indeed, early time-domain formulations of the density-operator RTRG [83, 181] were motivated by considerations similar to those given in Sec. 5.1, but encountered technical

issues. These were initially resolved by reformulations which abandoned the time-domain [85, 182] and started from a renormalized perturbation theory which was later identified as describing the $T = \infty$ limit [135, 136] as used here. This renormalization by the $T = \infty$ reference solution plays a crucial role in the construction of a well-defined RG flow for the open-system dynamics, in particular, for the special treatment required for the stationary state. This is problematic when starting from a standard bare perturbation expansion ("zero eigenvalue problem", see the discussion preceding Eq. (199) in Ref. [23]).

In the present chapter we instead returned to the time-domain by exploiting the insights gained in the above cited works. This has the advantage that the similarities and differences with Wilson's RG [70] become apparent, in particular the focus on the long-range correlations which become explicit in the renormalized perturbation theory about $T = \infty$. The ordinary perturbation expansion does not reveal the relevant correlations since the $T = \infty$ and $T < \infty$ contributions are completely mixed up [135, 136]. This constitutes a key difference of the T-flow to other RG approaches. Its apparently successful application here warrants further, more detailed consideration of these physical underpinnings, in particular its close connection to the *generation of memory effects*. Importantly, here memory is characterized as retardation with characteristic time $1/T$, which is related but not the same as non-divisibility of dynamical maps [122] (non-Markovianity).

The return to the time-domain achieved by our work may also enable general physical arguments to be applied more easily to technical considerations, especially since our RG flow parameter can in principle be changed physically in the lab. A T-flow step establishes a mapping between two *entire physical evolutions* at adjacent temperatures. Operationally this corresponds to an intervention on the initially decoupled reservoir state $\rho_R(T) \to \rho_R(T - \delta T)$ before the interaction with the system is started and before the environment is discarded (integrated out) [Eq. (2.1)]. It has been stressed [122] that interventions on the environment represent yet another way of characterizing memory effects beyond the framework of retardation and non-divisibility of the reduced evolution mentioned above. Operationally defined mappings of entire evolutions have been studied in detail in quantum information using the supermap [183] and process-tensor formalisms [184] and these may find new applications here. To apply such considerations here it is a crucial advantage that the T-flow allows one to stay in the time-domain, since transformation to frequency domain tends to complicate rather than simplify operational properties of time-evolutions [47].

6

Conclusions and outlook

In this thesis we studied the dynamics of open quantum systems using the time-local and time-nonlocal quantum master equations on which most research about dynamical maps Π of open systems is based. A major theme was relating these two fundamental approaches quantitatively, connecting the more complicated but often physically more interesting time-local representation to the technically more powerful time-nonlocal one. A second theme concerned systematic approximations beyond semigroups, where we explored, in particular, slip corrections, different perturbative schemes, and renormalization groups. The thread connecting these themes was the recurrent issue of memory, understood as either retardation or divisibility of the dynamics.

6.1 | Connecting time-(non)local descriptions of open quantum systems

Motivated by our initial detailed case study published in Ref. [1], we investigated the unsolved problem of how the two canonical QMEs of open quantum systems are related. We found that the time-local generator $\mathcal{G}$ and the time-nonlocal memory kernel $\mathcal{K}$ are connected by a simple, yet general fixed-point relation $\mathcal{G} = \hat{\mathcal{K}}[\mathcal{G}]$.

Especially in the stationary limit, it was possible to exploit this result directly, analytically revealing several non-perturbative insights. Most importantly, we proved the sampling relation (3.15) relating spectral properties of $\mathcal{G}(\infty)$ and $\hat{\mathcal{K}}(\omega)$ at pole frequencies of $\hat{\Pi}(\omega)$. We showed that this interesting interrelation between $\mathcal{G}(\infty)$, $\hat{\mathcal{K}}(\omega)$ and $\hat{\Pi}(\omega)$ has important implications for the construction of semigroup Markov approximations. First, the semigroup generators $\hat{\mathcal{K}}(0)$ and $\mathcal{G}(\infty)$ "naturally" suggested by proponents of time-local and time-nonlocal approaches respectively are not identical,

raising the question which one is "better". We found that, while the low-frequency kernel $\hat{\mathcal{K}}(0)$ has the advantage of always being well-defined, it is the long-time generator $\mathcal{G}(\infty)$ that is contained within the propagator as $\Pi(t) = e^{-it\mathcal{G}(\infty)}\mathcal{S} + \ldots$. Here $\mathcal{S}$ is an inital slip correction, which we constructed non-perturbatively from linearizations around the sampled eigenvalue poles [Eq. (3.17)]. Applied to fermionic systems in particular, this slip operator can be further analyzed as we reported in a separate publication [3]. Second, the expansion (3.18), which in the time-nonlocal approach is purported to account for "memory" corrections, can be exactly resummed to a non-perturbative expression with the surprising result that is equal to $\mathcal{G}(\infty)$, which is obtained in the time-local approach by manifestly ignoring memory effects. This makes quantitative the difference between memory as retardation/frequency dependence and memory as described by non-divisible evolutions.

The discovered fixed-point relation is also applicable to much more complicated transient effects. We have shown that $\mathcal{G}(t)$ can be constructed from iterations of the fixed-point functional $\hat{\mathcal{K}}[\bullet]$ and illustrated the numerical stability for several examples. This can work even in the most challenging case where $\mathcal{G}(t)$ has singularities at isolated times, for which perturbative computations of $\mathcal{G}(t)$ are known to break down beyond the first singularity. This underscores that our iterative construction of $\mathcal{G}(t)$ via the memory kernel $\mathcal{K}(t)$ is by nature non-perturbative because it does not rely on the presence of a small parameter. This apparent success warrants the investigation of several further questions relating to the convergence of the (transient and stationary) functional iteration, the uniqueness of the fixed-points in both procedures, and the possible connection of the iteration to renormalization group procedures, see also the discussion in Sec. 3.6. These questions highlight the fact that the relation between the time-local and time-nonlocal picture of the *same* quantum dynamics contains by itself deeper insights. The question "What does it take to make the description of the evolution time-local without introducing any error?" thus seems to be instructive.

6.2 | Perturbative series and renormalization groups

A second theme of this thesis was the construction and comparison of different approximation strategies in the context of QMEs. We investigated what happens to a given approximation scheme when altering its time locality by deriving translation rules between perturbative series for the memory kernel $\mathcal{K}$ and the generator $\mathcal{G}$ [Eqs. (4.4)–(4.5)]. Our result disentangles the more difficult $\mathcal{G}$-expansion in terms of the simpler, time-ordered $\mathcal{K}$-expansion, connected in an overarching anti-time-ordered structure. We

applied this in detail to the diagrammatic expansion of the memory kernel $\mathcal{K}$ [Eq. (4.19)] and showed how the generator $\mathcal{G}$ can be expressed using the same diagrams, i.e. without inventing a new language [Eq. (4.23)] obstructing the direct comparison.

This allowed us to compare the two approaches straightforwardly and in an unbiased way. Analyzing the complete positivity of approximations and comparing them with the exact solution for the non-interacting Anderson dot, we concluded that the time-local approach might be more advantageous than the time-nonlocal approach in bare expansions around the uncoupled limit $\Gamma = 0$. However, when considering the more powerful renormalized expansion around the $T = \infty$ limit this conclusion is reversed. Here, insisting on time-locality of the perturbation theory becomes problematic when running the dissipative reference evolution *backwards*. As a result only the time-nonlocal approach is reliable within a renormalized perturbative formulation. Thus, the question how to translate established advanced approximations (going beyond bare perturbation theory) within the time-local picture remains open.

The power of the renormalized perturbation theory became clear in the final analysis presented, where it provided the natural physically motivated starting point for the development of a new renormalization group scheme, which we called the T-flow. Here the main idea was that temperature sets the inverse correlation time of the reservoirs. Thus, decreasing temperature increases memory, here understood as the retardation contained in the kernel $\mathcal{K}$. We showed that the "memory" corrections obtained by lowering the temperature can be systematically computed within this RG scheme. A noteworthy technical feature of the T-flow method is that it can be formulated entirely in time-space. It is physically interesting that the RG flow parameter can, in principle, be changed in the lab, possibly allowing a more operational formulation of the technical scheme.

Despite the presented successful benchmarking of the T-flow with various other approaches, many questions remain unexplored. For example, the present time-space formulation is clearly disadvantageous if stationarity is only reached after very long times, which happens in the considered Anderson dot if $V, T \ll \Gamma$. In this case, a reformulation of the method in Laplace space might be favored. Additionally, the extension to models with bosonic environments would be of interest. This would require one to set up a renormalized perturbation theory around the infinite temperature limit for bosonic environments first, which seems possible.

A

Exact resummation of the memory expansion

In Sec. 3.2.4 we mentioned that the memory expansions of Refs. [41, 42] are contained in our fixed-point relation (3.4). Here we give an explicit formula for *all* terms. Moreover, we sum the series to a self-consistent form and recover our key results (3.4) and (3.9).

Memory-expansion. We essentially follow the approach of Ref. [41] noting that we have verified that Ref. [42] achieves exactly the same thing by manipulating partial integrations. Both works start from the time-*nonlocal* QME (2.3) and construct the time-*local* QME (2.9). Importantly, *no* weak coupling approximation is made in these works but they do restrict attention to the stationary limit $t_0 \to -\infty$ by constructing the approximate time-local QME $\frac{d}{dt}\Pi(t-t_0) \approx -i\mathcal{G}(\infty)\Pi(t-t_0)$. Ref. [41] considers only the leading memory-correction (3.18). Here we make none of the mentioned assumptions and specialize to the case of Refs. [41, 42] only at the end [Eq. (A.10)].

Thus, the summation of the memory expansion amounts to the construction of $\mathcal{G}(t,t_0)$ from $\mathcal{K}(t,s)$ such that we have $i\dot{\Pi}(t,t_0) = \int_{t_0}^{t} ds\, \mathcal{K}(t,s)\Pi(s,t_0) = \mathcal{G}(t,t_0)\Pi(t,t_0)$. In the main text this was solved by exploiting the divisor, $\mathcal{G}(t,t_0) = \int_{t_0}^{t} ds\, \mathcal{K}(t,s)\Pi(s,t|t_0)$. In our formulation, the approach taken in Refs. [41, 42] amounts to computing the inverse divisor as

$$\Pi(s,t|t_0) = \Pi(s,t_0)\Pi(t,t_0)^{-1} \tag{A.1a}$$

$$= \sum_{k=0}^{\infty} \frac{1}{k!}(-1)^k (t-s)^k \mathcal{F}^k(t,t_0) \tag{A.1b}$$

by inserting the *memory-expansion* $\Pi(s,t_0) = \sum_k \frac{1}{k!}(-1)^k (t-s)^k \partial_t^k \Pi(t,t_0)$ of quantities in the past time s around the present time $t > s$. For example, Eq. (3.18) discussed in Ref. [41] corresponds to the $k = 0, 1$ terms. Here the superoperator-valued Taylor

coefficients $\mathcal{F}^k(t,t_0)$ are the *time-local generators of the k-th derivative* of the propagator:

$$\partial_t^k \Pi(t,t_0) = \mathcal{F}^k(t,t_0)\Pi(t,t_0). \tag{A.2}$$

Written as $\mathcal{F}^k(t,t_0) := [\partial_t^k \Pi(t,t_0)]\Pi(t,t_0)^{-1}$ they are easily shown to obey the recursion relation

$$\mathcal{F}^k(t,t_0) = \partial_t \mathcal{F}^{k-1}(t,t_0) + \mathcal{F}^{k-1}(t,t_0)[-i\mathcal{G}(t,t_0)] \tag{A.3}$$

with starting condition $\mathcal{F}^0(t,t_0) = \mathcal{I}$ giving, for instance,

$$\mathcal{F}^1(t,t_0) = -i\mathcal{G}(t,t_0) \tag{A.4a}$$

$$\mathcal{F}^2(t,t_0) = -i\partial_t\mathcal{G}(t,t_0) + [-i\mathcal{G}(t,t_0)]^2 \tag{A.4b}$$

$$\begin{aligned}\mathcal{F}^3(t,t_0) = &-i\partial_t^2\mathcal{G}(t,t_0) + [-i\mathcal{G}(t,t_0)][-i\partial_t\mathcal{G}(t,t_0)] \\ &+ 2[-i\partial_t\mathcal{G}(t,t_0)][-i\mathcal{G}(t,t_0)] + [-i\mathcal{G}(t,t_0)]^3\end{aligned} \tag{A.4c}$$

This suggests inserting the ansatz

$$\mathcal{F}^k(t,t_0) = \sum_{n=1}^{k}\sum_{p_1=0}^{k-n}\cdots\sum_{p_n=0}^{k-n}\delta_{k-n,p_1+\ldots+p_n}F^n_{p_1\ldots p_n}[-i\partial_t^{p_1}\mathcal{G}(t,t_0)]\ldots[-i\partial_t^{p_n}\mathcal{G}(t,t_0)] \tag{A.5}$$

and deriving the recursion relations for the coefficients

$$F^n_{p_1\ldots p_n} = \sum_{j=1}^{n} F^n_{p_1\ldots(p_j-1)\ldots p_n} \quad \text{for } p_n \geq 1, \tag{A.6a}$$

$$F^n_{p_1\ldots p_{n-1}0} = \sum_{j=1}^{n-1} F^n_{p_1\ldots(p_j-1)\ldots p_{n-1}0} + F^{n-1}_{p_1\ldots p_{n-1}}. \tag{A.6b}$$

Together with the starting conditions $F^1_0 = 1$ these define *all* the coefficients of the memory expansion. Construction of the general solution of the recursion equations (A.6) is very cumbersome and hides the elegant functional fixed-point relation.

Fixed-point equation. We now show that the result (A.1b) with (A.5) equivalently follows from our fixed-point relation (3.4) by inserting into Eq. (3.3) the memory expansion $\mathcal{G}(s_i,t_0) = \sum_{p_i}\frac{1}{p_i!}(-t_i)^{p_i}\partial_t^{p_i}\mathcal{G}(t,t_0)$ and performing the nested integrations over variables $t_i = t - s_i$:

$$\Pi(s,t|t_0) = \mathcal{T}_{\rightarrow}e^{-\int_s^t d\tau[-i\mathcal{G}](\tau,t_0)} \tag{A.7a}$$

$$= \sum_{n=0}^{\infty}(-1)^n\int_{t>s_n>\ldots>s_1>s} ds_n\ldots ds_1[-i\mathcal{G}(s_1,t_0)]\ldots[-i\mathcal{G}(s_n,t_0)] \tag{A.7b}$$

$$= \sum_{k=0}^{\infty}\frac{(-1)^k}{k!}(t-s)^k\mathcal{F}^k(t,t_0). \tag{A.7c}$$

We obtain the *explicit general* form of *all* coefficients:

$$F^n_{p_1\ldots p_n} = \frac{(n+\sum_i p_i)!}{\prod_i p_i! \prod_{i=0}^{n-1}[\sum_{j=0}^{i} p_{n-j}]} \tag{A.8a}$$

$$= \prod_{i=1}^{n-1} \binom{p_{n-i} + \sum_{j=1}^{i-1}(p_{n-j}+1)}{p_{n-i}} \tag{A.8b}$$

$$= \prod_{i=1}^{n-1} F^2_{p_{i-1},p_i+\ldots+p_n+(n-i)}. \tag{A.8c}$$

The factorization (A.8b) into binomials shows that all coefficients are in fact integers. Using the form (A.8c) one verifies[1] that the coefficients are indeed the solutions to the recursion relations (A.6). With $\mathcal{G}(t,t_0) = \int_{t_0}^{t} ds\, \mathcal{K}(t,s)\Pi(s,t|t_0)$ this establishes that the laborious determination of the coefficients and subsequent summation of the memory expansion (A.1b) envisaged in Refs. [41, 42] ultimately leads to our general functional fixed-point equation (3.4). Our derivation of this self-consistent equation in the main text circumvents all above complications by immediately identifying the divisor in Eq. (3.2). However, even if one is interested in generating memory expansions, our approach (A.7) via the divisor is far simpler.

Noting the special coefficient values $F^n_{0\ldots0} = 1$ we see that

$$\mathcal{F}^k = [-i\mathcal{G}]^k + \text{ (terms involving at least one time-derivative of } \mathcal{G}) \tag{A.9}$$

Thus in the stationary limit where $\lim_{t_0\to-\infty} \partial_t^k \mathcal{G}(t,t_0) = 0$ and $\lim_{t_0\to-\infty} \mathcal{G}(t,t_0) = \mathcal{G}(\infty)$:

$$\Pi(s-t|-\infty) = \sum_{k=0}^{\infty} \frac{(-1)^k}{k!}(t-s)^k[-i\mathcal{G}(\infty)]^k$$

$$= e^{i\mathcal{G}(\infty)(t-s)}. \tag{A.10}$$

Inserted into $\mathcal{G}(\infty) = \int_0^\infty ds\, \mathcal{K}(t-s)\Pi(s-t|-\infty)$ we thus also directly recover our stationary fixed-point equation (3.9) for time-translational systems, $\mathcal{K}(t,s) = \mathcal{K}(t-s)$ by explicit summation of the *stationary* memory expansion. This is the specific expansion studied in Refs. [41, 42].

[1] One verifies Eq. (A.6a) first for $n = 2$, giving $F^2_{p_1p_2} = F^2_{(p_1-1)p_2} + F^2_{p_1(p_2-1)}$, and uses this relation for $n > 2$ to simplify the sum of the last two terms, $F^n_{p_1\ldots(p_{n-1}-1)p_n} + F^n_{p_1\ldots p_{n-1}(p_n-1)}$. Then one adds $F^n_{p_1\ldots(p_{n-2}-2)p_{n-1}p_n}$ and so forth. Eq. (A.6b) follows as special case of Eq. (A.6a) since $F^n_{p_1..p_{n-1}(-1)} = F^{n-1}_{p_1\ldots p_{n-1}}$.

B

Relation between $\mathcal{G}$ and gradient/Moyal expansion of $\mathcal{K}$

The memory expansion (A.1b) implies that the generator of the time-local QME (2.9) may be written as a gradient expansion

$$\mathcal{G}(t,t_0) = \sum_{k=0}^{\infty} \frac{(-1)^k}{k!} \Big[\int_{t_0}^{t} ds\, \mathcal{K}(t,s)(t-s)^k \Big] \mathcal{F}^k(t,t_0) \tag{B.1}$$

$$= \sum_{k=0}^{\infty} \frac{1}{k!} \Big[\frac{\partial^k}{(-i\partial\omega)^k} \hat{\mathcal{K}}(\omega,t,t_0) \Big] \Big|_{\omega=0} \mathcal{F}^k(t,t_0) \tag{B.2}$$

with frequency derivatives of the "finite-time Laplace transform"

$$\hat{\mathcal{K}}(\omega,t,t_0) := \int_0^{t-t_0} ds e^{i\omega s} \mathcal{K}(t,t-s) \tag{B.3}$$

of the memory kernel. Since $\mathcal{F}^k(t,t_0) := [\partial_t^k \Pi(t,t_0)]\Pi(t,t_0)^{-1} = f(\mathcal{G},\ldots,\partial_t^{k-1}\mathcal{G})$ has no simple structure as function of k [Eq. (A.5)] it is not clear how the series can be summed, not even formally. This reflects that it arises from the nontrivial anti-time-ordered exponential (A.7). If one instead considers its action on $\Pi(t,t_0)$,

$$\dot{\Pi}(t,t_0) = -i \sum_{k=0}^{\infty} \frac{(-1)^k}{k!} \Big[\int_{t_0}^{t} ds\, \mathcal{K}(t,s)(t-s)^k \Big] \partial_t^k \Pi(t,t_0) \tag{B.4a}$$

$$= -i \sum_{k=0}^{\infty} \frac{1}{k!} \Big[\frac{\partial^k}{(-i\partial\omega)^k} \hat{\mathcal{K}}(\omega,t,t_0) \Big] \Big|_{\omega=0} \partial_t^k \Pi(t,t_0), \tag{B.4b}$$

then the series can be *formally* summed to give a nonlinear *time-frequency-domain differential operator*. Its action on superoperator *functions* of t must coincide with the linear action of $\mathcal{G}(t,t_0)$ on the superoperator *evaluated at* t:

$$\hat{\mathcal{K}}(\omega,t,t_0) e^{i \frac{\overleftarrow{\partial}}{\partial\omega} \frac{\overrightarrow{\partial}}{\partial t}} \Big|_{\omega=0} \Pi(t,t_0) = \mathcal{G}(t,t_0)\Pi(t,t_0). \tag{B.5}$$

Thus, $\mathcal{G}(t,t_0)$ here plays the role of a (superoperator-valued) eigenvalue of this *time-domain* differential operator. This differential operator is constructed as *frequency-domain* differential operator acting to the *left* on the memory kernel transform $\hat{\mathcal{K}}(\omega,t,t_0)$. The above follows the well-known Moyal approach [139, 157] to quantum physics of closed systems, where one enforces locality at the price of introducing position- and momentum-space differential operators acting both to the right *and to the left*. Its extension to the *time-nonlocal evolution* of open systems within the density-operator approach is thus closely related to the time-convolutionless approach based on the time-local equation (2.9).

Clearly, this *formal* relation between the generator and the memory kernel is easily written down. However, our functional fixed-point result (3.4) goes beyond this by *explicitly* expressing the action of the time-domain differential operator on the left hand side of Eq. (B.5), evaluating $\partial_t^k \Pi(t,t_0) = \mathcal{F}^k(t,t_0)\Pi(t,t_0)$ [Eq. (A.5)], and summing the series to an anti-time-ordered exponential in terms of $\mathcal{G}(t,t_0)$. This is demonstrated by Eq. (A.7) read in reverse order. As the main text shows, this makes the fixed-point relation a powerful analytical and numerical tool.

For time-translational systems, $\mathcal{K}(t,s) = \mathcal{K}(t-s)$, taking the stationary limit leads to the simplification $\lim_{t_0\to-\infty}\mathcal{F}^k(t,t_0) = (-i\mathcal{G}(\infty))^k$, giving

$$\mathcal{G}(\infty) = \sum_{k=0}^{\infty}\frac{(-1)^k}{k!}\Big[\int_{-\infty}^{t} ds\,\mathcal{K}(t-s)(t-s)^k\Big](-i\mathcal{G}(\infty))^k \tag{B.6}$$

$$= \sum_{k=0}^{\infty}\frac{1}{k!}\Big[\frac{\partial^k}{\partial\omega^k}\hat{\mathcal{K}}(\omega)\Big]\Big|_{\omega=0}\mathcal{G}(\infty)^k \tag{B.7}$$

with frequency-derivatives of the Laplace-transformed memory kernel $\hat{\mathcal{K}}(\omega)$. In this case, the gradient expansion can be summed to give an alternative expression for our stationary fixed point relation (3.9):

$$\hat{\mathcal{K}}(\omega)e^{\frac{\overleftarrow{\partial}}{\partial\omega}\mathcal{G}(\infty)}\big|_{\omega=0} = \mathcal{G}(\infty). \tag{B.8}$$

This gives a nonlinear differential operator acting to the left on superoperator functions of ω and is a mere *formal* expression of our stationary fixed-point equation (3.9), $\hat{\mathcal{K}}(\mathcal{G}(\infty)) := \int_{-\infty}^{t} ds\mathcal{K}(t-s)e^{i\mathcal{G}(\infty)(t-s)}$. Equation (B.8) extends the shift property for ordinary Laplace transforms, $e^{\frac{\partial}{\partial\omega}\Delta}\hat{f}(\omega) = \hat{f}(\omega+\Delta)$, to our result (3.10) with superoperator-valued frequency argument $\Delta = \mathcal{G}(\infty)$. To ensure that the memory kernel generates a trace-preserving evolution [Eq. (3.6)] the frequency derivatives must *stand on the right* and therefore needs to *act to the left* to accomplish the shift.

C

Iteration in the resonant level model

For the resonant level model both the stationary [Sec. 3.3.1] and transient [Sec. 3.3.2] fixed-point iteration terminate at the first step when starting from any zero-trace-preserving superoperator X, i.e., $\mathrm{Tr}\, X\bullet = 0$. This can be seen by writing the time-nonlocal part of the kernel as [1, 136]

$$\mathcal{K}_N(t) = -i\Gamma \mathsf{k}(t) e^{-\Gamma t/2} G_+^+ G_-^+, \tag{C.1}$$

where we used the fermionic creation superoperators (4.13), which do not have a spin index σ in the RLM. Because of the superpauli principle they satisfy $G_+^+ G_-^+ G_\eta^+ = 0$ (note that this would not hold in the Anderson model because of the higher Hilbert space dimension). Expanding any zero-trace-preserving superoperator X in terms of products of superfields one verifies that in each term G_η^+ stands on the far *left*. This implies

$$\mathcal{K}_N(t-s) e^{iX(t-s)} = \mathcal{K}_N(t-s) \tag{C.2}$$

and by Eq. (3.20) the transient [Eq. (3.47)] and stationary [Eq. (3.46)] iteration find the exact generator in a *single* step. Starting from an *arbitrary* superoperator X, the first iteration will *make* it zero-trace by Eq. (3.6) and by the above result the second iteration will be converged.

D

Well-definedness of second and fourth order perturbation theory

It is at first unclear whether the diagrams in Eqs. (4.20a)–(4.20b) and Eqs. (4.28a)–(4.28b) of the bare and renormalized $\mathcal{K}$ perturbation theory respectively are actually well defined because of the singularity in the contraction function $\gamma^-_{\eta\sigma}(t)$ [Eq. (4.21)] at $t = 0$. This arises because we have taken the wideband limit from start. In Ref. [135] the bandwidth dependence was discussed [Eq. (75)–(76) loc. cit.] in the frequency representation but not in the time-representation used here. Here we specifically show the finiteness of the renormalized perturbation theory up to fourth order using corresponding arguments. By replacing $L_\infty \to L$ everywhere the exact same steps establish the finiteness of the bare perturbation theory. First note that $\gamma^-_{\eta\sigma}(t)$ diverges as $1/t$ for $t \to 0$, in particular

$$\lim_{t\to 0} t\,\gamma^-_{\eta\sigma}(t) = -i\sum_r \frac{\Gamma_{r\sigma}}{\pi}. \tag{D.1}$$

However, because the superfermion superoperators anticommute [Eq. (4.15)] we have

$$\sum_\eta \gamma^-_{\eta\sigma}(t) G^+_{\eta\sigma} G^+_{\bar\eta\sigma} = \frac{1}{2}\sum_\eta \left[\gamma^-_{\eta\sigma}(t) G^+_{\eta\sigma} G^+_{\bar\eta\sigma} + \gamma^-_{\bar\eta\sigma}(t) G^+_{\bar\eta\sigma} G^+_{\eta\sigma}\right] \tag{D.2a}$$

$$= \frac{1}{2}\sum_\eta \left[\gamma^-_{\eta\sigma}(t) - \gamma^-_{\bar\eta\sigma}(t)\right] G^+_{\eta\sigma} G^+_{\bar\eta\sigma} \tag{D.2b}$$

$$= \frac{-i}{2}\sum_{\eta r} \left[e^{i\bar\eta\mu_r t} - e^{i\eta\mu_r t}\right] \frac{\Gamma_{r\sigma} T_r}{\sinh(\pi T_r t)} G^+_{\eta\sigma} G^+_{\bar\eta\sigma} \tag{D.2c}$$

$$= \sum_{\eta r} \sin(\bar\eta\mu_r t) \frac{\Gamma_{r\sigma} T_r}{\sinh(\pi T_r t)} G^+_{\eta\sigma} G^+_{\bar\eta\sigma} \tag{D.2d}$$

$$= -2\sum_r \Gamma_{r\sigma} T_r \frac{\sin(\mu_r t)}{\sinh(\pi T_r t)} G^+_{+\sigma} G^+_{-\sigma}. \tag{D.2e}$$

Thus, we see that the apparent singularity in the left hand side of Eq. (D.2a) at $t = 0$ never contributes. The $t \to 0$ limit can be evaluated in Eq. (D.2e) and is given by

$$\lim_{t\to 0} \sum_{\eta} \gamma^{-}_{\eta\sigma}(t) G^{+}_{\eta\sigma} G^{+}_{\bar{\eta}\sigma} = -2 \sum_{r} \frac{\Gamma_{r\sigma}}{\pi} \mu_r G^{+}_{+\sigma} G^{+}_{-\sigma}. \tag{D.3}$$

We can now rewrite the second order renormalized $\mathcal{K}$ diagram as

$$= -\sum_{\eta\sigma} \gamma^{-}_{\eta\sigma}(t) G^{+}_{\eta\sigma} e^{-iL_\infty t} G^{+}_{\bar{\eta}\sigma} \tag{D.4}$$

$$= -\sum_{\eta\sigma} \gamma^{-}_{\eta\sigma}(t) G^{+}_{\eta\sigma} \left[e^{-iL_\infty t} - \mathcal{I} \right] G^{+}_{\bar{\eta}\sigma} - \sum_{\eta\sigma} \gamma^{-}_{\eta\sigma}(t) G^{+}_{\eta\sigma} G^{+}_{\bar{\eta}\sigma} \tag{D.5}$$

Using Eq. (D.1) and Eq. (D.3) this immediately shows that this diagram is finite for $t \to 0$:

$$\lim_{t\to 0} \quad = \sum_{\eta\sigma r} \frac{\Gamma_{r\sigma}}{\pi} G^{+}_{\eta\sigma} L_\infty G^{+}_{\bar{\eta}\sigma} + 2 \sum_{\sigma r} \frac{\Gamma_{r\sigma}}{\pi} \mu_r G^{+}_{+\sigma} G^{+}_{-\sigma}. \tag{D.6}$$

Since the second order diagram is contained within one of the fourth order diagrams [Eq. (4.28b)], it follows that

$$= \mathcal{O}(t) \text{ as } t \to 0. \tag{D.7}$$

This is because the outer contraction $\gamma^{-}_{\eta_1\sigma_1}(t)$ diverges as $1/t$, but the inner integrals $\int_0^t dt_1 \int_0^{dt_1} dt_2 \cdots = \mathcal{O}(t^2)$ vanish quadratically. To see the well-definedness of the other fourth order diagram we decompose it as

$$= F_1(t) + F_2(t), \tag{D.8}$$

$$F_1(t) := -\sum_{\eta_1\sigma_1} \sum_{\eta_2\sigma_2} \int_0^t dt_1 \int_0^{t_1} dt_2 \gamma^{-}_{\eta_1\sigma_1}(t - t_2) \gamma^{-}_{\eta_2\sigma_2}(t_1) \times G^{+}_{\eta_1\sigma_1} e^{-iL_\infty (t-t_1)} G^{+}_{\eta_2\sigma_2} \left[e^{-iL_\infty (t_1 - t_2)} - \mathcal{I} \right] G^{+}_{\bar{\eta}_1\sigma_1} e^{-iL_\infty t_2} G^{+}_{\bar{\eta}_2\sigma_2}, \tag{D.9}$$

$$F_2(t) := -\sum_{\eta_1\sigma_1} \sum_{\eta_2\sigma_2} \int_0^t dt_1 \int_0^{t_1} dt_2 \gamma^{-}_{\eta_1\sigma_1}(t - t_2) \gamma^{-}_{\eta_2\sigma_2}(t_1) \times G^{+}_{\eta_1\sigma_1} e^{-iL_\infty (t-t_1)} G^{+}_{\eta_2\sigma_2} G^{+}_{\bar{\eta}_1\sigma_1} e^{-iL_\infty t_2} G^{+}_{\bar{\eta}_2\sigma_2}. \tag{D.10}$$

The first contraction $\gamma^{-}_{\eta_1\sigma_1}(t - t_2)$ in $F_1(t)$ diverges if $t_2 \to t$. But in this limit the factor $e^{-iL_\infty (t_1 - t_2)} - \mathcal{I}$ vanishes with $\mathcal{O}(t_1 - t_2)$ because of the time ordering $t \geq t_1 \geq t_2$. Therefore the divergence in $\gamma^{-}_{\eta_1\sigma_1}(t - t_2)$ is always regularized. The second contraction $\gamma^{-}_{\eta_2\sigma_2}(t_1)$ in $F_1(t)$ diverges for $t_1 \to 0$, which is regularized by the inner integral $\int_0^{t_1} dt_2 = \mathcal{O}(t_1)$. Hence $F_1(t)$ is always finite. In the second term $F_2(t)$ one first uses the

anticommutation $G^+_{\eta_2\sigma_2}G^+_{\bar{\eta}_1\sigma_1} = -G^+_{\bar{\eta}_1\sigma_1}G^+_{\eta_2\sigma_2}$. Note again that in the limit $t_2 \to t$ we also have $t_1 \to t$ because of the time ordering. This means that the factor

$$\gamma^-_{\eta_1\sigma_1}(t - t_2)G^+_{\eta_1\sigma_1}e^{-iL_\infty(t-t_1)}G^+_{\bar{\eta}_1\sigma_1} \tag{D.11}$$

is always finite for $t_2 \to t$ following the same argument which established that Eq. (D.4) has the finite limit (D.6). For precisely the same reason the other factor

$$\gamma^-_{\eta_2\sigma_2}(t_1)G^+_{\eta_2\sigma_2}e^{-iL_\infty t_2}G^+_{\bar{\eta}_2\sigma_2} \tag{D.12}$$

is finite for $t_1 \to 0$. Therefore $F_2(t)$ is also always finite, establishing the well-definedness of this last diagram.

E

Exact generator at $U = 0$

Here we show that the renormalized *second* order generator $\mathcal{G} = L_\infty + \mathcal{G}^{(2)}_{\text{ren}}$ is already exact in the noninteracting case by showing that the fourth order correction is identically zero, $\mathcal{G}^{(4)}_{\text{ren}} = 0$, by a nontrivial cancellation of terms. To do so we split up the fourth order renormalized generator into two contributions

$$-i\mathcal{G}^{(4)}_{\text{ren}}(t) = A_1(t) - A_2(t), \tag{E.1}$$

$A_1(t) :=$ 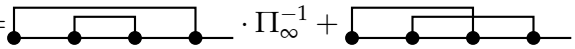 (E.2)

$A_2(t) :=$ 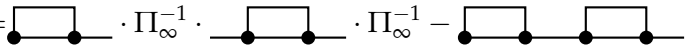 (E.3)

and show that $A_1(t) = A_2(t)$. The main simplification for $U = 0$ is that the renormalized free Liouvillian L_∞ and the superfermions satisfy the commutation relation

$$\left[L_\infty, G^+_{\eta\sigma}\right] = \left(\eta\epsilon - \tfrac{i}{2}\sum_r \Gamma_{r\sigma}\right) G^+_{\eta\sigma}, \tag{E.4}$$

see Eq. (118) in Ref. [136]. From this it follows that

$$G'_{\eta\sigma}(t) := e^{iL_\infty t} G^+_{\eta\sigma} e^{-iL_\infty t} \tag{E.5a}$$

$$= e^{\left(i\eta\epsilon + \frac{1}{2}\sum_r \Gamma_{r\sigma}\right)t} G^+_{\eta\sigma}. \tag{E.5b}$$

These transformed superfermions still anticommute $\left\{G'_{\eta_1\sigma_1}(t_1), G'_{\eta_2\sigma_2}(t_2)\right\} = 0$. We now rewrite $A_1(t)$ using the $G'_{\eta\sigma}$ as

$$\begin{aligned} A_1(t) = e^{-iL_\infty t} \int_{t>t_1>t_2>t_3>0} dt_1 dt_2 dt_3 \Big[&\gamma_{\eta_1\sigma_1}(t-t_3)\gamma_{\eta_2\sigma_2}(t_1-t_2) G'_{\eta_1\sigma_1}(t) G'_{\eta_2\sigma_2}(t_1) G'_{\bar{\eta}_2\sigma_2}(t_2) G'_{\bar{\eta}_1\sigma_1}(t_3) \\ &- \gamma_{\eta_1\sigma_1}(t-t_2)\gamma_{\eta_2\sigma_2}(t_1-t_3) G'_{\eta_1\sigma_1}(t) G'_{\eta_2\sigma_2}(t_1) G'_{\bar{\eta}_1\sigma_1}(t_2) G'_{\bar{\eta}_2\sigma_2}(t_3) \Big] e^{iL_\infty t} \end{aligned} \tag{E.6a}$$

$$\begin{aligned} = e^{-iL_\infty t} \int_{t>t_1>t_2>t_3>0} dt_1 dt_2 dt_3 \Big[&\gamma_{\eta_1\sigma_1}(t-t_3)\gamma_{\eta_2\sigma_2}(t_1-t_2) G'_{\eta_1\sigma_1}(t) G'_{\bar{\eta}_1\sigma_1}(t_3) G'_{\eta_2\sigma_2}(t_1) G'_{\bar{\eta}_2\sigma_2}(t_2) \end{aligned}$$

$$+ \gamma_{\eta_1\sigma_1}(t-t_2)\gamma_{\eta_2\sigma_2}(t_1-t_3)G'_{\eta_1\sigma_1}(t)G'_{\bar{\eta}_1\sigma_1}(t_2)G'_{\eta_2\sigma_2}(t_1)G'_{\bar{\eta}_2\sigma_2}(t_3)\Big]e^{iL_\infty t} \tag{E.6b}$$

$$= e^{-iL_\infty t}\Big[\int_{t>t_2>t_3>t_1>0} dt_2dt_3dt_1 + \int_{t>t_2>t_1>t_3>0} dt_2dt_1dt_3\Big]$$
$$\times \gamma_{\eta_1\sigma_1}(t-t_1)\gamma_{\eta_2\sigma_2}(t_2-t_3)G'_{\eta_1\sigma_1}(t)G'_{\bar{\eta}_1\sigma_1}(t_1)G'_{\eta_2\sigma_2}(t_2)G'_{\bar{\eta}_2\sigma_2}(t_3)e^{iL_\infty t} \tag{E.6c}$$

$$= e^{-iL_\infty t}\int_0^t dt_1\int_{t_1}^t dt_2\int_0^{t_2} dt_3$$
$$\times \gamma_{\eta_1\sigma_1}(t-t_1)\gamma_{\eta_2\sigma_2}(t_2-t_3)G'_{\eta_1\sigma_1}(t)G'_{\bar{\eta}_1\sigma_1}(t_1)G'_{\eta_2\sigma_2}(t_2)G'_{\bar{\eta}_2\sigma_2}(t_3)e^{iL_\infty t} \tag{E.6d}$$

From Eq. (E.6a) to Eq. (E.6b) we used the anticommutation property of the $G'_{\eta\sigma}$. From Eq. (E.6b) to Eq. (E.6c) we relabeled the integration variables as $t_1 \to t_2 \to t_3 \to t_1$ in the first term and as $t_1 \leftrightarrow t_2$ in the second term. But for $A_2(t)$ we have similarly

$$A_2(t) = e^{-iL_\infty t}\Big[\int_0^t dt_1\int_0^t dt_2\int_0^{t_2} dt_3 - \int_{t>t_1>t_2>t_3>0} dt_1dt_2dt_3\Big]$$
$$\times \gamma_{\eta_1\sigma_1}(t-t_1)\gamma_{\eta_2\sigma_2}(t_2-t_3)G'_{\eta_1\sigma_1}(t)G'_{\bar{\eta}_1\sigma_1}(t_1)G'_{\eta_2\sigma_2}(t_2)G'_{\bar{\eta}_2\sigma_2}(t_3)e^{iL_\infty t} \tag{E.7a}$$

$$= e^{-iL_\infty t}\int_0^t dt_1\int_{t_1}^t dt_2\int_0^{t_2} dt_3$$
$$\times \gamma_{\eta_1\sigma_1}(t-t_1)\gamma_{\eta_2\sigma_2}(t_2-t_3)G'_{\eta_1\sigma_1}(t)G'_{\bar{\eta}_1\sigma_1}(t_1)G'_{\eta_2\sigma_2}(t_2)G'_{\bar{\eta}_2\sigma_2}(t_3)e^{iL_\infty t}. \tag{E.7b}$$

By comparison we thus see that $A_1(t) = A_2(t)$. Hence $\mathcal{G}^{(4)}_{\text{ren}} = 0$.

F

Effective supervertices in T-flow

Here we give the precise definition of the supervertices and show how the vertex diagrams can be translated into explicit equations. First, it is important to keep in mind that in contrast to the bare superfermion G_1^+ [Eq. (4.13)] the effective supervertex G_1 also has a dependence on time. Specifically we need to distinguish the time arguments of the latest, the uncontracted and the earliest vertex within G_1, which we label as t, τ and s respectively. Thus $t \geq \tau \geq s$ and we denote $G_1 = G_1(t, \tau, s)$. For time translation invariant systems this simplifies to $G_1(t - \tau, \tau - s)$. Every vertex *except the uncontracted one* is associated with a prefactor of $-i$, and every cut contraction line with a fermion minus sign. Importantly the contraction function associated with the uncontracted vertex is not part of G_1 itself. Thus, the first two diagrams in the definition of G_1 [Eq. (5.4)] are translated as

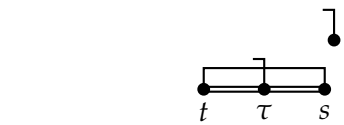

$$= G_1^+ \bar{\delta}(t - \tau)\bar{\delta}(\tau - s), \tag{F.1}$$

$$= \gamma_2^-(t - s) G_2^+ \Pi(t, \tau) G_1^+ \Pi(\tau, s) G_2^+, \tag{F.2}$$

where we indicated the time arguments in the second diagram. Higher order terms also contain internal vertices with time arguments labeled from left to right as $t_1 > \cdots > t_n$ over which one has to integrate in a time-ordered way. For example, the third term of (5.4) reads

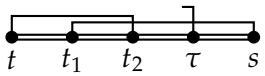

$$= \int_\tau^t dt_1 \int_\tau^{t_1} dt_2 \gamma_2^-(t - t_2)\gamma_3^-(t_1 - s) \times G_2^+ \Pi(t, t_1) G_3^+ \Pi(t_1, t_2) G_2^+ \Pi(t_2, \tau) G_1^+ \Pi(\tau, s) G_3^+. \tag{F.3}$$

The 2-point vertex $G_{12} = G_{12}(t, \tau_1, \tau_2, s)$ is defined such that the uncontracted vertex with index 1 (at time τ_1) is always to the left of the uncontracted vertex with index 2 (at

time τ_2), i.e., $\tau_1 > \tau_2$. Thus

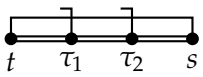

$$= -\gamma_3^-(t-s)G_3\Pi(t,\tau_1)G_1\Pi(\tau_1,\tau_2)G_2\Pi(\tau_2,s)G_{\bar{3}}. \tag{F.4}$$

G

Temperature dependence of the propagator Π

The propagator Π can be computed from the renormalized kernel Σ via the Dyson equation

$$\Pi(t) = \Pi_\infty(t) - i[\Pi_\infty * \Sigma * \Pi](t), \tag{G.1}$$

where $*$ denotes time convolution. Suppressing time arguments and taking a derivative with respect to the temperature T_r of the r-th reservoir it follows that

$$\begin{aligned}
\frac{\partial \Pi}{\partial T_r} =& \Pi_\infty * \frac{\partial\,[-i\Sigma]}{\partial T_r} * \Pi + \Pi_\infty * [-i\Sigma] * \frac{\partial \Pi}{\partial T_r} && \text{(G.2)}\\
=& -i\big(\Pi_\infty + \Pi_\infty * [-i\Sigma] * \Pi_\infty + \cdots\big) * \frac{\partial \Sigma}{\partial T_r} * \Pi && \text{(G.3)}\\
=& -i\Pi * \frac{\partial \Sigma}{\partial T_r} * \Pi. && \text{(G.4)}
\end{aligned}$$

To obtain Eq. (G.3) one iterates the self-consistent equation Eq. (G.2) for $\partial_T \Pi$ treating Π, Π_∞ and Σ as given. Eq. (G.4) follows by recognizing the term in parenthesis as the solution of the self-consistent equation (G.1) for Π. Setting T equal for all reservoirs we obtain Eq. (5.11) of the main text. Inserting the leading order term of $\partial_T \Sigma$ it is straightforward to show that the leading short-time dependence of $\partial_T \Pi$ is *quartic* for small times δt:

$$\frac{\partial \Pi}{\partial T_r}(\delta t) = -\frac{\pi}{36} T_r \Gamma_{r\sigma_1} \left(G_1^+ L_\infty G_{\bar{1}}^+ + \eta_1 \mu_r G_1^+ G_{\bar{1}}^+\right) \delta t^4. \tag{G.5}$$

This explains the T-independent short-time behavior discussed in the main text [Eq. (5.35)].

H

Finiteness of T-flow equations

Here we establish that the T-flow equations are explicitly free of time-divergences. The diagrams in Eq. (5.8) are explicitly given by


$$= -\int_s^t dt_1 \int_s^{t_1} dt_2 \frac{\partial \gamma_1}{\partial T}(t-t_2) G_1^+ \Pi(t,t_1) G_{\bar{1}}(t_1,t_2,s), \tag{H.1}$$


$$= -\int_s^t dt_1 \int_s^{t_1} dt_2 \gamma_1(t-t_2) G_1^+ \frac{\partial \Pi}{\partial T}(t,t_1) G_{\bar{1}}(t_1,t_2,s), \tag{H.2}$$


$$= -\int_s^t dt_1 \int_s^{t_1} dt_2 \gamma_1(t-t_2) G_1^+ \Pi(t,t_1) \frac{\partial G_{\bar{1}}}{\partial T}(t_1,t_2,s). \tag{H.3}$$

Whereas (H.1) does not contain any singularities, this is not immediately obvious for Eqs. (H.2) and (H.3). In Eq. (H.2) we use that $\partial_T \Pi(t) = \mathcal{O}(t^4)$, see Eq. (G.5). This small-time behaviour regularizes the $1/t$ divergence of the contraction function. The finiteness of (H.3) can be seen by switching the order of integrations:

$$\int_s^t dt_1 \int_s^{t_1} dt_2 \gamma_1(t-t_2) = \int_s^t dt_2 \gamma_1(t-t_2) \int_{t_2}^t dt_1 \tag{H.4}$$

Now the inner t_1 integral vanishes as $\mathcal{O}(t-t_2)$ making the term finite. Using very similar arguments one establishes that all diagrams in (5.12) and (5.13) are well behaved, making the T-flow equations explicitly time-singularity free.

I

Numerical solution of the T-flow equations

The truncated T-flow equations from the main text form a closed set of implicit (self-consistent) differential equations for Σ, G_1 and G_{12} and we here comment on their numerical discretization. Suppressing time arguments these equations are of the form

$$\frac{\partial \Sigma}{\partial T} = \mathcal{F}_0\left[\Sigma, \frac{\partial \Sigma}{\partial T}, G_1, \frac{\partial G_1}{\partial T}\right], \tag{I.1}$$

$$\frac{\partial G_1}{\partial T} = \mathcal{F}_1\left[\Sigma, \frac{\partial \Sigma}{\partial T}, G_1, \frac{\partial G_1}{\partial T}, G_{12}, \frac{\partial G_{12}}{\partial T}\right], \tag{I.2}$$

$$\frac{\partial G_{12}}{\partial T} = \mathcal{F}_2\left[\Sigma\right], \tag{I.3}$$

where the functionals $\mathcal{F}_i$ are given by the right-hand sides of Eqs. (5.8), (5.12) and (5.13). We do not explicitly indicate the dependence on the propagator Π and its temperature derivative $\partial_T \Pi$, since these can be computed using Σ and $\partial_T \Sigma$ as the solutions of Eqs. (2.3) and (5.11), respectively. Defining the vector $\Phi := (\Sigma, G_1, G_{12})$ the T-flow equations thus have the form

$$\frac{\partial \Phi}{\partial T} = \mathcal{F}\left[\Phi, \frac{\partial \Phi}{\partial T}\right]. \tag{I.4}$$

To simplify the discussion we assume an equidistant temperature grid $T_n := n\delta T$ for some small stepsize $\delta T > 0$, noting that in practice the stepsize should be varied based on local error estimates to reduce numerical effort and improve accuracy. Our goal is to compute $\Phi_n := \Phi(T_n)$ and $\partial_T \Phi_n := \partial_T \Phi(T_n)$ on this grid assuming $\Phi_{n+1}, \Phi_{n+2}, \ldots$ and $\partial_T \Phi_{n+1}, \partial_T \Phi_{n+2}, \ldots$ are already available. To do so we first approximate $\partial_T \Phi_n \approx (-3\Phi_n + 4\Phi_{n+1} - \Phi_{n+2})/(2\delta T)$ leading to

$$\Phi_n = \frac{4}{3}\Phi_{n+1} - \frac{1}{3}\Phi_{n+2} - \frac{2}{3}\mathcal{F}\left[\Phi_n, \frac{-3\Phi_n + 4\Phi_{n+1} - \Phi_{n+2}}{2\delta T}\right]\delta T + \mathcal{O}(\delta T^3). \tag{I.5}$$

This is the well-known second order backwards differentiation formula (BDF2) [185]. To evaluate Eq. (I.5) further we approximate on the right hand side $\Phi_n = \Phi_n^{(\mathrm{P})} + \mathcal{O}(T^3)$, where $\Phi_n^{(\mathrm{P})}$ denotes the Adams-Bashforth predictor [185]

$$\Phi_n^{(\mathrm{P})} := \Phi_{n+1} - \left(\frac{3}{2} \left. \frac{\partial \Phi}{\partial T} \right|_{n+1} - \frac{1}{2} \left. \frac{\partial \Phi}{\partial T} \right|_{n+2} \right) \delta T. \tag{I.6}$$

Thus we obtain both Φ_n and $\partial_T \Phi_n = \mathcal{F}\left[\Phi_n^{(\mathrm{P})}, (-3\Phi_n^{(\mathrm{P})} + 4\Phi_{n+1} - \Phi_{n+2})/(2\delta T)\right]$ as wanted.

References

[1] V. Reimer, M. R. Wegewijs, K. Nestmann, and M. Pletyukhov, "Five approaches to exact open-system dynamics: Complete positivity, divisibility, and time-dependent observables", J. Chem. Phys. **151**, 044101 (2019).

[2] K. Nestmann, V. Bruch, and M. R. Wegewijs, "How quantum evolution with memory is generated in a time-local way", Phys. Rev. X **11**, 021041 (2021).

[3] V. Bruch, K. Nestmann, J. Schulenborg, and M. R. Wegewijs, "Fermionic duality: General symmetry of open systems with strong dissipation and memory", SciPost Phys. **11**, 53 (2021).

[4] K. Nestmann and M. R. Wegewijs, "General connection between time-local and time-nonlocal perturbation expansions", Phys. Rev. B **104**, 155407 (2021).

[5] K. Nestmann and M. R. Wegewijs, "Renormalization group for open quantum systems using environment temperature as flow parameter", SciPost Phys. **12**, 121 (2022).

[6] W. H. Louisell, *Quantum statistical properties of radiation* (Wiley, 1973).

[7] C. C. Tannoudji, J. D. Roc, and G. Grynberg, *Atom - photon interactions: basic processes and applications* (Wiley, 1992).

[8] H. Carmichael, *An open systems approach to quantum optics* (Springer, 1993).

[9] L. L. Sohn, L. P. Kouwenhoven, and G. Schön, *Mesoscopic Electron Transport* (Springer, Dordrecht, The Netherlands, 1997).

[10] V. May and K. Oliver, *Charge and energy transfer dynamics in molecular systems* (Wiley-VCH, 2004).

[11] A. Nitzan, *Chemical dynamics in condensed phases: relaxation, transfer and reactions in condensed molecular systems* (Oxford University Press, 2006).

[12] M. A. Nielsen and I. L. Chuang, *Quantum computation and quantum information* (Cambridge University Press, Cambridge, 2010).

[13] C. Uchiyama, "Nonadiabatic effect on the quantum heat flux control", Phys. Rev. E **89**, 052108 (2014).

[14] J. Goold, M. Huber, A. Riera, L. del Rio, and P. Skrzypczyk, "The role of quantum information in thermodynamics - a topical review", J. Phys. A: Math. Theor. **49**, 143001 (2016).

[15] S. Vinjanampathy and J. Anders, "Quantum thermodynamics", Contemp. Phys. **57**, 545–579 (2016).

[16] H.-P. Breuer, E.-M. Laine, and J. Piilo, "Measure for the degree of non-markovian behavior of quantum processes in open systems", Phys. Rev. Lett. **103**, 210401 (2009).

[17] D. Chruściński, A. Kossakowski, and Á. Rivas, "Measures of non-markovianity: divisibility versus backflow of information", Phys. Rev. A **83**, 052128 (2011).

[18] Á. Rivas, S. F. Huelga, and M. B. Plenio, "Quantum non-markovianity: characterization, quantification and detection", Rep. Prog. Phys. **77**, 094001 (2014).

[19] J. Bae and D. Chruściński, "Operational Characterization of Divisibility of Dynamical Maps", Phys. Rev. Lett. **117**, 050403 (2016).

[20] B. Vacchini and H.-P. Breuer, "Exact master equations for the non-Markovian decay of a qubit", Phys. Rev. A **81**, 042103 (2010).

[21] A. Smirne and B. Vacchini, "Nakajima-Zwanzig versus time-convolutionless master equation for the non-Markovian dynamics of a two-level system", Phys. Rev. A **82**, 022110 (2010).

[22] N. Megier, D. Chruściński, J. Piilo, and W. T. Strunz, "Eternal non-Markovianity: from random unitary to Markov chain realisations", Sci. Rep. **7**, 6379 (2017).

[23] H. Schoeller, "A perturbative nonequilibrium renormalization group method for dissipative quantum mechanics", Eur. Phys. Journ. Special Topics **168**, 179–266 (2009).

[24] H. Schoeller, "Dynamics of open quantum systems", arXiv:1802.10014 (2018).

[25] G. Cohen and E. Rabani, "Memory effects in nonequilibrium quantum impurity models", Phys. Rev. B **84**, 075150 (2011).

[26] L. Kidon, H. Wang, M. Thoss, and E. Rabani, "On the memory kernel and the reduced system propagator", J. Chem. Phys. **149**, 104105 (2018).

[27] M. Pletyukhov and H. Schoeller, "Nonequilibrium kondo model: crossover from weak to strong coupling", Phys. Rev. Lett. **108**, 260601 (2012).

[28] E. Y. Wilner, H. Wang, G. Cohen, M. Thoss, and E. Rabani, "Bistability in a nonequilibrium quantum system with electron-phonon interactions", Phys. Rev. B **88**, 045137 (2013).

[29] C. J. Lindner and H. Schoeller, "Dissipative quantum mechanics beyond the Bloch-Redfield approximation: A consistent weak-coupling expansion of the Ohmic spin boson model at arbitrary bias", Phys. Rev. B **98**, 115425 (2018).

[30] C. J. Lindner, F. B. Kugler, V. Meden, and H. Schoeller, "Renormalization group transport theory for open quantum systems: Charge fluctuations in multilevel quantum dots in and out of equilibrium", Phys. Rev. B **99**, 205142 (2019).

[31] A. Braggio, J. König, and R. Fazio, "Full Counting Statistics in Strongly Interacting Systems: Non-Markovian Effects", Phys. Rev. Lett. **96**, 026805 (2006).

[32] C. Flindt, T. Novotný, A. Braggio, M. Sassetti, and A.-P. Jauho, "Counting Statistics of Non-Markovian Quantum Stochastic Processes", Phys. Rev. Lett. **100**, 150601 (2008).

[33] K. H. Thomas and C. Flindt, "Electron waiting times in non-Markovian quantum transport", Phys. Rev. B **87**, 121405(R) (2013).

[34] F. Shibata, Y. Takahashi, and N. Hashitsume, "A generalized stochastic liouville equation. Non-Markovian versus memoryless master equations", J. Stat. Phys. **17**, 171 (1977).

[35] F. Shibata and T. Arimitsu, "Expansion Formulas in Nonequilibrium Statistical Mechanics", J. Phys. Soc. Jpn. **49**, 891 (1980).

[36] S. Chaturvedi and F. Shibata, "Time-convolutionless projection operator formalism for elimination of fast variables. Applications to Brownian motion", Z. Phys. B: Condens. Matter **35**, 297–308 (1979).

[37] H.-P. Breuer, B. Kappler, and F. Petruccione, "Stochastic wave-function method for non-Markovian quantum master equations", Phys. Rev. A **59**, 1633–1643 (1999).

[38] H.-P. Breuer, B. Kappler, and F. Petruccione, "The time-convolutionless projection operator technique in the quantum theory of dissipation and decoherence", Ann. Phys. **291**, 36–70 (2001).

[39] C. Timm, "Time-convolutionless master equation for quantum dots: perturbative expansion to arbitrary order", Phys. Rev. B **83**, 115416 (2011).

[40] J. Splettstoesser, M. Governale, J. König, and R. Fazio, "Adiabatic pumping through a quantum dot with coulomb interactions: a perturbation expansion in the tunnel coupling", Phys. Rev. B **74**, 085305 (2006).

[41] L. D. Contreras-Pulido, J. Splettstoesser, M. Governale, J. König, and M. Büttiker, "Time scales in the dynamics of an interacting quantum dot", Phys. Rev. B **85**, 075301 (2012).

[42] C. Karlewski and M. Marthaler, "Time-local master equation connecting the Born and Markov approximations", Phys. Rev. B **90**, 104302 (2014).

[43] Á. Rivas, S. F. Huelga, and M. B. Plenio, "Entanglement and Non-Markovianity of Quantum Evolutions", Phys. Rev. Lett. **105**, 050403 (2010).

[44] D. Chruściński and A. Kossakowski, "Markovianity criteria for quantum evolution", J. Phys. B: At. Mol. Opt. Phys. **45**, 154002 (2012).

[45] M. J. W. Hall, J. D. Cresser, L. Li, and E. Andersson, "Canonical form of master equations and characterization of non-Markovianity", Phys. Rev. A **89**, 042120 (2014).

[46] G. Amato, H.-P. Breuer, and B. Vacchini, "Microscopic modeling of general time-dependent quantum Markov processes", Phys. Rev. A **99**, 030102 (2019).

[47] V. Reimer and M. R. Wegewijs, "Density-operator evolution: Complete positivity and the Keldysh real-time expansion", SciPost Phys. **7**, 12 (2019).

[48] D. Chruściński and A. Kossakowski, "Sufficient conditions for memory kernel master equation", Phys. Rev. A **94**, 020103(R) (2016).

[49] D. Chruściński and A. Kossakowski, "Generalized semi-Markov quantum evolution", Phys. Rev. A **95**, 042131 (2017).

[50] B. Vacchini, A. Smirne, E.-M. Laine, J. Piilo, and H.-P. Breuer, "Markovianity and non-Markovianity in quantum and classical systems", New J. Phys. **13**, 093004 (2011).

[51] B. Vacchini, "Non-Markovian master equations from piecewise dynamics", Phys. Rev. A **87**, 030101 (2013).

[52] F. Ciccarello, G. M. Palma, and V. Giovannetti, "Collision-model-based approach to non-Markovian quantum dynamics", Phys. Rev. A **87**, 040103 (2013).

[53] S. N. Filippov and D. Chruściński, "Time deformations of master equations", Phys. Rev. A **98**, 022123 (2018).

[54] M. M. Wolf and J. I. Cirac, "Dividing Quantum Channels", Commun. Math. Phys. **279**, 147–168 (2008).

[55] A. Müller-Hermes, D. Reeb, and M. M. Wolf, "Quantum Subdivision Capacities and Continuous-Time Quantum Coding", IEEE Trans. Inf. Theory **61**, 565–581 (2015).

[56] E. Nielsen, J. K. Gamble, K. Rudinger, T. Scholten, K. Young, and R. Blume-Kohout, "Gate Set Tomography", Quantum **5**, 557 (2021).

[57] R. Vasile, S. Olivares, M. A. Paris, and S. Maniscalco, "Continuous-variable quantum key distribution in non-Markovian channels", Phys. Rev. A **83**, 042321 (2011).

[58] E.-M. Laine, H.-P. Breuer, and J. Piilo, "Nonlocal memory effects allow perfect teleportation with mixed states", Sci. Rep. **4**, 1–5 (2014).

[59] B. Bylicka, M. Tukiainen, D. Chruściński, J. Piilo, and S. Maniscalco, "Thermodynamic power of non-Markovianity", Sci. Rep. **6**, 1–7 (2016).

[60] M. S. Sarandy and D. A. Lidar, "Adiabatic approximation in open quantum systems", Phys. Rev. A **71**, 012331 (2005).

[61] M. S. Sarandy and D. A. Lidar, "Abelian and non-Abelian geometric phases in adiabatic open quantum systems", Phys. Rev. A **73**, 062101 (2006).

[62] D. O. Krimer and M. Pletyukhov, "Few-Mode Geometric Description of a Driven-Dissipative Phase Transition in an Open Quantum System", Phys. Rev. Lett. **123**, 110604 (2019).

[63] F. Li, J. Ren, and N. A. Sinitsyn, "Quantum Zeno effect as a topological phase transition in full counting statistics and spin noise spectroscopy", EPL **105**, 27001 (2014).

[64] R.-P. Riwar, "Fractional charges in conventional sequential electron tunneling", Phys. Rev. B **100**, 245416 (2019).

[65] N. A. Sinitsyn, "The stochastic pump effect and geometric phases in dissipative and stochastic systems", J. Phys. A: Math. Theor. **42**, 193001 (2009).

[66] R.-P. Riwar and J. Splettstoesser, "Transport fluctuation relations in interacting quantum pumps", New J. Phys. **23**, 013010 (2021).

[67] W. de Haas, J. de Boer, and G. van dën Berg, "The electrical resistance of gold, copper and lead at low temperatures", Physica **1**, 1115–1124 (1934).

[68] J. Kondo, "Resistance Minimum in Dilute Magnetic Alloys", Progress of Theoretical Physics **32**, 37–49 (1964).

[69] D. Goldhaber-Gordon, J. Göres, M. A. Kastner, H. Shtrikman, D. Mahalu, and U. Meirav, "From the Kondo Regime to the Mixed-Valence Regime in a Single-Electron Transistor", Phys. Rev. Lett. **81**, 5225–5228 (1998).

[70] K. G. Wilson, "The renormalization group: Critical phenomena and the Kondo problem", Rev. Mod. Phys. **47**, 773–840 (1975).

[71] L. P. Kadanoff, "Scaling laws for ising models near T_c", Physics Physique Fizika **2**, 263–272 (1966).

[72] L. P. Kadanoff, W. Götze, D. Hamblen, R. Hecht, E. A. S. Lewis, V. V. Palciauskas, M. Rayl, J. Swift, D. Aspnes, and J. Kane, "Static Phenomena Near Critical Points: Theory and Experiment", Rev. Mod. Phys. **39**, 395–431 (1967).

[73] P. W. Anderson, G. Yuval, and D. R. Hamann, "Exact Results in the Kondo Problem. II. Scaling Theory, Qualitatively Correct Solution, and Some New Results on One-Dimensional Classical Statistical Models", Phys. Rev. B **1**, 4464–4473 (1970).

[74] H. T. M. Nghiem and T. A. Costi, "Generalization of the time-dependent numerical renormalization group method to finite temperatures and general pulses", Phys. Rev. B **89**, 075118 (2014).

[75] F. B. Anders and A. Schiller, "Real-Time Dynamics in Quantum-Impurity Systems: A Time-Dependent Numerical Renormalization-Group Approach", Phys. Rev. Lett. **95**, 196801 (2005).

[76] F. B. Anders, "Steady-State Currents through Nanodevices: A Scattering-States Numerical Renormalization-Group Approach to Open Quantum Systems", Phys. Rev. Lett. **101**, 066804 (2008).

[77] A. J. Daley, C. Kollath, U. Schollwöck, and G. Vidal, "Time-dependent density-matrix renormalization-group using adaptive effective Hilbert", J. Stat. Mech.: Theory Exp. **2004**, P04005 (2004).

[78] S. R. White and A. E. Feiguin, "Real-Time Evolution Using the Density Matrix Renormalization Group", Phys. Rev. Lett. **93**, 076401 (2004).

[79] S. G. Jakobs, V. Meden, and H. Schoeller, "Nonequilibrium functional renormalization group for interacting quantum systems", Phys. Rev. Lett. **99**, 150603 (2007).

[80] S. G. Jakobs, M. Pletyukhov, and H. Schoeller, "Nonequilibrium functional renormalization group with frequency-dependent vertex function: a study of the single-impurity anderson model", Phys. Rev. B **81**, 195109 (2010).

[81] J. E. Han and R. J. Heary, "Imaginary-Time Formulation of Steady-State Nonequilibrium: Application to Strongly Correlated Transport", Phys. Rev. Lett. **99**, 236808 (2007).

[82] S. Weiss, J. Eckel, M. Thorwart, and R. Egger, "Iterative real-time path integral approach to nonequilibrium quantum transport", Phys. Rev. B **77**, 195316 (2008).

[83] H. Schoeller and J. König, "Real-Time Renormalization Group and Charge Fluctuations in Quantum Dots", Phys. Rev. Lett. **84**, 3686–3689 (2000).

[84] H. Schoeller, "An Introduction to Real-Time Renormalization Group", in *Low-Dimensional Systems* (Springer, Berlin, Germany, 2000), pp. 137–166.

[85] T. Korb, F. Reininghaus, H. Schoeller, and J. König, "Real-time renormalization group and cutoff scales in nonequilibrium applied to an arbitrary quantum dot in the Coulomb blockade regime", Phys. Rev. B **76**, 165316 (2007).

[86] H. Schoeller and F. Reininghaus, "Real-time renormalization group in frequency space: A two-loop analysis of the nonequilibrium anisotropic Kondo model at finite magnetic field", Phys. Rev. B **80**, 045117 (2009).

[87] H. Schoeller and F. Reininghaus, "Erratum: Real-time renormalization group in frequency space: A two-loop analysis of the nonequilibrium anisotropic Kondo

model at finite magnetic field [Phys. Rev. B 80, 045117 (2009)]", Phys. Rev. B **80**, 209901 (2009).

[88] M. Pletyukhov, D. Schuricht, and H. Schoeller, "Relaxation versus decoherence: spin and current dynamics in the anisotropic kondo model at finite bias and magnetic field", Phys. Rev. Lett. **104**, 106801 (2010).

[89] F. Reininghaus, M. Pletyukhov, and H. Schoeller, "Kondo model in nonequilibrium: Interplay between voltage, temperature, and crossover from weak to strong coupling", Phys. Rev. B **90**, 085121 (2014).

[90] C. Karrasch, S. Andergassen, M. Pletyukhov, D. Schuricht, L. Borda, V. Meden, and H. Schoeller, "Non-equilibrium current and relaxation dynamics of a charge-fluctuating quantum dot", Europhys. Lett. **90**, 30003 (2010).

[91] O. Kashuba, D. M. Kennes, M. Pletyukhov, V. Meden, and H. Schoeller, "Quench dynamics of a dissipative quantum system: a renormalization group study", Phys. Rev. B **88**, 165133 (2013).

[92] O. Kashuba and H. Schoeller, "Transient dynamics of open quantum systems", Phys. Rev. B **87**, 201402 (2013).

[93] H.-P. Breuer and F. Petruccione, *The theory of open quantum systems* (Oxford University Press, London, 2002).

[94] D. Chruściński and A. Kossakowski, "Non-Markovian Quantum Dynamics: Local versus Nonlocal", Phys. Rev. Lett. **104**, 070406 (2010).

[95] D. Chruściński, Á. Rivas, and E. Størmer, "Divisibility and Information Flow Notions of Quantum Markovianity for Noninvertible Dynamical Maps", Phys. Rev. Lett. **121**, 080407 (2018).

[96] S. Chakraborty and D. Chruściński, "Information flow versus divisibility for qubit evolution", Phys. Rev. A **99**, 042105 (2019).

[97] U. Chakraborty and D. Chruściński, "Construction of propagators for divisible dynamical maps", New J. Phys. **23**, 013009 (2021).

[98] N. Kirstaedter, N. N. Ledentsov, M. Grundmann, D. Bimberg, V. M. Ustinov, S. S. Ruvimov, M. V. Maximov, P. S. Kop'ev, Z. I. Alferov, U. Richter, P. Werner, U. Gösele, and J. Heydenreich, "Low threshold, large To injection laser emission from (InGa)As quantum dots", Electron. Lett. **30**, 1416–1417 (1994).

[99] C.-H. M. Chuang, P. R. Brown, V. Bulović, and M. G. Bawendi, "Improved performance and stability in quantum dot solar cells through band alignment engineering - Nature Materials", Nat. Mater. **13**, 796–801 (2014).

[100] T.-H. Kim, K.-S. Cho, E. K. Lee, S. J. Lee, J. Chae, J. W. Kim, D. H. Kim, J.-Y. Kwon, G. Amaratunga, S. Y. Lee, B. L. Choi, Y. Kuk, J. M. Kim, and K. Kim, "Full-colour quantum dot displays fabricated by transfer printing - Nature Photonics", Nat. Photonics **5**, 176–182 (2011).

[101] A. Imamog¯lu, D. D. Awschalom, G. Burkard, D. P. DiVincenzo, D. Loss, M. Sherwin, and A. Small, "Quantum Information Processing Using Quantum Dot Spins and Cavity QED", Phys. Rev. Lett. **83**, 4204–4207 (1999).

[102] J. R. Schrieffer and P. A. Wolff, "Relation between the Anderson and Kondo Hamiltonians", Phys. Rev. **149**, 491–492 (1966).

[103] K. E. Hellwig and K. Kraus, "Pure operations and measurements", Commun. Math. Phys. **11**, 214 (1969).

[104] K. Kraus, "General state changes in quantum theory", Ann. Phys. **64**, 311 (1971).

[105] P. Pechukas, "Reduced dynamics need not be completely positive", Phys. Rev. Lett. **73**, 1060–1062 (1994).

[106] K. Kraus, *States, effects and operations: fundamental notions of quantum theory* (Springer-Verlag, Berlin, 1983).

[107] R. Alicki, "Comment on "reduced dynamics need not be completely positive"", Phys. Rev. Lett. **75**, 3020–3020 (1995).

[108] P. Pechukas, "Pechukas replies:" Phys. Rev. Lett. **75**, 3021–3021 (1995).

[109] D. Schmid, K. Ried, and R. W. Spekkens, "Why initial system-environment correlations do not imply the failure of complete positivity: a causal perspective", Phys. Rev. A **100**, 022112 (2019).

[110] S. Nakajima, "On quantum theory of transport phenomena", Prog. Theor. Phys. **20**, 948 (1958).

[111] R. Zwanzig, "Ensemble method in the theory of irreversibility", J. Chem. Phys. **33**, 1338 (1960).

[112] M. Tokuyama and H. Mori, "Statistical-Mechanical Approach to Random Frequency Modulations and the Gaussian Memory Function", Progress of Theoretical Physics **54**, 918–920 (1975).

[113] M. Tokuyama and H. Mori, "Statistical-Mechanical Theory of Random Frequency Modulations and Generalized Brownian Motions", Prog. Theor. Phys. **55**, 411 (1976).

[114] T. Yu and J. H. Eberly, "Finite-Time Disentanglement Via Spontaneous Emission", Phys. Rev. Lett. **93**, 140404 (2004).

[115] M. P. Almeida, F. de Melo, M. Hor-Meyll, A. Salles, S. P. Walborn, P. H. S. Ribeiro, and L. Davidovich, "Environment-Induced Sudden Death of Entanglement", Science **316**, 579–582 (2007).

[116] J. Laurat, K. S. Choi, H. Deng, C. W. Chou, and H. J. Kimble, "Heralded Entanglement between Atomic Ensembles: Preparation, Decoherence, and Scaling", Phys. Rev. Lett. **99**, 180504 (2007).

[117] T. Yu and J. H. Eberly, "Sudden Death of Entanglement", Science **323**, 598–601 (2009).

[118] V. Gorini, A. Kossakowski, and E. C. G. Sudarshan, "Completely positive dynamical semigroups of n-level systems", J. Math. Phys. **17**, 821 (1976).

[119] G. Lindblad, "On the generators of quantum dynamical semigroups", Commun. Math. Phys. **48**, 119–130 (1976).

[120] H.-P. Breuer, E.-M. Laine, J. Piilo, and B. Vacchini, "Colloquium: Non-Markovian dynamics in open quantum systems", Rev. Mod. Phys. **88**, 021002 (2016).

[121] H. M. Wiseman and G. J. Milburn, *Quantum measurement and control* (Cambridge University Press, 2009).

[122] L. Li, M. J. W. Hall, and H. M. Wiseman, "Concepts of quantum non-Markovianity: A hierarchy", Phys. Rep. **759**, 1–51 (2018).

[123] M. Hell, M. R. Wegewijs, and D. P. DiVincenzo, "Coherent backaction of quantum dot detectors: Qubit isospin precession", Phys. Rev. B **89**, 195405 (2014).

[124] M. Hell, M. R. Wegewijs, and D. P. DiVincenzo, "Qubit quantum-dot sensors: Noise cancellation by coherent backaction, initial slips, and elliptical precession", Phys. Rev. B **93**, 045418 (2016).

[125] W. F. Stinespring, "Positive functions on C^*-algebras", Proc. Amer. Math. Soc. **6**, 211 (1955).

[126] C. W. Helstrom, "Quantum detection and estimation theory", J. Stat. Phys. **1**, 231–252 (1969).

[127] B. Bylicka, M. Johansson, and A. Acin, "Constructive method for detecting the information backflow of non-markovian dynamics", Phys. Rev. Lett. **118**, 120501 (2017).

[128] U. Geigenmüller, U. M. Titulaer, and B. U. Felderhof, "Systematic elimination of fast variables in linear systems", Physica A **119**, 41 (1983).

[129] F. Haake and M. Lewenstein, "Adiabatic drag and initial slip in random processes", Phys. Rev. A **28**, 3606–3612 (1983).

[130] F. Haake and R. Reibold, "Strong damping and low-temperature anomalies for the harmonic oscillator", Phys. Rev. A **32**, 2462–2475 (1985).

[131] P. Gaspard and M. Nagaoka, "Slippage of initial conditions for the Redfield master equation", J. Chem. Phys. **111**, 5668–5675 (1999).

[132] H. Schoeller and G. Schön, "Mesoscopic quantum transport: resonant tunneling in the presence of a strong coulomb interaction", Phys. Rev. B **50**, 18436–18452 (1994).

[133] J. König, H. Schoeller, and G. Schön, "Zero-bias anomalies and boson-assisted tunneling through quantum dots", Phys. Rev. Lett. **76**, 1715 (1996).

[134] J. König, J. Schmid, H. Schoeller, and G. Schön, "Resonant tunneling through ultrasmall quantum dots: zero-bias anomalies, magnetic-field dependence, and boson-assisted transport", Phys. Rev. B **54**, 16820 (1996).

[135] R. B. Saptsov and M. R. Wegewijs, "Fermionic superoperators for zero-temperature nonlinear transport: real-time perturbation theory and renormalization group for anderson quantum dots", Phys. Rev. B **86**, 235432 (2012).

[136] R. B. Saptsov and M. R. Wegewijs, "Time-dependent quantum transport: causal superfermions, exact fermion-parity protected decay modes, and pauli exclusion principle for mixed quantum states", Phys. Rev. B **90**, 045407 (2014).

[137] J. Schulenborg, R. B. Saptsov, F. Haupt, J. Splettstoesser, and M. R. Wegewijs, "Fermion-parity duality and energy relaxation in interacting open systems", Phys. Rev. B **93**, 081411(R) (2016).

[138] J. Schulenborg, J. Splettstoesser, and M. R. Wegewijs, "Duality for open fermion systems: energy-dependent weak coupling and quantum master equations", Phys. Rev. B **98**, 235405 (2018).

[139] J. E. Moyal, "Quantum mechanics as a statistical theory", Math. Proc. Cambridge Philos. Soc. **45**, 99 (1949).

[140] J. Rammer and H. Smith, "Quantum field-theoretical methods in transport theory of metals", Rev. Mod. Phys. **58**, 323 (1986).

[141] S. Onoda, N. Sugimoto, and N. Nagaosa, "Theory of Non-Equilibirum States Driven by Constant Electromagnetic Fields— Non-Commutative Quantum Mechanics in the Keldysh Formalism —", Prog. Theor. Phys. **116**, 61 (2006).

[142] D. Sternheimer, "Deformation quantization: twenty years after", AIP Conference Proceedings **453**, 107 (1998).

[143] C. Zachos, "A Survey of Star Product Geometry", arXiv:hep-th/0008010 (2000).

[144] F. Buscemi and N. Datta, "Equivalence between divisibility and monotonic decrease of information in classical and quantum stochastic processes", Phys. Rev. A **93**, 012101 (2016).

[145] A. Smirne, L. Mazzola, M. Paternostro, and B. Vacchini, "Interaction-induced correlations and non-Markovianity of quantum dynamics", Phys. Rev. A **87**, 052129 (2013).

[146] S. Wißmann, H.-P. Breuer, and B. Vacchini, "Generalized trace-distance measure connecting quantum and classical non-Markovianity", Phys. Rev. A **92**, 042108 (2015).

[147] F. Benatti, D. Chruściński, and S. Filippov, "Tensor power of dynamical maps and positive versus completely positive divisibility", Phys. Rev. A **95**, 012112 (2017).

[148] H.-P. Breuer, G. Amato, and B. Vacchini, "Mixing-induced quantum non-Markovianity and information flow", New J. Phys. **20**, 043007 (2018).

[149] D. Chruściński, C. Macchiavello, and S. Maniscalco, "Detecting non-markovianity of quantum evolution via spectra of dynamical maps", Phys. Rev. Lett. **118**, 080404 (2017).

[150] B. M. Garraway, "Decay of an atom coupled strongly to a reservoir", Phys. Rev. A **55**, 4636 (1997).

[151] L. Mazzola, S. Maniscalco, J. Piilo, K.-A. Suominen, and B. M. Garraway, "Pseudomodes as an effective description of memory: Non-Markovian dynamics of two-state systems in structured reservoirs", Phys. Rev. A **80**, 012104 (2009).

[152] A. J. van Wonderen and L. G. Suttorp, "Kraus map for non-markovian quantum dynamics driven by a thermal reservoir", EPL **102**, 60001 (2013).

[153] A. J. van Wonderen and L. G. Suttorp, "Continued-fraction representation of the kraus map for non-markovian reservoir damping", J. Phys. A: Math. Gen. **51**, 175304 (2018).

[154] A. J. van Wonderen and L. G. Suttorp, "Exact density matrix of a discrete quantum system immersed in a thermal reservoir", arXiv:1808.04198 (2018).

[155] K. Siudzińska and D. Chruściński, "Quantum evolution with a large number of negative decoherence rates", J. Phys. A: Math. Theor. **53**, 375305 (2020).

[156] F. Cavaliere, M. Governale, and J. König, "Nonadiabatic Pumping through Interacting Quantum Dots", Phys. Rev. Lett. **103**, 136801 (2009).

[157] H. J. Groenewold, *On the Principles of Elementary Quantum Mechanics* (Springer Netherlands, Dordrecht, 1946).

[158] N. Megier, A. Smirne, and B. Vacchini, "The interplay between local and non-local master equations: exact and approximated dynamics", New J. Phys. **22**, 083011 (2020).

[159] A. Oppenheim, A. S. Willsky, and I. Young, *Signals and Systems* (Prentice-Hall, New York, 1983).

[160] J. N. Pedersen, B. Lassen, A. Wacker, and M. H. Hettler, "Coherent transport through an interacting double quantum dot: Beyond sequential tunneling", Phys. Rev. B **75**, 235314 (2007).

[161] S. Koller, M. Grifoni, M. Leijnse, and M. R. Wegewijs, "Density-operator approaches to transport through interacting quantum dots: simplifications in fourth-order perturbation theory", Phys. Rev. B **82**, 235307 (2010).

[162] J. Kern and M. Grifoni, "Transport across an Anderson quantum dot in the intermediate coupling regime", Eur. Phys. J. B **86**, 1–18 (2013).

[163] M. S. Ferguson, O. Zilberberg, and G. Blatter, "Open quantum systems beyond Fermi's golden rule: Diagrammatic expansion of the steady-state time-convolutionless master equations", Phys. Rev. Res. **3**, 023127 (2021).

[164] P. P. Mazza, D. Zietlow, F. Carollo, S. Andergassen, G. Martius, and I. Lesanovsky, "Machine learning time-local generators of open quantum dynamics", Phys. Rev. Res. **3**, 023084 (2021).

[165] S. Andergassen, M. Pletyukhov, D. Schuricht, H. Schoeller, and L. Borda, "A renormalization-group analysis of the interacting resonant level model at finite bias: generic analytic study of static properties and quench dynamics", Phys. Rev. B **83**, 205103 (2011).

[166] R. P. Feynman and F. L. Vernon, "The theory of a general quantum system interacting with a linear dissipative system", Ann. Phys. **24**, 118 (1963).

[167] M. M. Wolf, *Quantum channels and operations - guided tour (lecture notes)*, (2012) `http://www-m5.ma.tum.de/foswiki/pub/M5/Allgemeines/MichaelWolf/QChannelLecture.pdf`.

[168] R. Horodecki, P. Horodecki, M. Horodecki, and K. Horodecki, "Quantum entanglement", Rev. Mod. Phys. **81**, 865–942 (2009).

[169] M. Leijnse and M. R. Wegewijs, "Kinetic equations for transport through single-molecule transistors", Phys. Rev. B **78**, 235424 (2008).

[170] C. Emary, "Self-consistent electron counting statistics", J. Phys.: Condens. Matter **23**, 025304 (2010).

[171] C. Emary and R. Aguado, "Quantum versus classical counting in non-markovian master equations", Phys. Rev. B **84**, 085425 (2011).

[172] J. Maciejko, J. Wang, and H. Guo, "Time-dependent quantum transport far from equilibrium: an exact nonlinear response theory", Phys. Rev. B **74**, 085324 (2006).

[173] T. L. Schmidt, P. Werner, L. Mühlbacher, and A. Komnik, "Transient dynamics of the anderson impurity model out of equilibrium", Phys. Rev. B **78**, 235110 (2008).

[174] P. Werner, T. Oka, and A. J. Millis, "Diagrammatic monte carlo simulation of nonequilibrium systems", Phys. Rev. B **79**, 035320 (2009).

[175] P. Werner, T. Oka, M. Eckstein, and A. J. Millis, "Weak-coupling quantum monte carlo calculations on the keldysh contour: theory and application to the current-voltage characteristics of the anderson model", Phys. Rev. B **81**, 035108 (2010).

[176] J. Eckel, F. Heidrich-Meisner, S. G. Jakobs, M. Thorwart, M. Pletyukhov, and R. Egger, "Comparative study of theoretical methods for non-equilibrium quantum transport", New Journal of Physics **12**, 043042 (2010).

[177] T. A. Costi, A. C. Hewson, and V. Zlatic, "Transport coefficients of the anderson model via the numerical renormalization group", Journal of Physics: Condensed Matter **6**, 2519–2558 (1994).

[178] S. Bock, A. Liluashvili, and T. Gasenzer, "Buildup of the kondo effect from real-time effective action for the anderson impurity model", Phys. Rev. B **94**, 045108 (2016).

[179] N. M. Gergs, C. B. M. Hörig, M. R. Wegewijs, and D. Schuricht, "Charge fluctuations in nonlinear heat transport", Phys. Rev. B **91**, 201107 (2015).

[180] N. Walldorf, A.-P. Jauho, and K. Kaasbjerg, "Thermoelectrics in Coulomb-coupled quantum dots: Cotunneling and energy-dependent lead couplings", Phys. Rev. B **96**, 115415 (2017).

[181] M. Keil and H. Schoeller, "Nonperturbative analysis of coupled quantum dots in a phonon bath", Phys. Rev. B **66**, 155314 (2002).

[182] H. Schoeller and F. Reininghaus, "Real-time renormalization group in frequency space: A 2-loop analysis of the nonequilibrium anisotropic Kondo model at finite magnetic field", arXiv, `10.1103/PhysRevB.80.045117` (2009).

[183] G. Chiribella, G. M. D'Ariano, and P. Perinotti, "Transforming quantum operations: quantum supermaps", EPL **83**, 30004 (2008).

[184] F. A. Pollock, C. Rodríguez-Rosario, T. Frauenheim, M. Paternostro, and K. Modi, "Non-markovian quantum processes: complete framework and efficient characterization", Phys. Rev. A **97**, 012127 (2018).

[185] J. C. Butcher, *Numerical methods for ordinary differential equations* (Wiley, 2008).